Design of Anthropomorphic Robot Arm: ARA-1

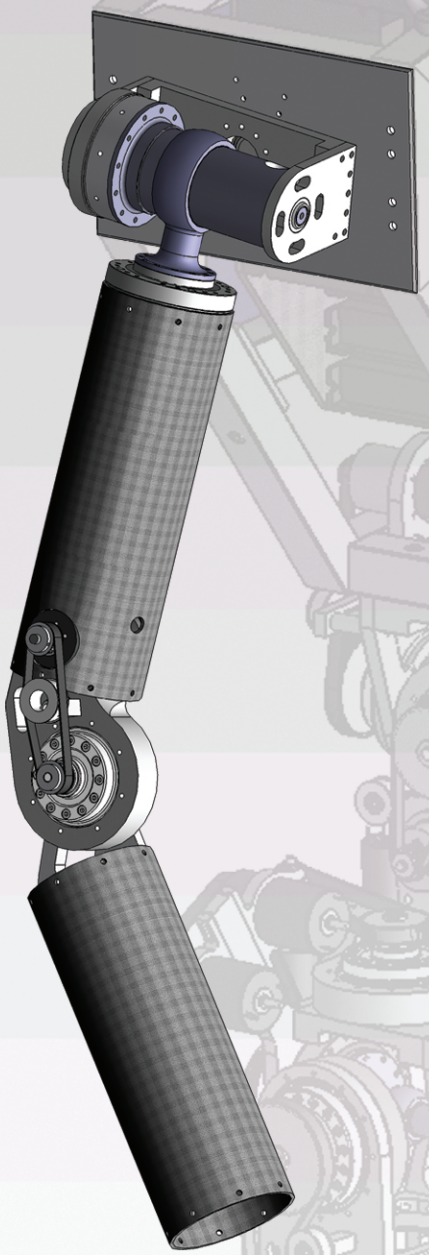

DESIGN OF MECHANICAL SYSTEMS

DMS 10 M.Sc.
INS

2008
AALBORG UNIVERSITY

AALBORG UNIVERSITY

Title :	**Design of Anthropomorphic Robot Arm: ARA-1**
Topic :	**Design of Mechanical Systems**
Project period :	**10th Semester (M.Sc.)**
Project start :	**February 3rd 2008**
Report submitted :	**June 3rd 2008**
Page count :	**66**
Appendix :	**A-E**
Supplement :	**Enclosed CD**
Number printed :	**4**
Supervisor :	**Associate Professor, PhD, Michael Rygaard**
Co.Supervisor :	**Associate Professor, Shaoping Bai**
Department :	**Department of Mechanical Engineering**
Written by :	

Lee R. L. Nielsen

Abstract

An anthropomorphic biped robot called AAU-Bot1 has been developed at Aalborg University. This robot is a part of cooperation between Department of Mechanical Systems and Department of Electrical Systems. Initially the robot was designed to perform the human gait or more precise the heel-toe gait. Currently the AAU-Bot1 is subjected to implementation of control schemes at Department of Electrical Systems. The arms of the robot are attached to the torso by means of revolute joints on the current robot. However it has been the aim from start of the cooperation to develop a robot that also could interact with humans in the form of a handshake.

As the AAU-Bot1's current arms are limited to a pitching motion around the shoulder joints. The focus of this project is to create a light and low power consuming mechanical design of an anthropomorphic robot arm (ARA) with seven degrees of freedom with the same working space as a human arm. The redundant setup of the robot arm will enhance the flexibility when it is to perform human-like motion. The robot arm is set to minimum perform two types of motion, standard gait and a human handshake motion. After manufacturing the designed ARA is to be mounted on AAU-Bot1.

The design is limited to a system with four degrees of freedom. From a literature study the human wrist trajectories for gait and handshake was determined. To determine the unknown trajectory for the four degrees of freedom, a combination of weighed and damped pseudo inverse Jacobian has been used. Together with standard kinematic and inverse dynamic analysis, ARA motion and forces was determined. The weighed-damped pseudo inverse Jacobian method has been used together with an optimisation procedure based on the Complex method. The optimisation procedure was introduced to minimise ARA power usage and remove trajectories that would collide with the torso of AAU-Bot1. Kinematic and inverse dynamic analysis results have been used to select gear and actuators from catalogues. Simple calculation and intuitive design procedures have been used to design the structural parts of the robot arm.

The work has resulted in a four degree of freedom conceptual design with human-like proportions and manipulability. The total mass of the initial design is approximately 5.8 *kg* that gives an additional mass for AAU-Bot1 of 4 *kg* per arm because of shared design parts. The arm can carry a payload of 2 *kg*. The distribution of joint degree of freedom follows the one of a human arm and is obtained with revolute joints in series. The design can perform standard human gait and handshake motion. At the same time the concept have been created sufficiently strong to perform other tasks.

The designed anthropomorphic robot arm is designed to work for standard gait and handshake motion. The redundant setup ensures a flexible arm that can imitate the human arm. It should be investigated if the mass can be reduced with use of special purpose designed gears and extra gearing to minimise motor sizes. The design is to be expanded with three extra degrees of freedom so an anthropomorphic robot arm design with seven degree of freedom can be manufactured.

Preface

This thesis has been created over one semester from February 3rd to June 3rd of 2008 at the Department of Mechanical Engineering. The report describes the concept design of a robot arm called ARA (Anthropomorphic Robot Arm). This arm is to be mounted on the anthropomorphic AAU-Bot1 robot [17] that is a biped robot constructed at Aalborg University.

From the initial stated problem a detailed specification for the design was established A concept design was established based on the established specification for the design.

The project has been supported by researchers from Department of Mechanical Engineering and from Department of Electronic Systems.

CD-ROM is enclosed in the back of this report, which contains; Matlab programs, a SolidWorks CAD model, technical data for gears and motors as well as a report in PDF format. Besides are results from the Matlab programs placed in the folder ”dynamic_results”. A complete overview of the different result can be viewed in the result files or by running the Matlab program ”main.m”.

Tables and figures have been enumerated with the number of the chapter and the number of the figure in that chapter, *e.g.* ”Figure 3.1”. This figure will be the first figure in chapter 3. Appendixes are indicated with letters, *e.g.* ”Appendix A”. Citations in the report have been made as, *e.g.* [23].

Contents

Abstract v

1 Introduction Problem description **1**

2 Problem Analysis **3**
2.1 Human Arm 3
2.1.1 Range of motion 4
2.2 AAU-Bot1 5
2.2.1 General 5
2.3 Other Projects 7
2.3.1 Robota 7
2.3.2 ARMAR-III arm 10
2.4 Summary 12

3 ARA Specification Problem formulation **13**
3.1 Demands 13
3.2 Wishes 14
3.3 Summary 14

4 Load Cases **15**
4.1 Walk Motion 15
4.2 Handshake Motion 16
4.3 Summary 18

5 Dynamic Analysis **19**
5.1 Initial Assumptions/Definitions 19
5.2 Kinematic Analysis 21
5.2.1 Kinematic Setup 21
5.2.2 Kinematic Constraint 22
5.2.3 Solving Unknown Driving Constraints 25
5.2.4 ARA Motion 27
5.2.5 Discussion 28
5.3 Inverse Dynamic Analysis 29
5.3.1 Equation of motion 29
5.3.2 Equations of motion - ARA 31
5.4 Optimisation Procedure 32
5.4.1 Complex 32
5.4.2 Overall Optimisation 34
5.4.3 Start Position 36

5.5 Dynamic Program . . . 38
5.6 Results . . . 39
5.6.1 Kinematic Results . . . 39
5.6.2 IDA Results . . . 41
5.6.3 Optimisation Results . . . 43
5.7 Summary . . . 43

6 ARA Concept Design 45
6.1 Power Transmission . . . 45
6.1.1 Harmonic Drive Gears . . . 46
6.1.2 Maxon Motors . . . 51
6.2 Mechanical Design . . . 57
6.2.1 Design Overview . . . 57
6.2.2 Design Considerations . . . 58
6.2.3 Design Details . . . 59
6.3 Summary . . . 62

7 Conclusion and Future Work 63

Bibliography 64

Nomenclature 67

Appendiks 70

A Constraint Equations 71

B Equation of Motion - ARA 79

C Dynamic Program 81

D Technical Data CPU units 133

E Technical Data Maxon Motors 141

1
Introduction Problem description

It was suggested that a new and better set of arms should be developed for the AAU-Bot1. The main goal for this project is to develop a new anthropomorphic robot arm (ARA) with higher manipulability than the current arms mounted on AAU-Bot1. An extract of the initial project description from Department of Mechanical Engineering is:

> *The project attempts to develop an anthropomorphic (human-like) robotic arm with a high degree of manipulability. A two-portion anthropomorphic robotic arm with seven degree of freedom (DOF) is to be built. The redundant DOF helps to eliminate singularity, to enhance flexibility in avoiding obstacles and to improve the dexterity. By introducing the redundancy DOF in the arm, it is expected to improve the performance of the arm so it can be comparable to human arms.*

There was beside the project description suggested different technical specification for the design. First of all a final arm should have 7 DOF, the same amount as a human arm. To imitate the human hand it was suggested that a gripper with 1 DOF should be mounted at wrist joint. As well it was suggested that the arm should be able to handle a payload up to 4 *kg*. It was also noted that the weight and power consumption is important factors for the designed arm. [22]

The AAU-Bot1 was developed by three students at Aalborg University in 2006/2007. The task was to develop a mechanical design of a humanoid biped robot with human-like proportion and DOF that could perform human walking. The project is a cooperation between Dept. of Mechanical Engineering and Department of Electronic Systems. Final assembly and control implementation is still under development by Department of Electronic Systems and the robot is expected to walk in the summer of 2008. Figure 1.1 shows a kinematic and CAD model of the developed robot [17].

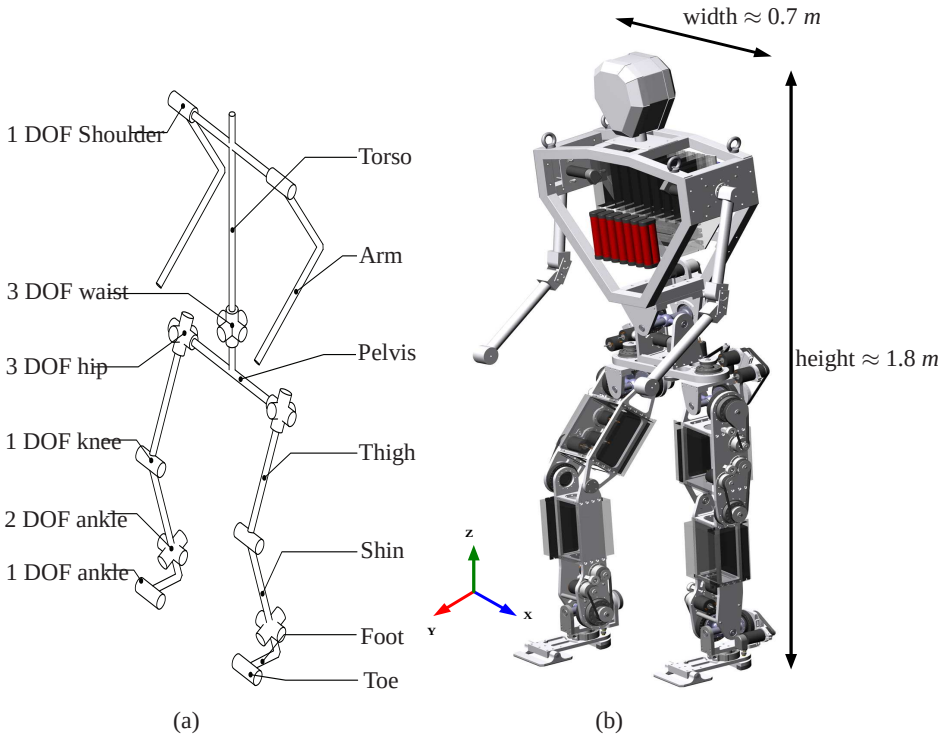

Figure 1.1: *DOF and CAD model of the AAU-Bot1 robot. [17]*

AAU-Bot1 is a relatively expensive project and it is important that the project also gives some form of payoff for the university. When the robot is completely finished and ready for public appearance the success criteria can be measured differently. But one factor could be how much the robot impresses or relates to the public or people reviewing the project. Because the AAU-Bot1 is a humanoid robot, humans will relate to the robot both physical and psychical. If the robot is able to interact with humans or imitate human behaviour, it will create a simple relation to humans. The chance of a successful presentation of the AAU-Bot1 would therefore increase.

2
Problem Analysis

2.1 Human Arm
2.2 AAU-Bot1
2.3 Other Projects
2.4 Summary

As the overall project description states that an anthropomorphic arm of 7 DOF is to be designed. It will from information collected in this chapter be established a detailed design specification for the ARA design. Human arm is being reviewed for important properties. The AAU-Bot1 design approach as well as experience is collected. Final some projects that have created anthropomorphic arms are reviewed. Based on the collected information a detailed ARA specification is worked out.

2.1 Human Arm

The human arm is a complex structure that is hard to copy in mechanical designs. But there are different parameters that general describe the properties of a human arm, i.e. degree of freedom, range of motion and size. Mass is not important because ARA is to be as light as possible. If normal kinematics notations are used the human arm DOF can be simplified to be represented with 3 DOF at shoulder joint, one at elbow, three at wrist. See figure 2.1.

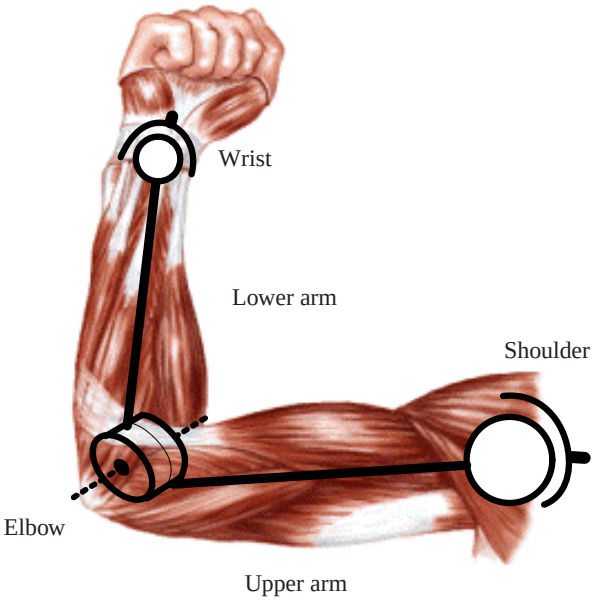

Figure 2.1: *Human arm represented with simple kinematic joints.*

2.1.1 Range of motion

The human arm DOF defined at figure 2.1 is limited to different outer position that together defines the human arm work space or range of motion. The general range of motion for an adult human can be shown with figure 2.2, 2.3.

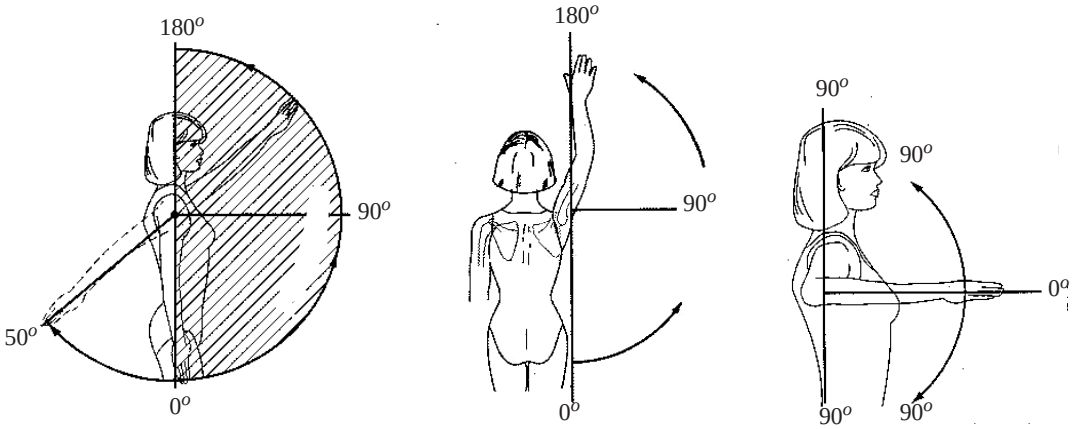

(a) Shoulder Pitch (b) Shoulder Roll (c) Shoulder Yaw

Figure 2.2: *Range of motion for human shoulder joint. [14]*

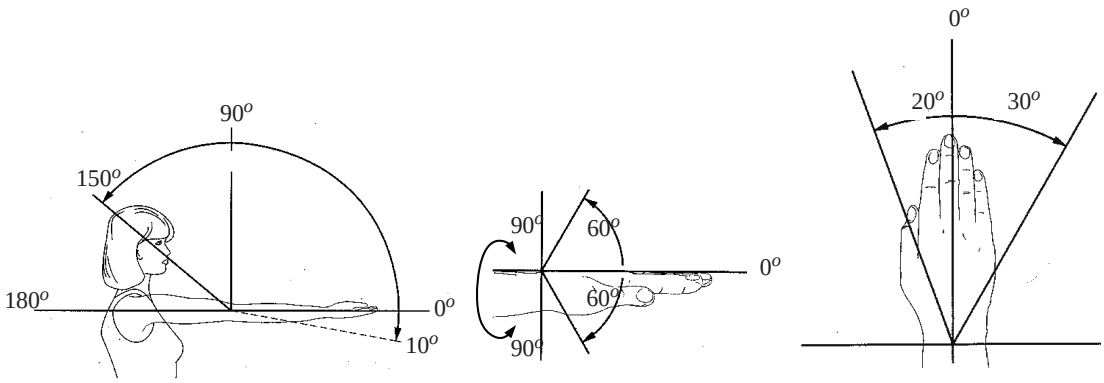

(a) Elbow Pitch (b) Wrist Yaw/Pitch (c) Wrist Roll

Figure 2.3: *Range of motion for human elbow joint, and wrist joint. [14]*

The data is summarised in table 2.1

Joint	**Movement limit**	**Angle [°]**
Elbow	Pitch upper/lower	140 / 0
Wrist	Pitch upper/lower	60 / 60
	Roll upper/lower	20 / 30
	Yaw upper/lower	90 / 90
Shoulder	Pitch upper/lower	180 / 50
	Roll upper/lower	90 / 0
	Yaw upper/lower	90 / 90

Table 2.1: *Human arm range of motion.*

These data for the human arm is to be passed on to the design of ARA as it is to perform human

motion.

Size

The size of a human arm is dependent on many factors where age and gender are primary dependencies. An investigation of human segment length have been conducted by [13]. The result of this work can be represented table 2.2, where the data is for males.

Upper arm length (mm)

Age	nr.	Mean	Stddv.	Interval		Median	5%	95%
				Lower	Upper			
20-29	42	368	18	332	404	370	341	395
30-39	63	370	21	327	413	370	341	405
40-49	61	370	23	324	416	370	340	410
50-59	55	371	21	329	412	365	344	410

Lower arm- and hand length (mm)

Age	nr.	Mean	Stddv.	Interval		Median	5%	95%
				Lower	Upper			
20-29	42	480	17	445	515	480	450	505
30-39	63	484	24	436	532	480	456	515
40-49	61	483	19	444	522	480	455	510
50-59	55	485	24	436	534	480	455	530

Hand length (mm)

Age	Numb	Mean	Stddv.	Interval		Median	5%	95%
				Lower	Upper			
20-29	42	194	19	155	232	195	175	210
30-39	63	195	12	172	219	195	180	210
40-49	61	194	13	168	219	195	175	210
50-59	55	194	13	168	220	195	179	215

Table 2.2: *Human arm length based on the working Danish male. [13]*

It is chosen to use the median values from the age 20 to 29.

2.2 AAU-Bot1

It is important to bear in mind that the ARA has to be mounted on the AAU-Bot1 and therefore mechanical parts, actuators etc. have to work together with the types of components already used in AAU-Bot1. So to establish a foundation for AAU-Bot1 component usage and design approach the design is shortly reviewed. At the same time experience from AAU-Bot1 project is taken in to consideration for ARA design.

2.2.1 General

The AAU-Bot1 is designed to perform walking motion for a minimum of 1000 hours. This include start/stop, turn and straight walk. The walking motion should be performed for a minimum of 15 minutes with on board power supply. As the AAU-Bot1 is to perform walking motion for at least 1000 hours the ARA design is to withstand that as well. Besides the walking motion the robot is also dimensioned to stand up from sitting on a chair as well as climb a 0.15 *m* high obstacle. The dimensioning of the AAU-Bot1 was initial based on arms that has a mass

of 5.8 *kg* this is therefore also set as maximum weight for initial ARA design.

The current AAU-Bot1 has a total of 17 actuated and 2 unactuated DOF, approximately a height of 1.8 *m* and a mass of 70 *kg*, see figure 1.1. Structural parts are created with aluminium to minimise the overall weight, but high stressed parts have been created with steel. Besides the structural parts the AAU-Bot1 is generally build from commercial components. These components are the DC RE series motors from Maxon [18]. Different sizes of the RE series are used to comply with the different power requirements associated with the walk motion. Position measurement through a working cycle is determined by digital encoders, also from Maxon, and integrated in the motor. The gearing between motor and joint is done with different CPU-S unit sizes from Harmonic Drive [5]. Connection between motor and gear is done with toothed belt drive. This also means that an extra gearing can be introduced.

It is noted that absolute position information is needed for control purpose. As the AAU-Bot1 is an open design that it is easy to modify and fix if any problems occur, but at the same time has disadvantages for moving parts that can get damaged or can damage persons working around the robot. Hence belt drives and motors should be shielded to both protect robot and people working with it.

AAU-Bot1 Arms

Current arms mounted on the AAU-Bot1 have a pitching motion placed at the shoulder joint. This pitch was included so the walking stability would be improved. But with only a pitching motion the arms have a low manipulability and have a limited usability for other task then walking. The current arms mounted on AAU-Bot1 are illustrated in figure 2.4.

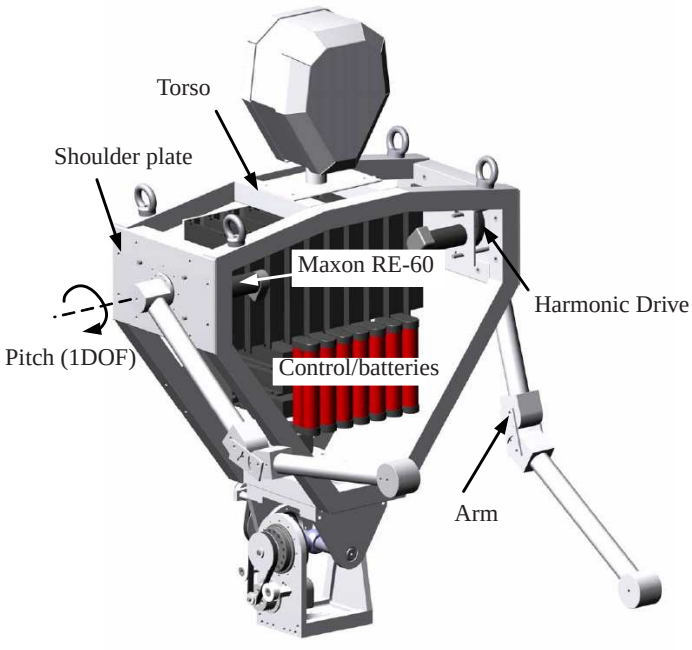

Figure 2.4: *Illustration of AAU-Bot1 arms and upper body. [17]*

As the figure illustrate it can been seen that AAU-Bot1 arms have one DOF at the shoulder.

This DOF is a pitching motion and is actuated with a Maxon RE-60W DC motor that then is connected to a Harmonic Drive CPU-S gear with a toothed belt drive. This consultation with Maxon motor, Harmonic Drive gear and toothed belt drive is used for all actuating DOF in the AAU-Bot1 design.

2.3 Other Projects

Several anthropomorphic robots have been created over time, some of these are the ASIMO [28], ARMAR [1], WABIAN-2 [27] and of course Aalborg University own AAU-Bot1 [17]. There are as well projects that focus on creating a high mobility robot arm, e.g. the WAM arm [24, 3], Robota [11]. Below three different robots/arms are illustrated, first the ROBOTA arm, figure 2.5(a) second the ARMAR III, figure 2.5(b) and last the Wabian-2, figure 2.5(c).

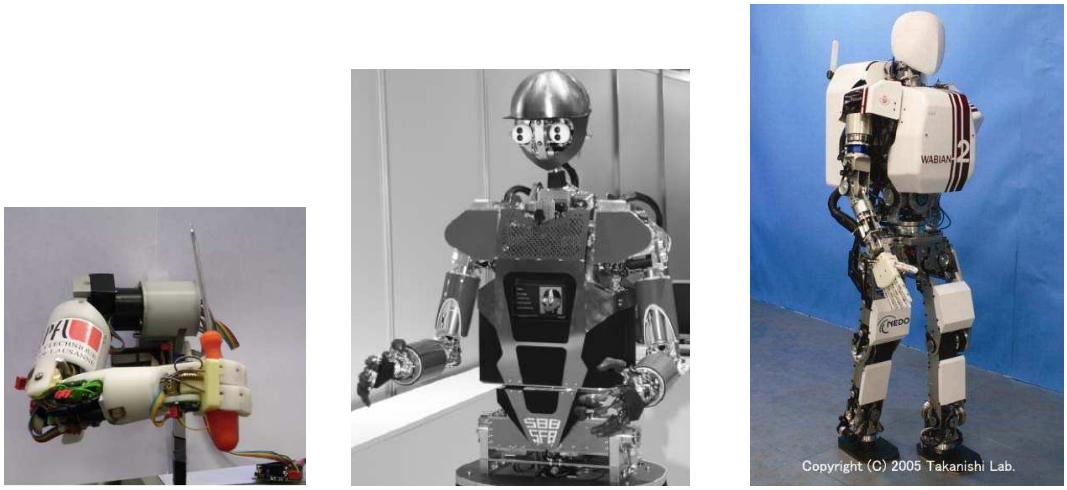

(a) (b) (c)

Figure 2.5: *Three different humanoid robots. (a) Illustrate the ROBOTA arm. (b) ARMAR III robot. (c) WABIAN-2 robot.*

2.3.1 Robota

Description of Robota arm is based on [11, 10]. The idea with the project is to design a multiple DOF doll-shaped humanoid robot. Physical appearance and features should resemble those of a baby or doll. The project started in 1997 with a robot that had a total of 5 DOF, one DOF for each leg, one for each arm and one for the head. Each of the DOF is controlled with a 1:6 geared DC motor. The newest project includes the design of arms that each has 6 DOF, three at the shoulder, one at elbow and two at wrist joint. The arm is designed to carry external loads up to 200 grams, where its own mass is around 700 grams.

General

The arm DOF is created with several revolute joints in series. Each DOF on the arm are actuated with DC motors of the type Faulhauber or Maxon. The motors are either direct drive or connected to a gearing of either bevel gear or notched belt. Absolute positions in work space of

each joint are determined with a potentiometer. This is done to remove an alignment procedure when the robot is switched on. For position measurement through a working cycle, digital motor encoders are used. On-board control and batteries are placed inside the torso of the doll; this is done to reduce the mass moment of inertia. The Robota segment sizes and kinematic model can be seen in figure 2.6.

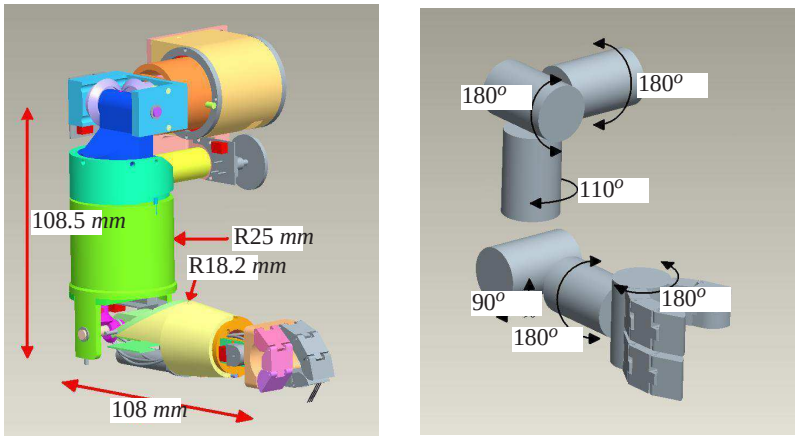

(a) (b)

Figure 2.6: *(a) Robota segment size. (b) Robota DOF. [11]*

Cables used in the arm were fixed inside upper and lower arm. The wire connection from upper body to arm is done outside the shoulder joint, the wires are hidden with a cosmetic shield.

Shoulder joint

To imitate the human shoulder the Robota arm has divided shoulder 3 DOF in to three separate revolute joints where all three joint axes intersects at a common point. Figure 2.7 from [11] shows how the three first DOF of the shoulder is created.

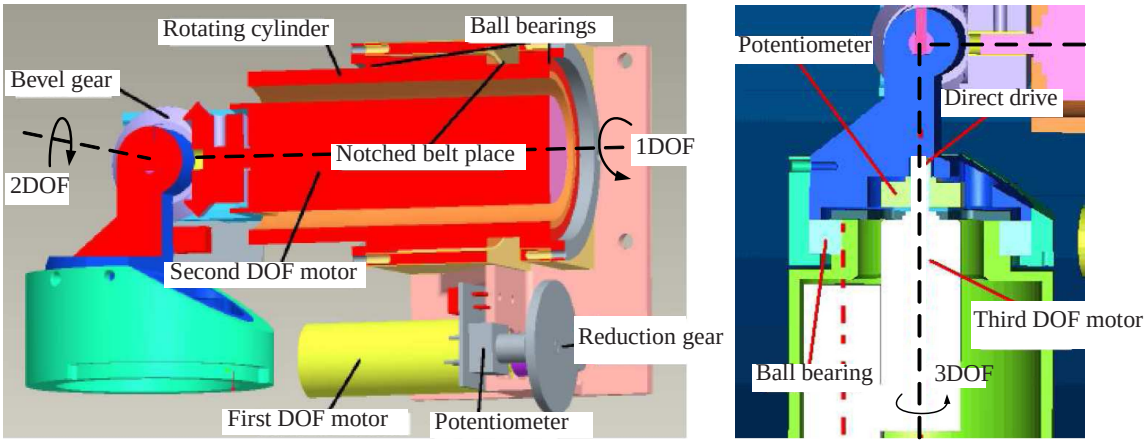

(a) (b)

Figure 2.7: *The design of the Robota shoulder joint to imitate a human 3 DOF shoulder. [11]*

The first DOF is created by designing a cylinder that is supported with ball bearings, to rotate the cylinder the DC motor is connected to the cylinder through a reduction gear which is connected to the cylinder by a notched drive belt. The backlash of this DOF is very little and generally only from the reduction gear. This joint has a moving range of complete 180^o.

The second DOF is controlled by a motor where a bevel gear makes sure that the upper arm is rotated around the second revolute joint. Because the bevel gear has relatively large teeth, backlash as well relatively large. The special part of this design is that the second DOF motor is fitted inside the first DOF cylinder. This make the design very compact but still relative simple. Joint range is 180^o.

The third DOF motor is placed inside the upper arm and then directly connected to the last body, this again make the design very compact and relative simple. For this DOF there are no or very little backlash from the motor itself. Joint range is 115^o.

The rest of the joints are more or less a derivative of the fist three joints. For further details see [11].

2.3.2 ARMAR-III arm

Description of ARMAR-III arm is based on [1, 2]. The goal with the ARMAR project is to create a humanoid robot that is able to support humans in different tasks either alone or in cooperation with humans. The current arms on the ARMAR-III have 7 DOF and motion range and size approximately the same as a human. The arm has a mass around 6 *kg* and can carry a payload up to 3 *kg*.

General

To imitate human kinematics the ARMAR-III arm is designed with several revolute joints in series. Each DOF of the arm is actuated with standard servo motors. The motors are either connected to a worm gear, belt drive or a Harmonic Drive gear [5]. Absolute position of joint work space is determined with optical sensors placed close to the joint rotational point. For position measurement through a working cycle, motor encoders were used. On-board control systems are placed in the torso. The ARMAR segment sizes and kinematic model can be reviewed in figure 2.8.

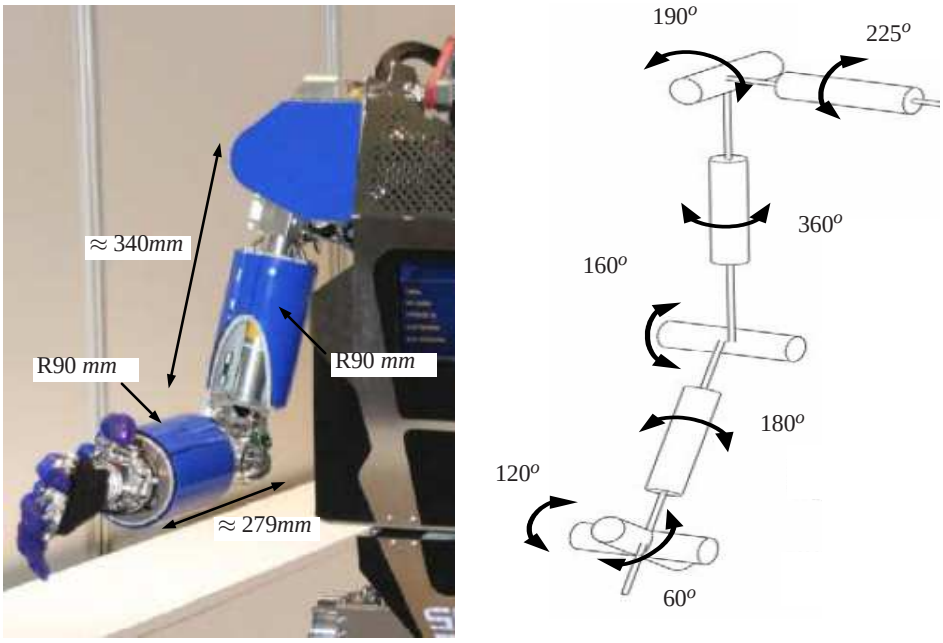

Figure 2.8: *(a) ARMAR segment size. (b) ARMAR DOF. [1]*

Cables in the ARMAR-III are placed inside the arm design. Elbow motion is actuated by motors placed in the torso.

The ARMAR-III have onboard force control of the arm, here several different techniques are used. To determine forces acting on the different shoulder DOF's there are placed strain gages at each worm gear shaft that measure the axial force. The elbow force is determined with use of load cells that have been integrated in the wire ropes that is used to actuate the elbow motion. At wrist point a six axis force and torque sensor is mounted. One special feature with the ARMAR-III is the addition of tactile skin sensor several places on the upper body.

Shoulder joint

The shoulder joint is created by three independent revolute joints that are actuated by commercially available servo motors and geared with Harmonic Drives, toothed belt transmission and worm gears. Figure 2.9 illustrate the shoulder design.

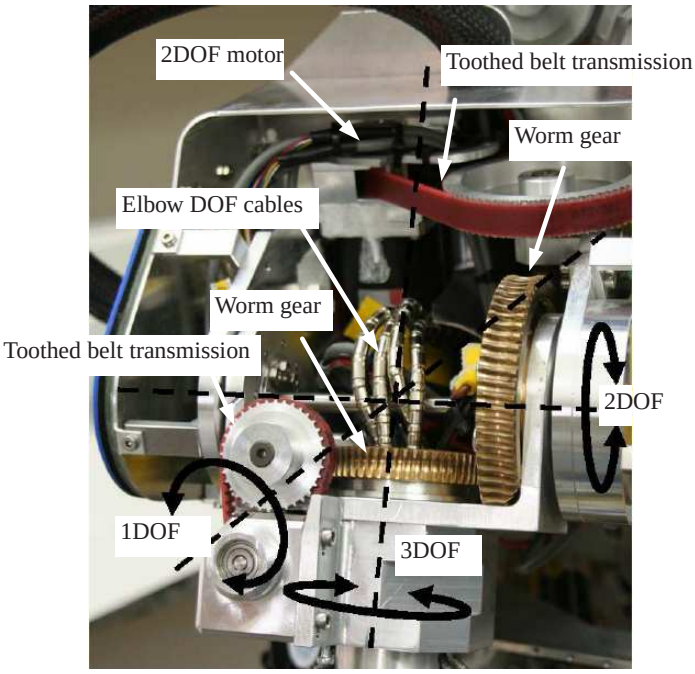

Figure 2.9: *ARMAR-III shoulder design. [1]*

The first DOF design is placed at torso and therefore this part of the arm is not contributing to the overall arm inertia. The DOF is geared with a Harmonic Drive where the motor is connected to the drive with a toothed belt drive. This joint has an angular range that goes from -45^o to 180^o with initial position straight down along the torso.

The second DOF is geared with both toothed belt transmission and worm gear. This means that the motor can be placed orthogonal to the rotational axis. With orthogonal placed motors the size of the shoulder is greatly reduced compared to earlier ARMAR models. Another aspect of the worm gears are that they are self locking. That means that if the robot is shut down the arms stay in position. The DOF is supported by two ball bearings on each side of the third DOF rotation axis. This joint has an angular range of -10^o to 180^o.

The third DOF is geared and actuated like the second DOF and is supported by ball bearings.

The elbow joint of the ARMAR-III arm is a 2 DOF joint. The first is the normal human arm bending and the second is the rotational principle between elbow and wrist. The elbow joint uses Harmonic Drive and servo motors to actuate the joint, but they are placed inside the torso. Wires are lead from the torse through the shoulder and out to the elbow with use of rolls and bowden cables. To ensure an uncoupling of motion the cables are placed at axis's of rotation..

2.4 Summary

Because the ARA should be an anthropomorphic robot arm it is necessary that the ARA design imitate the human arm, therefore ARA properties is to be the same as of a human arm. Segment length of ARA are based on the median values of a Danish male in the age between 20-29 years. The mass of the complete 7 DOF arm should be below 5.8 *kg*, that is the mass of AAU-Bot1 arms for initial calculation. The mass of the ARA is to be minimised because this will reduce power consumption of ARA and improve dynamic behaviour because of a lowered mass moment of inertia. The stiffness of a robot arm is generally important because this increase end-point accuracy and simplify control. Increasing stiffness do generally increase the mass, therefore a compromise between the two has to be taken.

Generally, the design of the different humanoid robots uses angular electrical actuators at each joint. For several of the robot projects DC motors are used along with gears from Harmonic Drive. The Harmonic drive gear has a relatively high gear ratio, small backlash, relative low mass, compact design and as well a relative high efficiency and therefore seems to be preferable and reasonable components to use with ARA design. As AAU-Bot1 uses Maxon RE series, that seem preferable for robot design, they are as well selected for ARA design.

The AAU-Bot1 robot is dimensioned to withstand 1000 hour of walking, which included different stop/start and turning task. Therefore this lifespan is the lifetime criteria for ARA when AAU-Bot1 is walking. ARA is from initial project description required to perform human handshake motion, this motion is set to be performed minimum 100 times.

It was suggested to create an arm with 7 DOF, but limited to only consist of 4 DOF. These four are the three at the shoulder joint and one at the elbow joint. Removal of the wrist joint DOF do not degrade the manipulability to place the arm in space when performing human walking and handshake motion. Because the two load cases, gait and handshake, only cover a small margin of possible load cases, static load cases is taken in to consideration.

It was stated that the ARA should be able to carry a payload up 4 *kg*, this will be close to the maximum mass of complete ARA design. Compared to other robot arms the payload/mass ratio will then be relative large. And to reach a payload of 4 *kg* the ARA mass would possibly increase drastically. Therefore initial the payload is lowered to 2 *kg* that seemed more reasonable for the arm design.
General experience from the projects dealing with anthropomorphic robots is that backlash from designed gear or selected gears are an important factor to take in to account. This property affects the dynamic behaviour and control of the system. General problem with the designs is the minimisation of weight and at the same time have motors to be sufficient large to give a required motion. Absolute control was recommended to simplify control implementation at the same time should any form of position control in a working state be applied.

3
ARA Specification Problem formulation

3.1 Demands
3.2 Wishes
3.3 Summary

The ARA specification is divided in to two aspects, demands and wishes. The demands and wishes are created based on the information found from the project description as well as details from conducted problem analysis. The demands is seen as the minimum specification that has to be fulfilled. The wishes is properties that it is recommended to optimise as they will improve performance of ARA design. As some of the wishes contradicts the best possible combination of the wishes has to be taken.

3.1 Demands

- To be mounted on AAU-Bot1
- 1000 hours of walking motion
- 100 times <Handshake motions
- Maximum mass of 5.8 *kg*
- 4 DOF. Three at the shoulder joint and one at the elbow joint.
- Carry a payload up to 2 *kg*
- Human like proportions [13]
  - Upper arm, 0.37 *m*
  - Lower arm, 0.285 *m*
- Human like mobility [14]
  - Shoulder roll -50^o to 180^o
  - Shoulder pitch 0^o to 180^o
  - Shoulder yaw -90^o to 90^o
  - Elbow pitch 0^o to 140^o
- Gears from Harmonic Drive [5]
- Actuators from Maxon motors [18]

3.2 Wishes

- Minimise weight
- Minimise power usage
- Maximise stiffness

3.3 Summary

From the problem description and conducted problem analysis a problem formulation is worked out in the form of a design specification for the ARA design. The specification is divided in to two aspects, technical data in the form of demands and secondly some wishes of parameters that will improve the ARA performance. A compromise between the wishes has to be taken.

4
Load Cases

4.1 Walk Motion
4.2 Handshake Motion
4.3 Summary

As the ARA is to work for 1000 hours for AAU-Bot1 walking motion and minimum 100 times of handshake these motion are investigated and determined based on human walking and handshake motion. The walking motion and handshake motion are collected from different external experimental data that do not directly have any association with the design of ARA. The gait data have been collected from AAU-Bot1 laboratory experiments. The handshake data have been collected from different articles, which have either investigated the handshake approach or the shake motion of a handshake. None of the data shown in this chapter is therefore collected from laboratory experiments that direct were intended to create the ARA. But experimental determination in-house would minimise available time for other important steps for designing the ARA and therefore collection of the data from available experiments conducted for separate projects seemed preferable.

All experimental data illustrated in this chapter is based on the right arm of the test person. Data shown in the different graphs have been converted to follow a standard right handed system with the global position at the shoulder joint, see figure 5.1(b) in chapter 5. Data is at the same time shown relative to the initial position of the wrist motion.

4.1 Walk Motion

Experimental data for human walk have been determined by [17] as a part of designing the AAU-Bot1. The experiment was performed in the ”Gait Laboratory facility of the Center for Sensory-Motor Interaction department of AAU”. To determine the gait a test person had several reflecting markers mounted several places on the body. The marker positions were captured with a motion capture system and logged over a time period.

The motion for test person arm where captured with one sensor at wrist point and one sensor at shoulder point. Walking was performed with a constant velocity of 1 m/s over a given time period. Logging was done while the test person walks along a specified path, where the logging starts and stops when passing a force platform.

To remove the dependency of upper body motion the wrist trajectory is computed relative to the motion of the shoulder point. The wrist trajectory from the experimental data for straight walking is plotted in figure 4.1.
The data at $t = 0$ does only show the relative position of wrist at the point when the test person passes the force board and does not imply what the position of the arm is at this time. It is

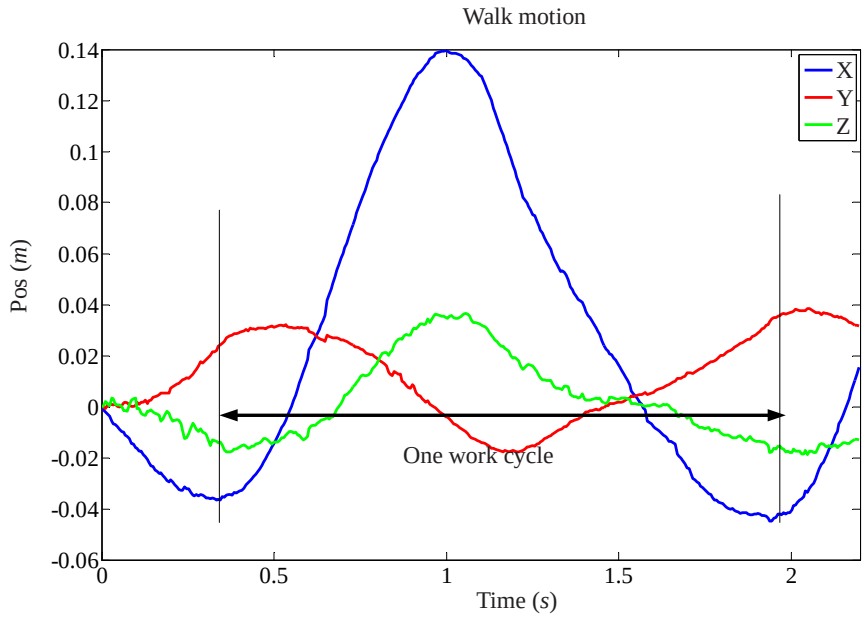

Figure 4.1: *Wrist trajectory for human walking. The work cycle starts when the arm is straight down along the torso.*

obvious that for position straight down along the torso, no negative motion in z direction of the wrist point can occur. The motion data with the arm position initially straight down along torso can then be approximated to start at t=0.35 *s* and end at t=1.9 *s*.

The motion data from the experiment are fitted with a sum of sinus curves to create a continuous function that yields realistic values for the velocity when differentiated with respect to time.

4.2 Handshake Motion

Human handshake motion will for simplicity sake be divided into two parts, firstly the handshake approach and secondly the shake. The division of the handshake will eliminate some information from the period just before handshake approach ends and the shake begins, but with the data available the interaction here is not considered important. The handshake approach has been investigated by [15] and the shake information is available from [26]. For the handshake approach a complete set of information is available to determine arm trajectory over a time period. For the shake there is only limited information and therefore different assumptions are taken to complete the trajectory this part. An entire handshake work cycle is defined as the total time for handshake approach, the shake and the return motion. The return motion is set to the opposite of the handshake approach.

Handshake Approach

The handshake approach experiment was performed with two test persons standing face to face at a distance of 1 *m*, and with arms straight down along torso. Each test person had four reflecting markers placed on their arms; shoulder, elbow and wrist. To capture the markers position a 3D capture system was used to log position over a time period. The test was performed 50

times with 10 pairs of test persons.

The wrist trajectory extracted from the experimental test is shown in figure 4.2. The extracted data from [15] is based on figures where the curve has been divided into several discrete steps. These data have been fitted with a sum of sinus curves to create a continuous function.

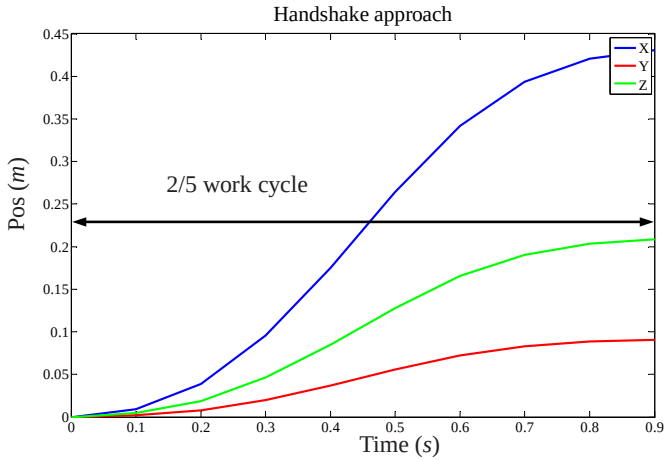

Figure 4.2: *Wrist trajectory for handshake approach.*

The handshake approach is only done for test persons standing completely still and face to face. In real life a handshake varies from time to time, where approach velocity, start position, type of person and many other factors can have influence on the wrist trajectory. In this work the data from [15] is used to determine the approach motion.

The shake

Some information of shake trajectory is available from [26]. Emphasis of this work is to control human-robot handshaking with neural oscillators. A frequency of 1.48 Hz for handshaking between human and robot is used based on information from [26]. The amplitude is a variable parameter that reported in [26] change depending on human handshake intensity.

To finalise the missing data, it is assumed that the handshake motion starts from where handshake approach ends. The amplitude for the motion is assumed to be 0.08 m and the time period for the handshake is three cycles or approximately 2 s. The amplitude and shake cycle are based on different shake observations. It is also assumed that the motion only takes place along the Z-axis; motion in X-axis and Y-axis is set to zero. The used shake motion is plotted in figure 4.3.

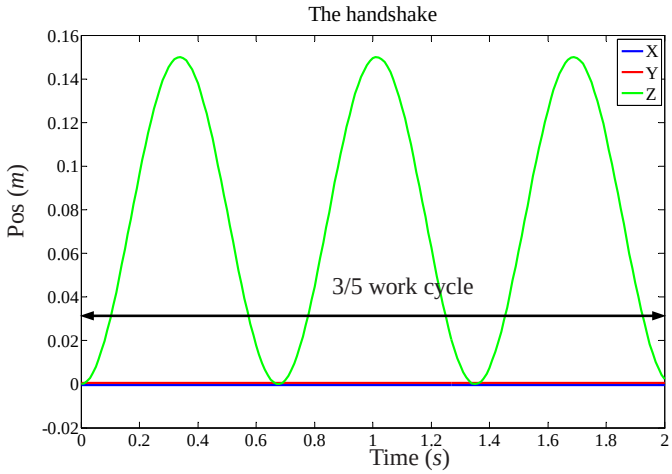

Figure 4.3: *Wrist trajectory for the shake motion.*

The amplitude and the frequency affect each other, which mean that a high frequency would minimise the amplitude and vise verse. But for the shake motion high amplitude is used along the frequency to ensure a safety factor when designing the ARA. With the shake motion simplified some motion data are lost.

4.3 Summary

In this chapter the motion associated with walking and handshake has been determined. The data shown in this chapter is only displacement plots, but velocity curves are as well available and can be viewed on "*CD-rom → load_cases*". The motion collected for walk and handshake do only include the XYZ trajectory of the wrist point, motion for the 3 DOF at the shoulder joint and the DOF at elbow joint are therefore unknown. The handshakes do not have a complete data set and therefore it has been necessary to simplify and make different assumptions to complete this data set.

5
Dynamic Analysis

5.1 Initial Assumptions/Definitions
5.2 Kinematic Analysis
5.3 Inverse Dynamic Analysis
5.4 Optimisation Procedure
5.5 Dynamic Program
5.6 Results
5.7 Summary

The kinematic analysis is carried out to determine the ARA joint motion that generates the wrist joint motion described in chapter 4. At the same time the inverse dynamic analysis is carried out to determine reactive forces in the design and the required from the actuators. Results from the analysis will be used to select gears, actuators and design structural parts that together give the ARA concept design. ARA is set to have four actuated revolute joints. Position of wrist joint (WJ) can be described with three translating positions (XYZ) and therefore the ARA setup is a redundant system. Motion of the four revolute joint can be determined using an optimisation approach. In this work the pseudo inverse Jacobian method (PIJ) [4] [12] [20] has been applied. The method is used in combination with standard kinematic methods used for rigid multi-body systems described in [23]. The dynamic analysis is divided into two main steps; first the kinematics analysis that is the study of motion regardless of the forces that produce the motion. Secondly the inverse dynamic analysis that deals with motion and its relationship with forces in a kinematically determined system. To ensure ARA capability for other tasks a short static analysis is also conducted.

The dynamic analysis is conducted by with a written Matlab program called DyP, which is created to ease to dynamic calculation and result overview. The overview of the program will shortly be showed in section 5.5. A detailed view of the code can be seen in Appendix C or on ”*CD-rom → dynamic_program*”.

Notations

Different notation is used to describe the general dynamic analysis. Here i refer to a body number and if two relative to one and another j index is used to describe the $i\pm1$ body. A vectors is symbolised with an letter underlined e.g. ”$\underline{a}$”, a matrix is symbolised with double underline e.g. ”$\underline{\underline{a}}$”. Scalars are donated just by a letter e.g. ”a”. References to global and local coordinate system is represented as $\underline{a}$ and $\underline{a}'$ or $\underline{\underline{a}}$ and $\underline{\underline{a}}'$ respectively.

5.1 Initial Assumptions/Definitions

The global coordinate system is established at the shoulder point, see figure 5.1. In the analysis the shoulder joint will not be represented by a spherical joint but by three revolute joints. The

initial calculation is performed where the three shoulder revolute joints are placed in the same position. The elbow joint is represented by one revolute joint. The start position of the ARA is defined by the upper and lower arm hanging down along the torso of AAU-Bot1.

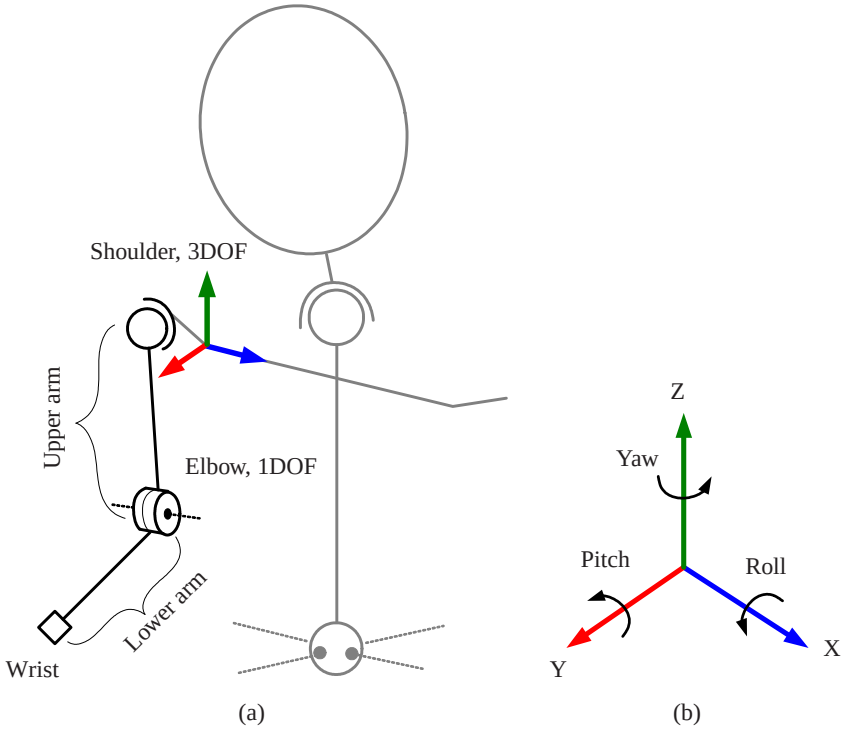

Figure 5.1: *Overall naming and definition of ARA setup for dynamic analysis.*

Constant Data

The complete mass of the ARA is initial set to 5.8 *kg*, the mass used for arms in [17]. The lower and upper arms are initially set to half of the estimated mass. The segment length is based on [13], where the upper and lower arm are 0.37 *m* and 0.285 *m* respectively. Moments of inertia for the upper and lower arm are based on a cylinder with a diameter of 0.09 *m*. The moment of inertia is for centre of mass (CoM) and in each segment local coordinate system. The complete set of initial used values are listed i table 5.1.

	Upper arm	Lower arm	Wrist (payload)
mass [kg]	2.9	2.9	2
Segment length [m]	0.37	0.285	0
Moment of inertia [$kg \cdot m^2$]	$j_{\xi\xi}$ = 0.034699	$j_{\xi\xi}$ = 0.02078589	0
	$j_{\eta\eta}$ = 0.034699	$j_{\eta\eta}$ = 0.02078589	0
	$j_{\zeta\zeta}$ = 0.002350	$j_{\zeta\zeta}$ = 0.00231961	0

Table 5.1: *Constant data for dynamic calculation.*

Start Position

For the experimental data it should be noticed that the test persons rest positions of their arms are not completely straight down, but that the joints have small offset angles. And as the start position has a large impact on the kinematic computed motion of ARA selection of start position have been selected to be done with a start guess routine. This routine will be described in details in section 5.4.

5.2 Kinematic Analysis

The kinematic analysis is done to determine angular and translating motion of bodies of ARA. Motion determined with the kinematic analysis will be used in an inverse dynamic analysis. The kinematic analysis is conducted to determine actuated joint motion as well as ARA general motion in space.

The kinematic analysis is conducted for a rigid multi-body system. This means that it is a system that consists of a set of rigid objects that can not deform, called links or bodies, joined together by kinematic joints. The kinematic joints restrict the relative motion of the two connected bodies. The type of the kinematic joint is characterised by the way the relative motion of two bodies is constrained. The relative motion allowed by a joint is described by joint's degrees of freedom.

To perform the kinematic analysis several steps have to be taken, according to [23] the steps can be divided into 6.

1. Assign index to each body
2. Define local coordinate systems
3. Select coordinates to describe the motion of the system.
4. Analyse kinematic constraints and derive equations
5. Define driving constraints
6. Find position, velocity and accelerations

5.2.1 Kinematic Setup

The ARA has been divided into five rigid bodies. Each are notated with a 1 to 5 or also defined as "Shoulder mount", "upper arm 1", "upper arm 2", "lower arm" and "wrist/payload". These bodies are connected with kinematic joints named A to E, where the joints A to D are actuated revolute joints and the joint E is an unactuated spherical joint that simply connects the wrist/payload to the lower arm. The actuated joints are also called the driving constraints through in this thesis. Body 1 to 3 define the upper arm represented in figure 5.1. The segment lengths of body 1 and 2 are for the initial calculations set to zero. This means that Body 3 have the upper arm properties from table 5.1. All local coordinate systems are placed at the centre of gravity (CoG). The position of joints according to the local coordinate systems of the bodies are defined with $\underline{s}_i'^{\,p}$, where i is the index of the body and p is the index of the joint. Figure 5.2(a) shows all local coordinate systems, joint and bodies. Figure 5.2(b) shows the geometrical position of each joint according to the local coordinate system of the corresponding bodies.

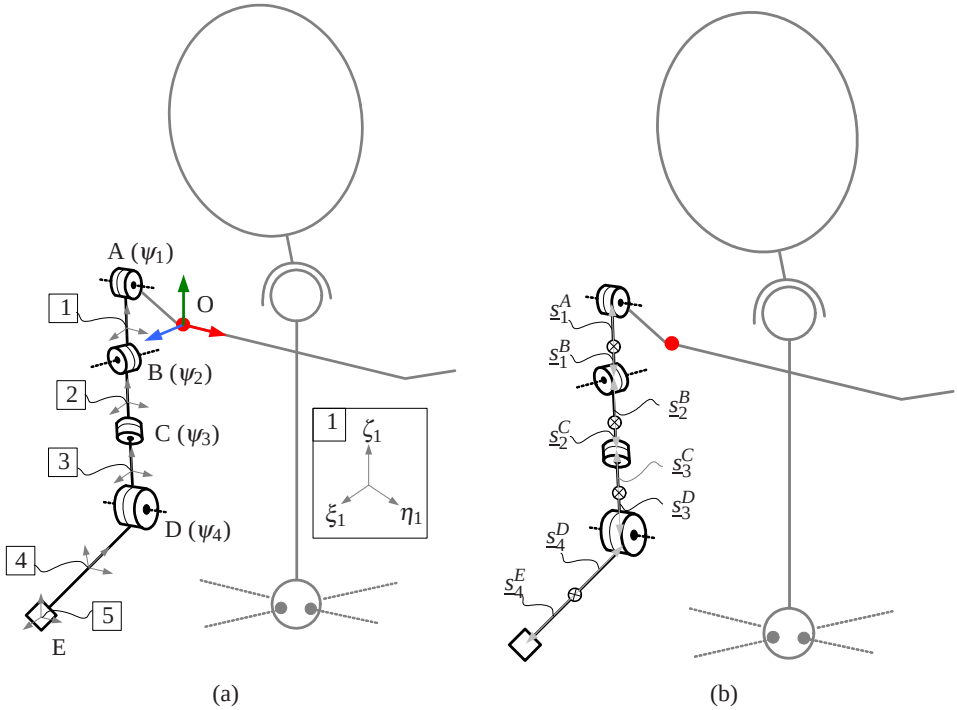

Figure 5.2: *Kinematic definitions for the ARA.*

The global coordinate system is placed at point ”O” and is defined in figure 5.2. The notation for the global coordinate system is (X, Y, Z) and the notation for local coordinate systems is (ξ_i, η_i, ζ_i), both coordinate system follow the right hand rule. Each body (ξ_i, η_i, ζ_i) axes are placed so they follow global (X, Y, Z) coordinate system for ARA initial position. It should also be noted that body 5 local coordinate system is placed at joint E and $\underline{s}_5^E$ is therefore zero. The four actuated joints are rotated with $\underline{\psi} = [\psi_1\ \psi_2\ \psi_3\ \psi_4]^T$

5.2.2 Kinematic Constraint

The kinematic joint define the constraint between two bodies e.g. between body 1 and 2 where the constraint reduces the number of DOF in the space for each body. The constraint equation can be written in the form of equation 5.1.

$$\underline{\Phi}(\underline{q}) = 0 \tag{5.1}$$

Where $\underline{q} = [\underline{q}_1^T\ \underline{q}_2^T \dots \underline{q}_n^T]^T$ is the coordinate vector. Where $\underline{q}_i = [\underline{r}_i^T\ \underline{\phi}_i^T]^T$. Here the vector is a combination of dependent and independent coordinates. For the ARA setup the independent coordinates are the actuated joints shown in figure 5.1(a). They are defined as $\underline{\psi} = [\psi_1\ \psi_2\ \psi_3\ \psi_4]^T$. $\underline{r}_i^T$ describes the position of the local coordinate system of body *i* according to the reference coordinate system. $\underline{\phi}_i^T$ describe the orientation of body *i* relative to the reference system.

The constraint equations between two bodies are represented in figure 5.3.

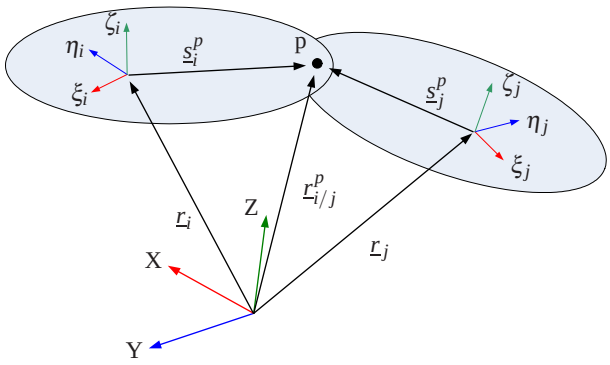

Figure 5.3: *Constraint definition between two bodies.*

The general constraint equations between the two bodies is formulated in equation 5.2. This equation does only restrict body location according to point p, this is the same as constraining the three translating motion. The constraint does not restrict any rotation around p.

$$\underline{\Phi}^3 = \underline{r}_i + \underline{\underline{A}}_i \underline{s}'^p_i - \underline{\underline{A}}_j \underline{s}'^p_j - \underline{r}_j = 0 \tag{5.2}$$

Φ^3 defines that the constraint equation restrict three DOF.

To restrict the rotation around p according to a revolute joint, two of the remaining three DOF have to be removed. The standard formulation to constrain one rotating DOF can be written as

$$\Phi^1 = \underline{u}_i^T \underline{u}_j = (\underline{\underline{A}}_i \underline{u}'_i)^T (\underline{\underline{A}}_j \underline{u}'_j) = 0 \tag{5.3}$$

This restraint states that two unit vectors represented in each of the two connected bodies local coordinate system at all time must remain orthogonal.

In equation 5.3 5.2, $\underline{\underline{A}}$ is the transformation matrix that either give the relation between body i and global coordinate system. In equation form the relation of global $\underline{s}_i$ and local $\underline{s}'_i$ is given by

$$\underline{s}_i^p = \underline{\underline{A}}_i \underline{s}'^p_i \tag{5.4}$$

The inverse version of equation 5.4 is

$$\underline{s}'^p_i = \underline{\underline{A}}_i^{-1} \underline{s}_i^p = \underline{\underline{A}}_i^T \underline{s}_i^p \tag{5.5}$$

This are used in the cases where the local information of and component are in interest.

Orientation

The transformation matrix for the ARA is formulated by means of Bryant angles. For Bryant angles the complete rotation of a body is defined by rotating each axis in the following order (x, η'', ζ'), see figure 5.4.

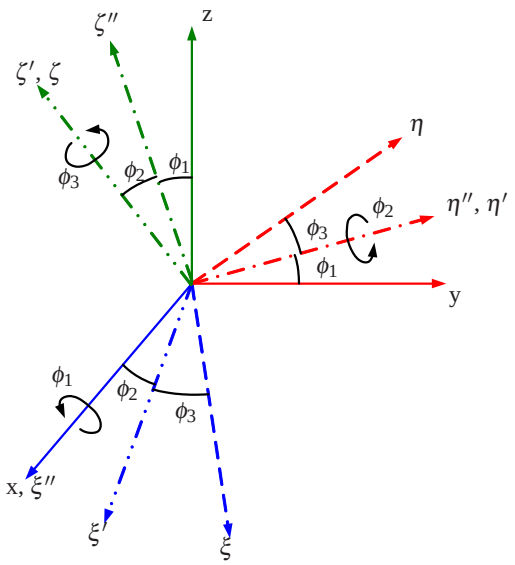

Figure 5.4: *Bryant angles.*

The initial xyz coordinate system of figure 5.4 have been rotated to a $\xi\eta\zeta$ coordinate system. This rotation can be represented by three single rotations. Each of the three rotations corresponds to a transformation matrix i.

$$\underline{\underline{D}} = \begin{bmatrix} 1 & 0 & 0 \\ 0 & c\phi_1 & -s\phi_1 \\ 0 & s\phi_1 & c\phi_1 \end{bmatrix} \qquad \underline{\underline{C}} = \begin{bmatrix} c\phi_2 & 0 & s\phi_2 \\ 0 & 1 & 0 \\ -s\phi_2 & 0 & c\phi_2 \end{bmatrix} \qquad \underline{\underline{B}} = \begin{bmatrix} c\phi_3 & -s\phi_3 & 0 \\ s\phi_3 & c\phi_3 & 0 \\ 0 & 0 & 1 \end{bmatrix}$$

With the combination of the three transformation matrices the complete transformation matrix for one body can be established, $\underline{\underline{A}} = \underline{\underline{DCB}}$.

$$\underline{\underline{A}} = \begin{bmatrix} c\phi_2 c\phi_3 & -c\phi_2 s\phi_3 & s\phi_2 \\ c\phi_1 s\phi_3 + s\phi_1 s\phi_2 c\phi_3 & c\phi_1 c\phi_3 - s\phi_1 s\phi_2 s\phi_3 & -s\phi_1 c\phi_2 \\ s\phi_1 s\phi_3 - c\phi_1 s\phi_2 c\phi_3 & s\phi_1 c\phi_3 + c\phi_1 s\phi_2 s\phi_3 & c\phi_1 c\phi_2 \end{bmatrix}$$

For bodies in series the transformation matrix can be expanded to describe the rotation of the next body in the series. This can be done with $D_i C_i B_i D_j$. This means the j^{th} body have been rotated the same as the i^{th} but is also rotated about the ξ of body i. The transformation matrix is an orthogonal matrix [23] and therefore $A^{-1} = A^T$. It the transformation matrix is represented between global coordinate system and local coordinate system i it is donated $\underline{\underline{A}}_i$. If the transformation is of body j with respect to body i the transformation matrix is donated $\underline{\underline{A}}_{j/i}$.

ARA Constraint Equations

The constraint equations derived from figure 5.2. The constraints for body 1 as an example are represented below. A detailed description of body 1 constraint equation are found in appendix A.

$$\begin{aligned} \underline{\Phi}_{1-3} &= \underline{r}_1 + \underline{\underline{A}}_1 \underline{s}_1'^A - \underline{s}_0^A = \underline{0} \\ \Phi_4 &= \phi_{11} = 0 \\ \Phi_5 &= \phi_{12} - \psi_1 = 0 \\ \Phi_6 &= \phi_{13} = 0 \end{aligned}$$

The time dependent driving constraint for the first body is ψ_1. The transformation matrix for body 1 is represented below.

$$\underline{\underline{A}}_1 = \begin{bmatrix} c\phi_{12}c\phi_{13} & -c\phi_{12}s\phi_{13} & s\phi_{12} \\ c\phi_{11}s\phi_{13} + s\phi_{11}s\phi_{12}c\phi_{13} & c\phi_{11}c\phi_{13} - s\phi_{11}s\phi_{12}s\phi_{13} & -s\phi_{11}c\phi_{12} \\ s\phi_{11}s\phi_{13} - c\phi_{11}s\phi_{12}c\phi_{13} & s\phi_{11}c\phi_{13} + c\phi_{11}s\phi_{12}s\phi_{13} & c\phi_{11}c\phi_{12} \end{bmatrix}$$

The complete 27 constraint equations as well the four transformation matrixes are placed in appendix A.

5.2.3 Solving Unknown Driving Constraints

As the time dependent driving constraints are unknown the PIJ (Pseudo Inverse Jacobian) method is applied to solve them. With this method the unknown driving constraint can be solved directly for each time step with relation to wrist joint velocity. The time derivative of equation 5.1 yields:

$$\underline{\underline{\Phi}}_q \dot{\underline{q}} = \underline{0} \tag{5.6}$$

$\underline{\underline{\Phi}}_q$ is the Jacobian matrix that is the partial derivative of the constraint equation with respect to $\underline{q}$, see equation 5.7.

$$\underline{\underline{\Phi}}_q = \frac{\partial \underline{\Phi}}{\partial \underline{q}} \tag{5.7}$$

Introducing the independent variables from the driving constraint, that refer to the revolute joints, and is donated with $\underline{\psi} = [\psi_1\ \psi_2\ \psi_3\ \psi_4]^T$ we get:

$$\underline{\underline{\Phi}}_q \dot{\underline{q}} + \underline{\underline{\Phi}}_\psi \dot{\underline{\psi}} = \underline{0} \tag{5.8}$$

If the equation is rewritten the dependent velocity vector can be expressed as a function of independent vector, see equation 5.9.

$$\dot{\underline{q}} = -\underline{\underline{\Phi}}_q^{-1} \underline{\underline{\Phi}}_\psi = \underline{\underline{\Phi}}_{q\psi} \dot{\underline{\psi}} \tag{5.9}$$

The last three entries in $\dot{\underline{q}}$ are the wrist velocity, i.e. we get:

$$\dot{\underline{r}}_5 = \underline{\underline{\Phi}}_{r_5\psi} \dot{\underline{\psi}} \tag{5.10}$$

Here $\underline{\underline{\Phi}}_{r_5\psi}$ is the last three rows of $\underline{\underline{\Phi}}_{q\psi}$ because $\dot{\underline{r}}_5$ is the last three rows of $\dot{\underline{q}}$.

$\underline{\underline{\Phi}}_{r_5\psi}$ is not a square matrix, hence, it cannot be inverted directly to yield a set of joint velocities $\underline{\dot{\psi}}$. Therefore a weighed PIJ method [20] combined with a damped PIJ [12] method is introduced. The weighed-damped PIJ is derived based on an optimisation problem that try to minimise.

$$||\underline{\underline{\Phi}}_{r_5\psi}\underline{\dot{\psi}} - \underline{\dot{r}}_5||^2 + \rho||\underline{w}\underline{\dot{\psi}}||^2 \tag{5.11}$$

The equation can be derived that give an that direct optimum solution for the driving constraints, and is written in the form of equation 5.12.

$$\underline{\underline{\Phi}}_{\psi r_5} = \underline{\underline{\Phi}}_{r_5\psi}^{-1} = \underline{\underline{w}}^{-1}\underline{\underline{\Phi}}_{r_5\psi}^T(\underline{\underline{\Phi}}_{r_5\psi}\underline{\underline{w}}^{-1}\underline{\underline{\Phi}}_{r_5\psi}^T + \rho^2\underline{\underline{I}})^{-1} \tag{5.12}$$

Here $\underline{\underline{w}}$ is the weighing matrix that only has digonal positive values relating to each driving constraint. Therefore a [4x4] matrix. ρ is a damping factor.

$$\underline{\underline{w}} = \begin{bmatrix} w_1 & 0 & 0 & 0 \\ 0 & w_2 & 0 & 0 \\ 0 & 0 & w_3 & 0 \\ 0 & 0 & 0 & w_4 \end{bmatrix}$$

ρ^2 is a damping factor and $\underline{\underline{I}}$ is a identity matrix and $\underline{\underline{w}}$ is the weighing matrix. The weighing matrix is associated to each of the driving joints. In DyP the default values for the weighing matrix is set to 1. The values of the weighing matrix are always set to positive. The weighing matrix will be used along with an overall optimisation procedure, this is described in 5.4.

The damped part of the equation 5.12 can minimise the velocity for each driving joints but at the same time enlarge the error from $\underline{\dot{r}}_5 - \underline{\underline{\Phi}}\underline{\dot{\psi}}$. The damped part has been introduced to ensure that large velocities near singular configurations are reduced. The damping factor is associated with the manipulability of the ARA that here is defined as equation 5.13

$$\varepsilon = \sqrt{det(\underline{\underline{\Phi}}_{\psi r_5}^T\underline{\underline{\Phi}}_{\psi r_5})} \tag{5.13}$$

The manipulability, ε, increases when ARA move close to singularities. The damping factor will be calculated according to equation 5.14 that is a rewritten equation based on [4].

$$\rho^2 = \begin{cases} \rho_0^2(1-\varepsilon_{max}/\varepsilon_i)^2 & ,\varepsilon_i \geq \varepsilon_{max} \\ 0 & ,0 \leq \varepsilon_i < \varepsilon_{max} \end{cases} \tag{5.14}$$

Where ρ_0^2 is the chosen maximum damping factor that from the derivative of equation 5.12, it is in DyP set to 0.1 . ε_i is the singularity value in a given time step i. ε_{max} is maximum manipulability value allowed before velocity gets to large.

The unknown driving constraint can then from above derived equation be written as:

$$\underline{\dot{\psi}} = \underline{\underline{\Phi}}_{\psi r_5}\underline{\dot{r}}_5 \tag{5.15}$$

Here $\underline{\underline{\Phi}}_{\psi r_5}$ is shown as equation 5.12.

Equation 5.15 is used to determine each driving constraint velocity that give prescribed wrist point velocity found in chapter 4.

5.2.4 ARA Motion

This section describes how the complete set of $\underline{q}$ vector is determined.

Position Analysis

As $\underline{q}$ depends on the driving constraints the positions can be computed by solving the standard constraint equation, $\Phi(q) = 0$. For each time step where the unknown driving constraints have been determined the velocities are multiplied with a small time step. This yields new values for the driving constraints and the constraint equation will no longer be valid. To solve the unknown position values of $\underline{q}$ the constraint equation are solved with a Newton-Raphson iteration for each new time step. The idea of the method is illustrated by figure 5.5.

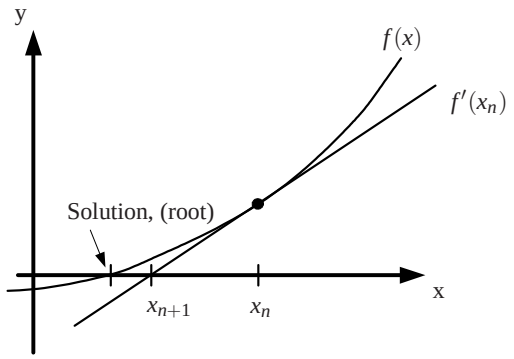

Figure 5.5: *Newton-Raphson method used to solve the constraint equation for each new time step.*

The tangent line of $f(x)$ with $x = x_n$ crosses at the x axis at x_{n+1}. This value is then used for the next step of the iteration until convergence is reached. The Newton-Raphson iteration can in general form be represented with equation 5.16.

$$x_{n+1} = x_n - \frac{f(x_n)}{f'(x_n)} \tag{5.16}$$

The iteration process can be stopped after a given number of steps or a given tolerance is fulfilled. The Newton-Raphson method is relatively easy and efficient to implement but can have some downsides, e.g. if $f(x)$ has several solutions and it is not sure that the same solution is found every time. Another problem can be if $f(x)$ is not strictly increasing or decreasing a local minimum could be found and $f(x) \neq 0$.

With the recalculated values of $\underline{q}$, that solve equation 5.2, the next time step is investigated. This means that the Jacobian are recalculated, new values of known wrist velocity are loaded and the driving constraint velocities are determined and again end op with the position analysis described in this section.

The constraint equations could have been determined analytically for the ARA setup that does require less calculation time than a numerical method. But the use of the Newton-Raphson method is chosen to ensure flexibility of the program, if there are applied any change to the ARA setup or an expansion of DyP.

Velocity/acceleration Analysis

Velocity and acceleration analysis are carried out using numerical differentiation.

$$\underline{\dot{q}} = \frac{\Delta \underline{q}}{\Delta t} \tag{5.17}$$

$$\underline{\ddot{q}} = \frac{\Delta \underline{\dot{q}}}{\Delta t} \tag{5.18}$$

The equations give the average velocity and acceleration between point ”n-1” and ”n” based on a given time step, Δt.

5.2.5 Discussion

The PIJ technique is a very powerful and fast method to solve redundant systems, but even if it is a fast technique it has some limitation.

One problem with the method is that if wrist point is moved towards positions that are outside the possible working space the Jacobian matrix go towards singularity and the PIJ will give large velocities and even for very small time steps the ARA will ”jump” around in its possible working space. For these singularity positions the second part of equation 5.11 are becoming secondary and the PIJ will find a solution that solves the fist part of this equation. An example can be viewed for the walking motion, see figure 4.1. Here if the ARA is placed straight down, the manipulability of the arm is limited compared to a position where XYZ motion can be performed in any direction. This can also be represented with the equation 5.13. The manipulability of ARA for the walking motion with initial position straight down along torso and a slight bend to elbow gives the curves illustrated in figure 5.6(a)

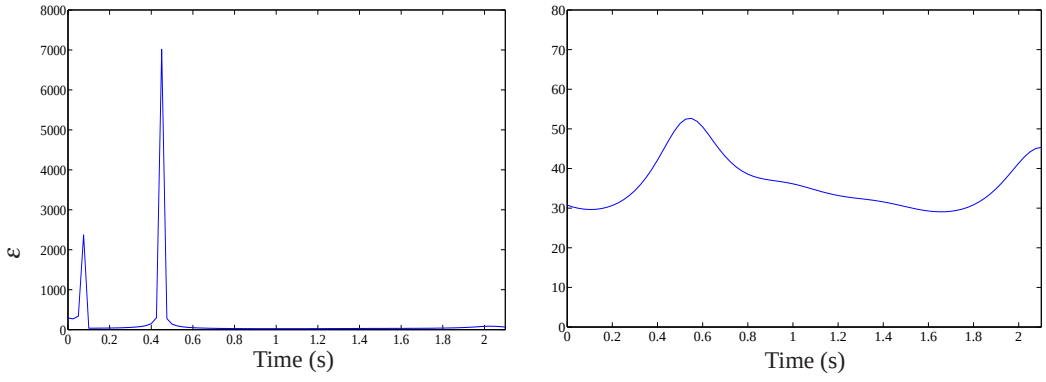

Figure 5.6: *Indication of ARA manipulability for the walking motion, low values equal high manipulability. (a) With the ARA start position straight down along torso. (b) With the ARA elbow slightly bend.*

It is seen the first time period of the walking movement gives high values of manipulability of the ARA. If the ARA are readjusted so the elbow is slight bended, like the arm of the test person, it can be shown that the singularities are avoided, figure 5.6(b).

5.3 Inverse Dynamic Analysis

The inverse dynamic analysis (IDA) is performed to determine the forces and moments based on calculated motion. IDA is placed inside the kinematic loop and therefore the forces and moments are determined for each time step. At the same time results from the kinematic and IDA analysis are used in the overall optimisation routine. Which minimise the average power usage, see section 5.4. The forces and moments are used to select gear, motors and dimensioning the mechanical parts in ARA design. The basis of the IDA analysis is based on the ”equations of motion” (EoM), Newton’s second law of linear motion 5.19 and Euler’s equation of rotational motion 5.21. These two equations establish a relationship between the motion and the forces and moments. If the equations are solved for each time step the complete set of unknown forces and moments that refer to the motion can be determined. The EoM is solved in global coordinate system.

5.3.1 Equation of motion

The general form Newton’s equation state that the force is equal the mass times the acceleration of the mass centre. And are in the general form written as equation 5.19 where reference frame do not move.

$$\sum \underline{F_i} = m_i \underline{\ddot{r}_i} \tag{5.19}$$

Here $\underline{F_i} = [F_i^x \, F_i^y \, F_i^z]^T$ equals the sum of mass (m) multiplied with body CoG acceleration $\underline{\ddot{r}_i} = [\ddot{r}_i^x \, \ddot{r}_i^y \, \ddot{r}_i^z]^T$. To simplify the equations the gravity parts of the equation have been separated from the normal equation 5.19 and can be written as.

$$\sum F_i = m\underline{\ddot{r}_i} + m_i \underline{g} \tag{5.20}$$

Where $\underline{g}$ is the gravity vector that define the direction of gravity according to used global coordinate system, in the coordinate system used for the ARA $\underline{g} = [0\,0\,-9.82]^T$. For simplicity $m_i\underline{g} = \underline{w_i}$

The rotational part of EoM also called Euler equation defines the momentum $M_i = [M_i^x \, M_i^y \, M_i^z]^T$ CoG. This way both the linear and gravity parts of the equation are removed and can be written in the form

$$\sum \underline{M_i} = \underline{\underline{J_i}}\,\underline{\dot{\omega}_i} + \underline{\underline{\tilde{\omega}_i}}\,\underline{\underline{J_i}}\,\underline{\omega_i} \tag{5.21}$$

$\underline{\underline{J}}$ represent the global inertia tensor that is associated with the rotational motion. $\underline{\omega_i} = [\omega_i^x \, \omega_i^y \, \omega_i^z]^T$ is the angular velocity and $\underline{\underline{\tilde{\omega}}}$ is the skew matrix of the angular velocity. Right side of equation 5.21 represent the rate of change of the angular momentum that is the same as right side of equation 5.19, the second part of equation 5.21 represent the moments because of centrifugal forces.

The angular velocity $\underline{\omega}$ is the velocity rotation around each of the original coordinate axes and is different than the time derivative of the Bryant angles, ϕ_i. When using the Bryant angles the relationship can be determined as equation 5.22, [23].

$$\underline{\omega}_i' = \begin{bmatrix} \omega_{i\xi} \\ \omega_{i\eta} \\ \omega_{i\zeta} \end{bmatrix} = \begin{bmatrix} c\phi_{i2}c\phi_{i3} & s\phi_{i3} & 0 \\ -c\phi_{i2}s\phi_{i3} & c\phi_{i3} & 0 \\ s\phi_{i2} & 0 & 1 \end{bmatrix} \begin{bmatrix} \dot{\phi}_{i1} \\ \dot{\phi}_{i2} \\ \dot{\phi}_{i3} \end{bmatrix} \tag{5.22}$$

As $\underline{\omega}'$ is the angular velocity around the $i'th$ local coordinate system measured in the local coordinate system.

The skew matrix is a method to e.g. take the cross products between two vectors and is defined for an arbitrary [3x1] as:

$$\underline{a} = \begin{bmatrix} a_x \\ a_y \\ a_z \end{bmatrix} \Rightarrow \underline{\tilde{a}} = \begin{bmatrix} 0 & -a_z & a_y \\ a_z & 0 & -a_x \\ -a_y & a_x & 0 \end{bmatrix} \tag{5.23}$$

Inertia tensor $\underline{\underline{J}}_i$ is associated to the angular motion as m_i is associated to the linear motion. The inertia tensor for a fixed axis coordinate system is defined as the volume integral for a given body as:

$$\underline{\underline{J}}' = -\int_v \underline{\tilde{s}}'\underline{\tilde{s}}' dm \Rightarrow \underline{\underline{J}}' = \begin{bmatrix} j_{\xi\xi} & j_{\xi\eta} & j_{\xi\zeta} \\ j_{\eta\xi} & j_{\eta\eta} & j_{\eta\zeta} \\ j_{\zeta\xi} & j_{\zeta\eta} & j_{\zeta\zeta} \end{bmatrix} \tag{5.24}$$

Where each input j_{ii} are the moments of inertia. The relation between inertia tensor that is based on fixed coordinate axis and global coordinate tensor $\underline{\underline{J}}$ are shown by [23] and is written as:

$$\underline{\underline{J}}_i = \underline{\underline{A}}_i \underline{\underline{J}}_i' \underline{\underline{A}}_i^T \tag{5.25}$$

5.3.2 Equations of motion - ARA

The complete set EoM for the ARA is represented with figure 5.7. EoM for the first body is represented with equations 5.27.

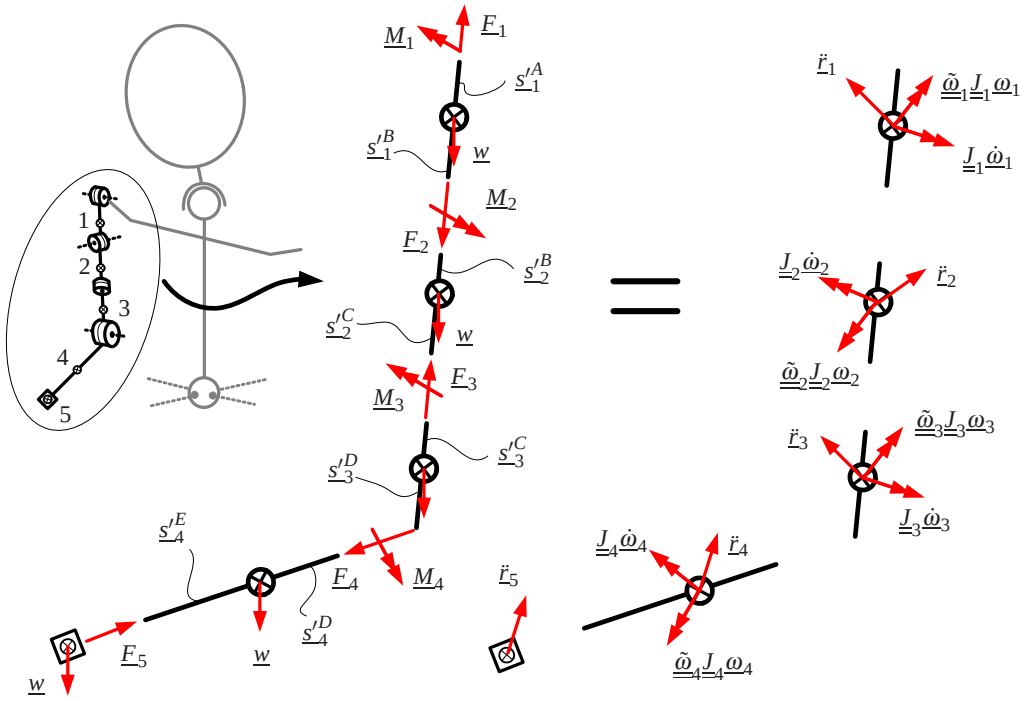

Figure 5.7: *Complete set of equations of motion for ARA.*

The FBD and KD are shown in figure 5.7. In equation form the EoM for body 1 (shoulder mount) is written as.

$$\sum \underline{F} \quad \Rightarrow \quad \underline{F}_1 - \underline{w}_1 - \underline{F}_2 = m_1 \ddot{\underline{r}}_1 \tag{5.26}$$

$$\sum \underline{M}_{CoG} \quad \Rightarrow \quad \underline{s}'^A_1 \underline{F}_1 + \underline{M}_1 - \underline{s}'^B_1 \underline{F}_2 - \underline{M}_2 = \underline{\underline{J}}_1 \dot{\underline{\omega}}_1 + \tilde{\underline{\omega}}_1 \underline{\underline{J}}_1 \underline{\omega}_1 \tag{5.27}$$

The complete set of EoM are placed in appendix B.

The EoM can be solved analytically. For simplicity and flexibility it, have been chosen to solve the equation with a Newton-Raphson routine, which is described in section 5.2.4. To solve the equations the EoM has been rewritten to.

$$\sum \underline{F}_i - m_i \ddot{\underline{r}}_i - \underline{w}_i = \underline{0} \tag{5.28}$$

$$\sum \underline{M}_i - \underline{\underline{J}}_i \dot{\underline{\omega}}_i - \tilde{\underline{\omega}}_i \underline{\underline{J}}_i \underline{\omega}_i = \underline{0} \tag{5.29}$$

The unknowns in the equation are $\underline{F}_i$ and $\underline{M}_i$ where i is the body index. The results are both represented in global forces $\underline{F}$,$\underline{M}$ and local forces $\underline{F}'$,$\underline{M}'$ depending on the use of data.

5.4 Optimisation Procedure

The overall optimisation routine is wrapped around the weighed-damped PIJ solution and try to tune the weighing matrix so that the driving constraints solution give minimum power usage with no AAU-Bot1 collision.

The optimisation procedure uses Complex method [25, 21]. The original Complex method try to find the maximum value of an objective function, but the used Complex method in the DyP try to find the minimum value of an objective function.

Besides the overall optimisation procedure an optimisation procedure is introduced to determine the initial start position of the ARA.

5.4.1 Complex

The complex optimisation routine is a non gradient based and works by the principle ”Survival of the fittest”. The Complex method tries to minimise a fitness function $f(\underline{x})$ $(\underline{x} \in \Re)$ that describes the fitness or quality of a design from explicit constraints

$$g_i < x_i < h_i \quad i = 1, 2, ..., n$$

and/or implicit constraints

$$g_j < f_j(x_j) < h_j \quad j = 1, 2, ..., m$$

The design is described by a set of design parameters $\underline{x} = [x_1\, x_2 \ldots x_n]$. The algorithm has a defined constant size population of n. It is recommended by [25] that the population size should be minimum the double amount as used design parameters. Design parameters can initially be chosen or generated randomly. Figure 5.8 represent a graphic interpretation of the Complex methods in a two-dimensional design space with a population size of n.

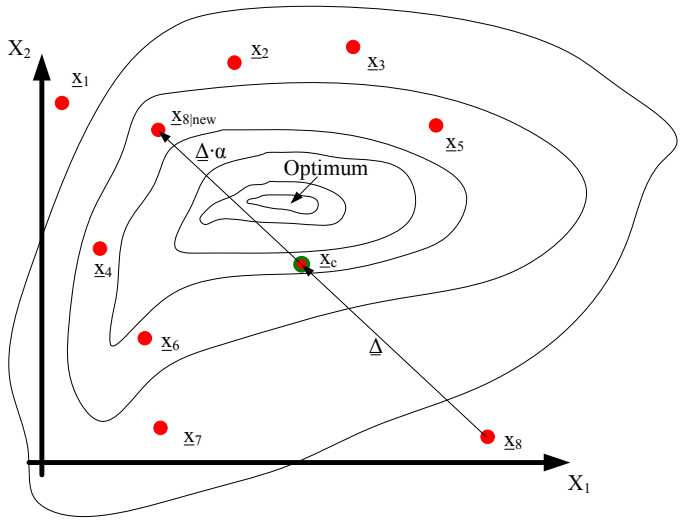

Figure 5.8: *A population size of 8 design parameters, Worst design is recalculated by mirroring around centroid.*

The worst set of design parameters ($\underline{x}_8$) are mirrored in the centroid ($\underline{x}_c$) of remaining design parameters and a new set of design parameters are created ($\underline{x}_{8|new}$). The centroid is calculated according to equation 5.30.

$$\underline{x}_c = \frac{1}{n-1}\left[\sum_{i\neq j}^{n} \underline{x}_i\right] \tag{5.30}$$

Here j represents the worst design and is not taken in to account when centroid is calculated. The new design parameter $\underline{x}_{j|new}$ is then calculated according to:

$$\underline{x}_{j|new} = \alpha(\underline{x}_c - \underline{x}_j) + \underline{x}_c \tag{5.31}$$

where α represent a value that define the length of the mirrored value, the value also indicates the search space of the mirrored design parameters. It is noted from [25] that the value should not be greater than 1.5, larger value would overshoot as it seeks global minimum. At the same time the value should not be too small, which would undershoot and possibly hit a local minimum. The value is set to 1.3 as recommended by [16].

Special Case 1: There can be a special case where the worst value keep being the worst value, if such a case is true the worst design is moved towards the best design and a random value is introduced. With this case the new set of design parameters are calculated according to equation 5.32. This equation will initially move the worst design half way towards the centroid value:

$$\underline{x}_{j|new} = 0.5(\underline{x}_j + \lambda\underline{x}_c + (1-\lambda)\underline{x}_k)) \tag{5.32}$$

where $\underline{x}_k$ is the best set of design parameters and λ is a tuning factor calculated as equation 5.33.

The tuning factor will change according to the number of times j have been the worst design. For continues worst design the tuning factor will force the worst design to go towards the best design.

$$\lambda = \frac{n_0}{n_0 + n_{rep} - 1}^{\frac{n_0+n_{rep}-1}{n_0}} \tag{5.33}$$

here n_0 is a tuning parameters that is set to 4 and n_{rep} is the number of iterations the set of design parameters have been the worst.

Fitness Value

The algorithm above is used to determine new set of design parameters where each population has been rated or punished with a fitness value(K) that is calculated according to a user defined fitness functions (f). If the optimisation problem has multiple objectives, the global fitness function is the sum of all fitness functions.

$$K = \sum f_i(\underline{x}) \quad , i = 1...n$$

n is the number of fitness functions. The optimisation procedure will then recalculate new set of design parameters from fitness values and keep doing that until a tolerance between best and worst fitness value (K) for each design of the population is reached or a given step number is reached. For the optimisation procedure the start design parameters are created based on random number that lay inside specified limits.

5.4.2 Overall Optimisation

The overall optimisation routine are divided in to two files, first the ”Complex” algorithm ”complex.m” and calculation of fitness values placed in ”Opti_factor.m”. The optimisation routine is performed over a complete working cycle from a load case and results from the cycle is used to calculate fitness values for each design of the population. Initial the design parameters are generated randomly with a value between 2 and 40.

Design parameters are the four values in the weighing matrix from equation 5.12. This means that a set of design parameters for each population are:

$$\underline{x}_n = [x_1\, x_2\, x_3\, x_4]^T$$

For each population number the weighing matrix is calculated as:

$$\underline{\underline{W}}_n = \begin{bmatrix} w_1 + x_1 & 0 & 0 & 0 \\ 0 & w_2 + x_2 & 0 & 0 \\ 0 & 0 & w_3 + x_3 & 0 \\ 0 & 0 & 0 & w_4 + x_4 \end{bmatrix}$$

Here w_i are set to 1.

Design Space

To limit the design parameters a fitness function has applied according to equation 5.34. Lower limit has been introduced because the weighing matrix is not allowed to take negative values. The higher value is introduced to shorten the optimisation calculation time and on the observation that larger values will not drastically minimise power usage. At the same time large values will give errors for the PIJ solution and ARA motion will not longer be smooth.

$$f_1 = \begin{cases} \exp\left(\frac{w_i}{w_{min}}\right)^{\beta} & , any\, w_{1,2,3,4} < w_{min} \\ \exp\left(\frac{w_i}{w_{max}}\right)^{\beta} & , any\, w_{1,2,3,4} > w_{max} \\ 0 & , otherwise \end{cases} \tag{5.34}$$

Here w_i is the index of the weighing matrix that has the lower and upper limits. w_{min} and w_{max} are the lower and upper limits respectively. The lower and upper limit is initially set to 2 and 40 respectively. β defines the influence of the fitness function.

Object function is to minimise the average power usage for the four driving constraints over a work cycle. The fitness function is defined as:

$$f_2 = \frac{P_{av}}{f_n} \tag{5.35}$$

where P_{av} is the root mean squared power usage for the four driving constraints over a work cycle. f_n is the normalising value that is set to the length of the upper arm. The square power usage for each driving constraint are determined according to equation 5.36.

$$P_{av} = \frac{1}{4}\sum_{i=1}^{4}\sqrt{\frac{1}{T}\int M'_i(t)^2 \dot{\psi}_i(t)^2 dt} \tag{5.36}$$

Here M_i' are the local moment around the rotational axis and $\dot{\psi}_i$ are the angular velocity of the i^{th} driving constraint

Constraint function is introduced to remove intrusion between ARA and AAU-Bot1 over a work cycle, where only the upper body (torso) from AAU-Bot1 is taken in to account. The fitness function is defined as equation 5.37, which is an indication of the maximum intrusion over the work cycle. To check the intrusion of any point of the ARA the upper and lower arms are divided in to small steps according to a given resolution.

$$f_{3|4} = \begin{cases} S^{\beta} & ,S > 1 \\ 0 & ,S < 1 \end{cases} \tag{5.37}$$

Here S defines a pseudo intrusion factor into an ellipsoid, that represent the AAU-Bot1 torso, β are the influence factor of the fitness function. S is represented by equation 5.38 and follow definitions represented by figure 5.9. This ellipsoid covers the outer dimension of the torso box on AAU-Bot1.

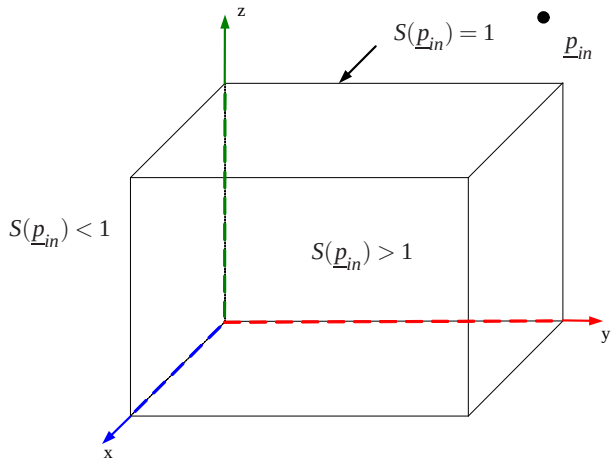

Figure 5.9: *Ellipsoid representing the torso of AAU-Bot1, the pseudo intrusion equation values follow the given limits represented in the figure.*

$$S = \left(\left(\frac{\underline{p}_{in}(x) - x}{a + \Delta a} \right)^{2\gamma} + \left(\frac{\underline{p}_{in}(y) - y}{b + \Delta b} \right)^{2\gamma} + \left(\frac{\underline{p}_{in}(z) - z}{c + \Delta c} \right)^{2\gamma} \right)^{-1} \tag{5.38}$$

Here $\underline{p}_{in}$ is the XYZ coordinates of a point of upper or lower arm that is checked for the intrusion with torso. x, y, z is the ellipsoid centre position in XYZ coordinates. a, b, c is the half width of the xyz direction of the ellipsoid. $\Delta a, \Delta b, \Delta c$ are a safety distance added on top of the ellipsoid. γ represents a parameter that tunes the shape of the ellipsoid.

The global fitness function is defined as.

$$K = f_1 + f_2 + f_3 + f_4 \tag{5.39}$$

5.4.3 Start Position

The start position routine is introduced because no exact data for initial position of arms is available for the different load cases, as well the singularity problems if the ARA is initially placed wrong, which has been shortly discussed in section 5.2.5. The start position routine is divided in to two aspects, first the MatLab file ”Start_pos.m” that is the ”complex” optimisation routine and second the file ”Dexterity.m” that calculates the fitness value of each design of the population based on created fitness functions.

Design parameters for the start position guess is chosen to be a angle at shoulder and at elbow. It is assumed that only shoulder joint has a rotational offset for the pitch motion and elbow joint has rotational offset angle compared to initial ARA position. This is also the same as the ARA only can have rotational movement in the XZ plane see figure 5.10.

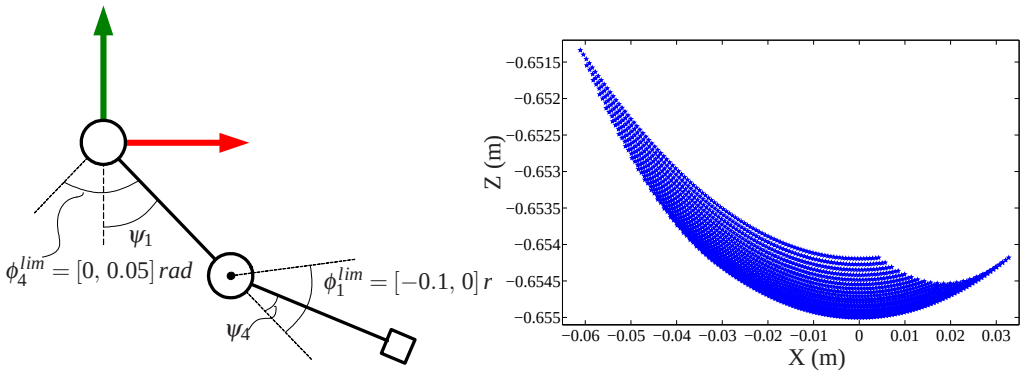

(a) (b)

Figure 5.10: *The two design parameters ψ_1, ψ_4. The design space in joint angles (a) and design space for wrist point (b). The design space value sign are according to right hand rule of reference coordinate system.*

The angles are directly associated with the first and fourth values in the driving constraint vector $\underline{\psi}$ and the design parameter is defined as:

$$\underline{x}_n = [x_1\, x_2]^T$$

where $x_1 = \psi_1$ and $x_2 = \psi_4$.

Design Space

For the start position it has been chosen to limit the design space, where shoulder joint is limited to $\underline{\phi}_1^{lim} = [0, 0.05] rad$ and the elbow to $\underline{\phi}_4^{lim} = [-0.1, 0] rad$ this can also be seen in figure 5.10. These limits have been chosen based on observation of the human arm hanging down along torso.

To limit the joint angles a fitness function for each design parameters is defined according to:

$$f_{1|2} = \begin{cases} \exp\left(\frac{||\phi_i||}{||\phi_i^{lim(1)}||}\right)^{\beta} & ,\phi_i < \phi_i^{lim(1)} \\ \exp\left(\frac{\phi_i}{\phi_i^{lim(2)}}\right)^{\beta} & ,\phi_i > \phi_i^{lim(2)} \\ 0 & ,otherwise \end{cases} \tag{5.40}$$

where β are a factor defining the influence of the fitness factor if joint limits are reached.

Object Function

The object is to minimise singularity at start position, more specific a fitness function that try to minimise the manipulability ε:

$$f_3 = \varepsilon \tag{5.41}$$

The manipulability is described in section 5.2.5.

The global fitness function is then defined as:

$$K = f_1 + f_2 + f_3 \tag{5.42}$$

5.5 Dynamic Program

Because the dynamic analysis of the ARA is a demanding and time consuming process a Matlab program is written to extract data like gear motion or force. The Matlab program structure does in general follow the same order as the described methods in previous sections. The dynamic program is for simplicity sake called DyP (Dynamic Program). The program is placed on "*CD-rom → dynamic_program → main.m*". DyP is only created to compute necessary information to design the ARA. A simple overview of DyP is illustrated in figure 5.11.

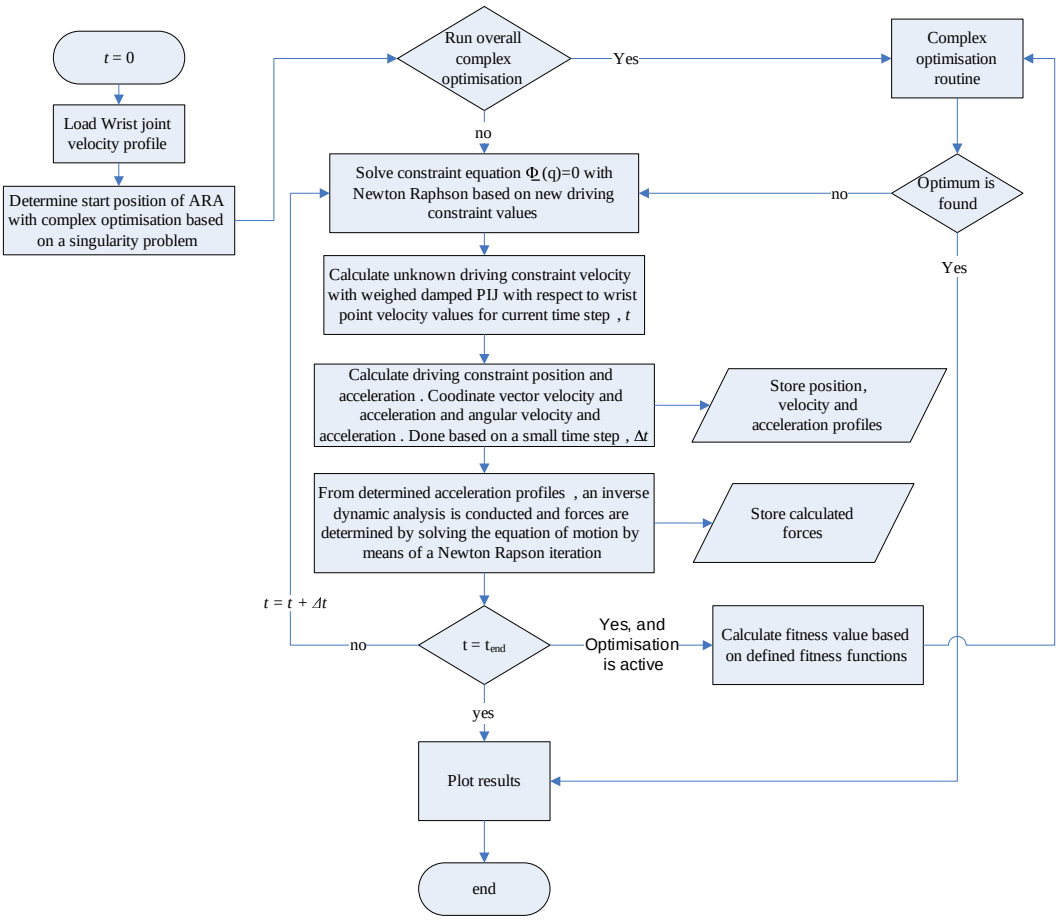

Figure 5.11: *Overall working principle of DyP.*

This do only give the general overview of the working principle program. Further details can be found in appendix C or on "*CD-rom → dynamic_program*".

5.6 Results

Results from the kinematic and IDA analysis will shortly be reviewed in this section. Results shown are with use of the overall optimisation procedure. The results shown have been limited to the handshake approach, the same data are available for the remaining load cases and can be reviewed with the DyP from ”*CD-rom → dynamic_program → main.m*” or from the result files placed on ”*CD-rom → dynamic_result*”.

5.6.1 Kinematic Results

ARA physical motion for handshake approach is illustrated in figure 5.12.

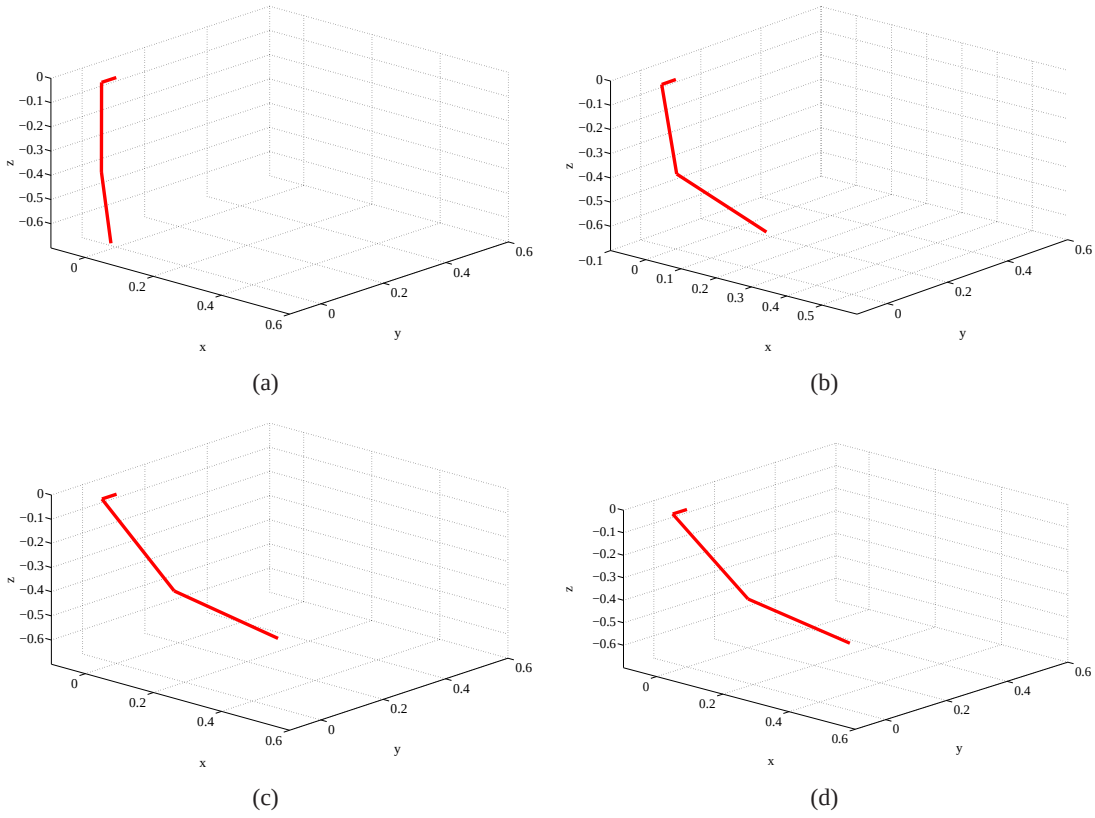

Figure 5.12: *Handshake approach illustrated with four time steps.*

A more detailed motion set for the driving constraints are illustrated in figure 5.13.

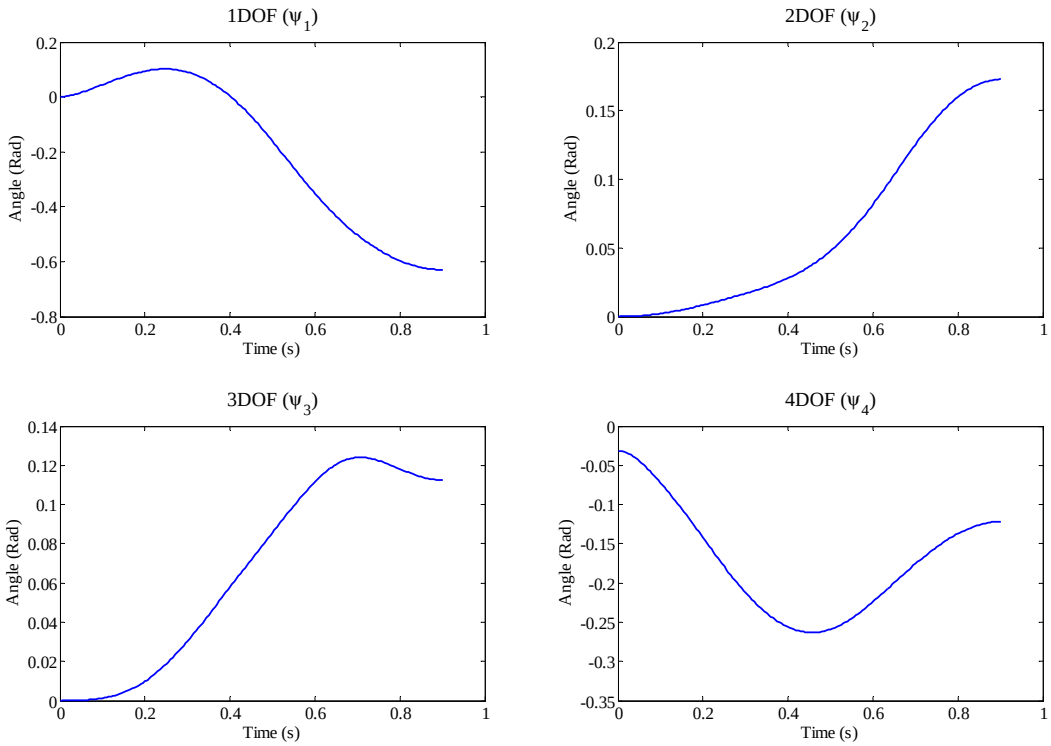

Figure 5.13: *Position over time curves for each of the four driving constraint for the handshake approach.*

The data shown above is only for the driving constraint but a complete set of motion data is available from DyP, both in global and local coordinates.

5.6.2 IDA Results

The results shown in this section are generated from the dynamic program.
The driving constraint torque is shown in figure 5.14. The force and moment data for remaining joints in either local or global reference can be reviewed by the DyP or the result files placed on *"CD-rom → dynamic_result"*.

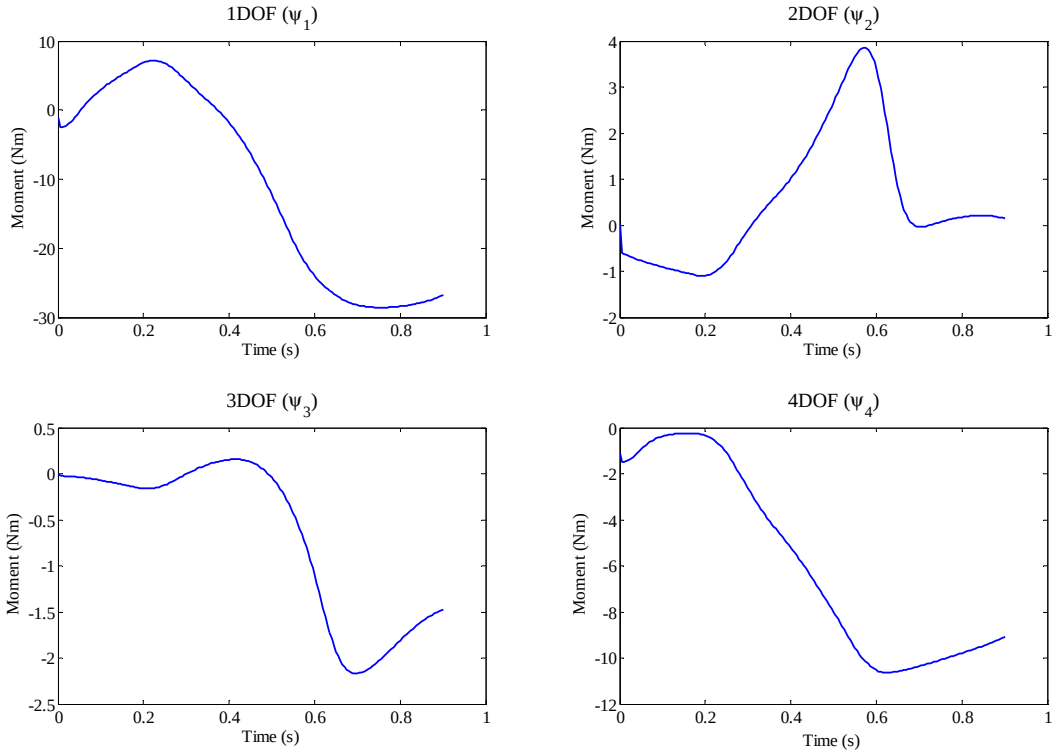

Figure 5.14: *Moment curve for the driving constraint around local axis for the handshake approach.*

The plot for the driving constraint moment can be used directly in the selection of gears and motors, for the mechanical design a complete set of force and moment vectors are needed for each body. These are available either from DyP or the result files.

Static Load

To ensure that the ARA is capable of placing the wrist point at any given point in space, positions where maximum static joint moment occurs are taken in to consideration. To take account of dynamic forces the static forces are multiplied with a safety factor. The moment for each joint can be divided in to an axial moment (A) and a tilting moment (T).

At the shoulder joint the local body pitch and roll moment is maximum when the ARA is placed in a horizontal position either pointing along the X-axis or the Y-axis. This is illustrated in figure 5.15. For this position the elbow joint do as well have maximum moment.

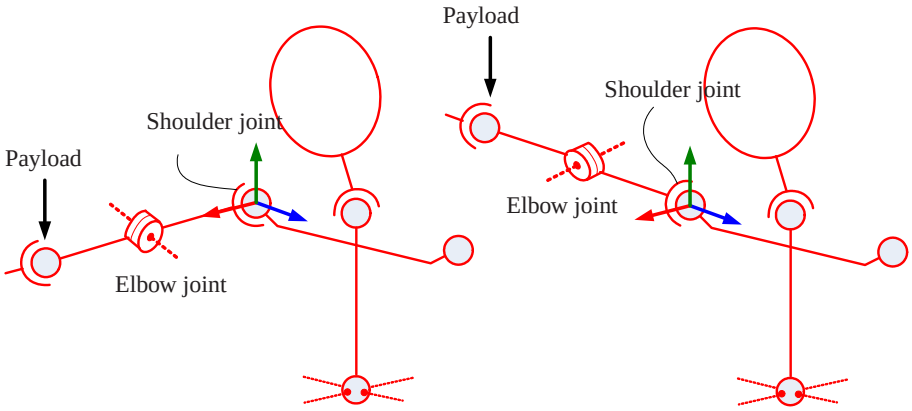

Figure 5.15: *Position of ARA for maximum static load at 1, 2 and 4th DOF.*

The maximum yaw is when the ARA upper arm is placed horizontal along either X-axis or Y-axis and the lower arm is placed along Y-axis or X-axis respectively. Figure 5.16 illustrates the position of ARA for maximum yaw moment of the 3 DOF.

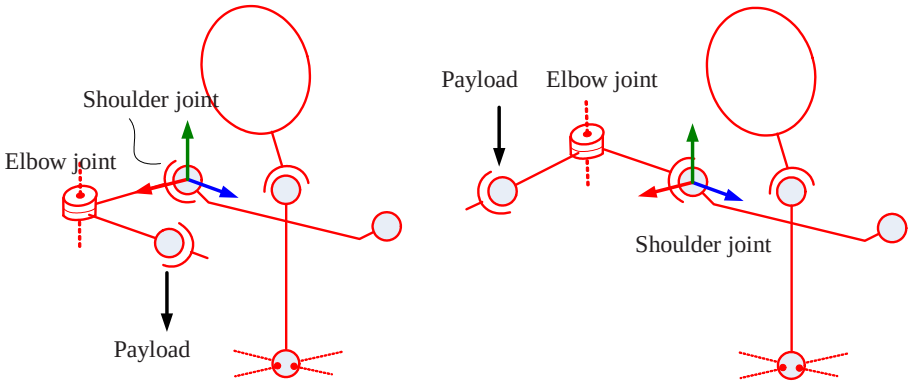

Figure 5.16: *Position of ARA for maximum static load at 3 DOF.*

The maximum moments for the shoulder joint in radial and axial moments are defined as:

$$M^{T}_{x|y} = (m_5 \cdot 0.655 + \sum(m_{1-4}) \cdot (0.655/2)) \cdot 9.82 \approx 44Nm$$

$$M^{A}_{x|y} = (m_5 \cdot 0.285 + m_4 \cdot (0.285/2)) \cdot 9.82 \approx 15Nm$$

The maximal moments at elbow joint are defined as:

$$M^T_{x|y} = (m_5 \cdot 0.285 + m_4 \cdot (0.285/2)) \cdot 9.82 \approx 15Nm$$

$$M^A_{x|y} = (m_5 \cdot 0.285 + m_4 \cdot (0.285/2)) \cdot 9.82 \approx 15Nm$$

The moments only represent a scalar value of the magnitude of the maximum moment.

5.6.3 Optimisation Results

As the kinematic and IDA results shown above is on the basis of the overall optimisation procedure it will in this section be shown the difference with use and without use of the optimisation procedure. The results shown are for the handshake approach and in overall power usage. First is without use of the overall optimisation procedure this means that the motion found is only based on direct method (PIJ) where the weighing matrix is set to an identity matrix. Second result is for the overall optimisation procedure where intrusion control (IC) is activated. Third is where the complete overall optimisation (CO) procedure is activated, here usage is to be minimised and intrusion removed. The values shown here is with a payload of 4 kg.

Direct PIJ solution
The results from the direct approach where $\underline{\dot{\psi}}^T \underline{I} \underline{\dot{\psi}}$ from equation 5.11 are minimised on the basis that the first part of the equation are fulfilled. From this approach the average absolute power usage for handshake approach is calculated as.

$$P_{PIJ} = \sqrt{\sum M'^2_i \dot{\psi}^2_i} \approx 13W \quad ,i = 1....n \tag{5.43}$$

where i is the timestep of a complete work cycle of n steps. If the motion trajectory for the arm is illustrated it can be seen that the arm will intersect with the box representing AAU-Bot1 upper body and therefore this motion will not be possible in real life motion.

Intrusion Control
The intrusion control is controlled by modifying the weighing matrix used in PIJ method. The optimisation procedure uses approximately 10 to 70 simulations to determine depending on the start guess values. When intrusion control is introduced the average power usage for the handshake approach will increase and is calculated to around $P_{IC} \approx 31W$.

Power minimisation and intrusion control
With use of the complete overall optimisation procedure where power is minimised and intrusion is removed, the weighing matrix values are determined after approximately 300 to 1000 simulations. The power usage from this simulation give an average of $P_{IC} \approx 28W$.

5.7 Summary

The dynamic analysis was performed both to determine unknown driving constraint motion and, furthermore, to determine the initial forces and moments acting on the ARA setup. From the initial assumption the motion and forces was determined using both PIJ methods along with

standard kinematic and inverse dynamic analysis. The method was wrapped inside an optimisation procedure that would determine the motion path for driving constraints that remove intrusion between ARA and AAU-Bot1 and minimise power consumption. It can be seen that the power usage improvement over a complete work cycle a relative small compared to the simulation steps used to determine an optimum motion path for the four driving constraints.

From the different load case results, selection of gear, motors can be done and the mechanical parts of the ARA can be designed. An overview of the magnitude of the maximum moments for each joint for the three load cases and static moments are listed in table 5.2.

Joint moment [Nm]	Walking	Handshake Approach	The shake	Static
Shoulder mount (A)				
Roll, ξ_1	4.5	4.5	7.5	44
Pitch, η_1	14	28	30	44
Yaw, ζ_1	0.5	3	4	15
Upper arm 1 (B)				
Roll, ξ_2	4.5	4	4.2	44
Pitch, η_2	14	28	30	44
Yaw, ζ_2	0.2	1	1.2	15
Upper arm 2 (C)				
Roll, ξ_3	4	3	2	44
Pitch, η_3	14	28	30	44
Yaw, ζ_3	0.7	0.9	0.3	15
Lower Arm (D)				
Roll, ξ_4	1.5	1.5	1.3	15
Pitch, η_4	8	11	14	15
Yaw, ζ_4	0	0	0	0

Table 5.2: *Collection of the magnitude of maximum moments for each of the three load cases and the static moments at each joint in respectively local coordinate system.*

Load shown in table above are listed in local coordinate system to respectively bodies. The grey marked areas are the driving constraint torque of the joint. It can be seen that for the three load cases the moments are generally smaller than the static loads. The only exception is the lower arm joint for the handshake that give 23.5 Nm compared to the static load that gives 15 Nm.

6

ARA Concept Design

6.1 Power Transmission
6.2 Mechanical Design
6.3 Summary

The ARA design shown in this chapter is the first conceptual design and is based on forces and moments determined in chapter 5. The motion and forces determined are based on different physical assumptions that do not comply with the concept design. When the concept design has been determined the physical properties from the design can be used to recalculate motion and forces. These can then again be used to redesign the first concept to a new and better. This iteration process would be efficient to put inside an optimisation procedure, where gear, actuators and mechanical design would be optimisation factors. This is not investigated as a part of this report. The concept design of the ARA is divided in to two steps. First the selection of gears and actuators and second step the ARA mechanical design.

The gear selection is based on the Harmonic Drive gears. The stock CPU type is used with AAU-Bot1 design and is as well selected for ARA design to keep design equivalent. Actuators are selected from the manufacture Maxon motors, the same as for AAU-Bot1. The same series as used in AAU-Bot1 will be used for ARA design.

The selections for gear and actuators are based on calculated motion and forces from DyP, here the driving constraint motion and forces. A short description of these results is presented in the end of chapter 5. The results are shown for the handshake approach. All load cases are considered in the selection of gear and actuators, but only maximum values for any given load case is used for the selection. The standard selection of gears and actuators are based on different procedures that will ensure high lifetime. As the ARA should only comply with the 1000 limit set for the AAU-Bot1, it can be necessary to modify the selection procedure to minimise gear and motor sizes and thereby keep the weight down.

6.1 Power Transmission

This section deals with the initial selection of power transmission, i.e. gears and actuators. The gears and actuators used for the AAU-Bot1 are Harmonic Drive and Maxon respectively. The gears used for the AAU-Bot1 are ”CPU” gear units. Actuators is of the type RE graphite brushes that are available in several sizes.

6.1.1 Harmonic Drive Gears

Harmonic Drive gears have been discussed in [17] but will shortly be introduced here to summarise the working principle of the gears and the overview of the ”CPU” series. This series is a unit gear that includes housing, bearings, input and output shaft and can be directly used without creating separate housing bearings etc. The gears can be acquired in different sizes. The gears used on the AAU-Bot1 are the type ”CPU-S” but the gear selection for ARA design will be considered for the complete ”CPU” series. The working principle of the Harmonic Drive gears is described base on information from [6].

As the CPU unit series is stock parts that use steel for all the parts in the gear, it is considered in the end of this chapter if the parts in the unit are to be replaced with in-house gear units created with Harmonic Drive gear component set where the housing etc. is created in aluminium. If such approach is taken, the designed gears have to be checked with extensive stress and strain analysis to ensure that the gear can work for the 1000 hours required for the ARA.

CPU series
CPU units have a high stiffness because of internal bearing support for the output shaft. The units support relative high axial and radial forces and at the same time relative large tilting moments, a summery of some of the properties of the units are shown in table 6.1, [7]. A cross section of the CPU unit M is shown in figure 6.1(a) and where figure 6.1(b) show the working principle of the units.

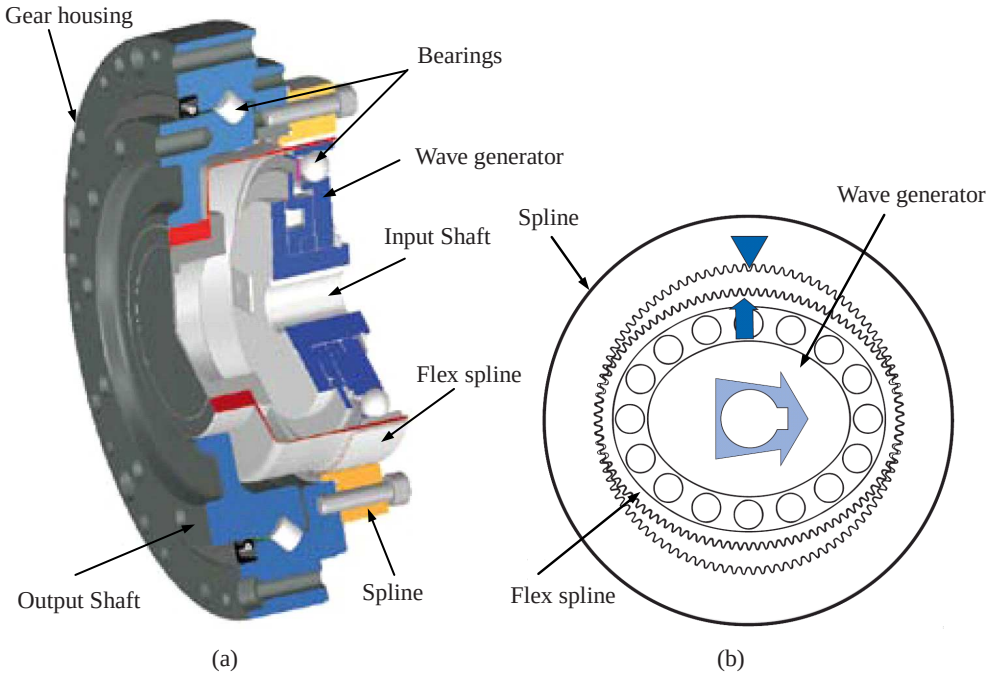

Figure 6.1: *(a) Cross section of the CPU-M unit gear, [6]. (b) Sketch of the Harmonic Drive working principle, sketch from [8].*

Here the Wave Generator is an assembly of a bearing and a steel disk which is called a Wave Generator plug. The outer surface of the Wave Generator plug is shaped as an ellipsoid. A special ball bearing is pressed around the plug forcing the bearing to take an elliptical shape. The

wave generator is general the input shaft. The flexspline is a thin wall steel cup with teeth on the outside surface near the opening of the spline. Wave generator is pressed inside the flexspline forcing the flexspline to take the form of and ellipsoid. This means that the outer surface of the flexspline is an elliptical shaped gear. The flexspline is in general the output shaft. The circular spline is a rigid steel ring with teeth placed on the inside diameter and is normally a fixed member either to a gear housing or other member. The circular spline is designed so the teeth of the flexpline fit inside the teeth of circular spline. This means that two regions of circular spline and flexspline are in contact, see figure 6.1(b).

The Harmonic Drive CPU series are available in three models, the ”CPU-H”, ”CPU-M” and ”CPU-S” see figure 6.2. The three models in the series have different designs for the input part but all follow the working principle described above.

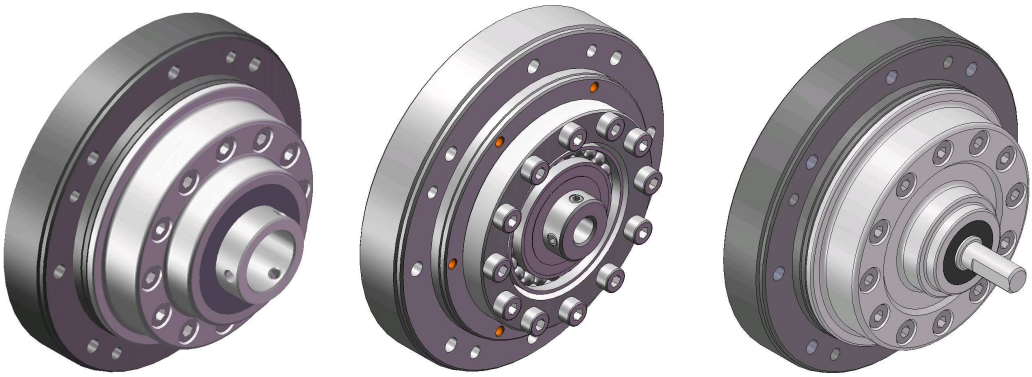

(a) (b) (c)

Figure 6.2: *The CPU series from Harmonic Drive. (a) CPU-H (b) CPU-M (c) CPU-S*

The CPU-H unit is different from the two remaining designs in the sense that the unit have a central hollow shaft. The hollow shaft can be used to pass cables, shafts, etc. through the centre of the gear. The unit would have advantages when considering cable distribution for the ARA.

The CPU-M unit can be used for direct mounting of any servo motor. To mount a servo motor on the gear, an adaptor part that connects motor and gear has to be designed.

The CPU-S unit is designed so it includes an input shaft that can be used with belt drives or simular. Here the input shaft is supported with bearings.

Table 6.1 show the important technical data that are common for the two smallest gears from CPU series.
The static tilting moment limit are based on a safety factor $f_s = 2$ that is recommended for vibrations/impact systems [7, p. 449]. Because the data are common for the CPU series it is not necessary at this point to decide model type. Only size of gear has to be selected, which is done in the next section.

Standard Gear Selection Procedure

The size selection of the CPU unit are based on calculation methods available from [9]. It is important that the sum of the gear weight is kept as low as possible so dynamic influence of the

CPU size	Mass [kg], -H, -M, -S	Ratio, R	Max dynamic/static tilting moment M_{TD}/M_{TS} [Nm]	Limit for avarage torque, T_A [Nm]	Limit for peak moment T_M [Nm]	Max input speed n_{max} [rpm]
14	0.67, 0.54, 0.64	50	73/122	6.9	35	8500
		80	73/122	11	47	
		100	73/122	11	54	
17	1, 0.79, 0.95	50	114/247	26	70	7300
		80	114/247	27	87	
		100	114/247	39	110	
		120	114/247	39	86	

Table 6.1: *Common data for the CPU unit series where static tilting moment are with a safety factor of $f_s = 2$. A complete set of data sheets for the three gears are placed in appendix D.*

gears are minimised. Besides, the stiffness of the gears should be relative high to ensure that tool-point do not vary compared to reference path described in chapter 4.

The gear selection procedure available from [9] states the selection of gears is divided in to criteria listed below.

1. Tilting moment $M_{g|T}$ <Limit for max tilting moment M_{TD}, M_{TS}
2. Avg. output torque, $T_{g|av}$ <Limit for avg. torque, T_A
3. Momentary repeated peak torque, $T_{g|R}$ <Limit for repeated peak torque, T_R
4. Momentary output torque, $T_{g|max}$ <Limit for momentary torque, T_M
5. Max input speed, $n_{g_{in}|max}$ <Limit for max input speed, n_{max}
6. Avg. input speed, $n_{g_{in}|av}$ <Limit for avg input speed, n_{av}

Table 5.2 gives a list of the moments at each joint where gears are to be used, where the values is given for local coordinate system of the respective body. The first selection criterion is based on the maximum tilting moment. It should be noted that the permissible tilting moments from table 6.1 are values when only bearings from the CPU units are used to carry the load. The gears for each of the joints are selected based on the static moments from table 5.2. This is done based on the fact they are larger than dynamic moments. The static moments are multiplied by a safety factor $f_s = 2$ from [7, p. 449]. The remaining criteria are compared with results from the load cases.

Shoulder Mount (A) gear selection

The selection of gear for this joint is based on the handshake because this gives the largest torques. But as the static moment is larger than dynamic loads, the first selection procedure is based on these values. The static tilting moment for joint A is shown in table 5.2 and states that the maximum inclusive safety factor is:

$$M_{g|T} = 88Nm \ < \ M_{TS} = 122Nm \tag{6.1}$$

The continuous load case criterions are easiest shown with a speed-torque plot. The handshake approach can be viewed in figure 6.3. For a torque-time plot see figure 5.14
It can be seen that the CPU unit of size 14 will fulfil the requirements. If the average torque from handshake approach and the handshake are calculated, it gives values larger then limitation for

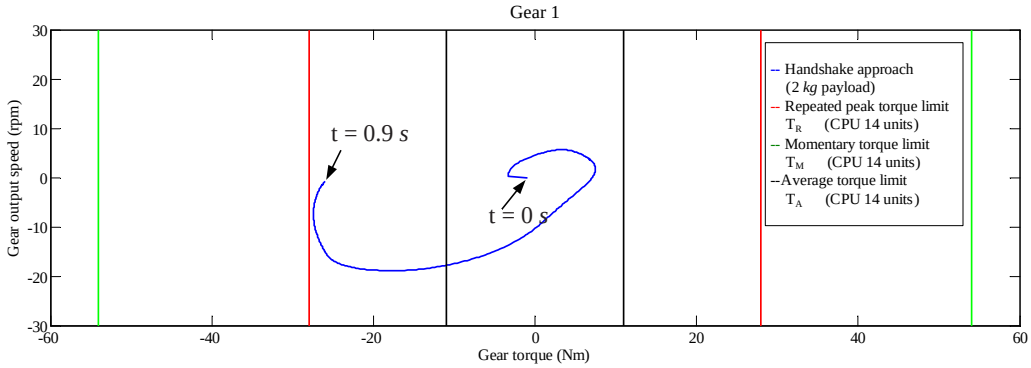

Figure 6.3: *Plot of gear work cycle in a speed-torque diagram. The velocity axis in the figure are for the output shaft, the input velocity are the output shaft velocity multiplied with the gear ratio. The limits for input velocity for the gears are shown in table 6.1.*

the average torque. This criterion is created to ensure a high working time. The rated working time for the CPU units are around 35000 hours and because the ARA have been set to work around 1000 hours this criterion are seen as a less critical limitation and are therefore not taken in to account.

Selected Gears

The selected gears for each joint are listed in table 6.2. The values in the table are a scalar size of the input velocity and the output torque.

Joint	Size	Mass	Gear ratio	Limit tilting moment M_{TS} [Nm]	Static tilting moment $M_{g\|T}$ [Nm]	$T_{g\|max}$ [Nm] / $n_{g_{in}\|max}$ [rpm]	T_M [Nm] / n_{av} [rpm]
Shoulder Mount (A)	14	≈ 0.6	100	122	88	30 / 2000	54 / 3500 (1100)$^{(1)}$
Upper Arm 1 (B)	14	≈ 0.6	100	122	88	4.2 / 700	54 / 3500 (1100)$^{(1)}$
Upper Arm 2 (C)	14	≈ 0.6	100	122	88	1 / 250	54 / 3500 (1100)$^{(1)}$
Lower Arm (D)	14	≈ 0.6	100	122	30	14 / 5000	54 / 3500 (1100)$^{(1)}$

Table 6.2: *List of selected CPU unit size for each revolute joint in the ARA design. Here the maximum torque and input speed from the load cases are shown along side the limits for the CPU units.* $^{(1)}$ *for CPU-H. A complete data list for the gears are found in appendix D.*

The gear selected for all joints are the smallest CPU unit available from stock program. The sum of the gear masses gives 2.4 *kg*, this is around 42 % of the allowed maximum ARA mass of 5.8 *kg*. This is at this point a relative large mass just for gear but these gears will at this point be selected for ARA design.

Gear Efficiency

The gear efficiency influences the motor selection and therefore has to be considered for the CPU series. The efficiency of the CPU units is depending on working temperature, input speed and output torque, unit size and gear ratio. Besides does the efficiency of the gears depends on the CPU type. For simplicity it is chosen to take the average efficiency from the three CPU types. This is of course conservative but will general ensure that the selected motors do work

with selected gears.

The total efficiency (η_L) of the gear can be calculated according to equation below. This is based on the CPU-H selection efficiency calculation.

$$\eta_L = K(\eta_R + \eta_e) \tag{6.2}$$

Here η_e is the efficiency value based on friction between input shaft sealing and input side, see figure 6.4(b). η_R is the efficient value based on input speed and working temperature, see figure 6.4(a).

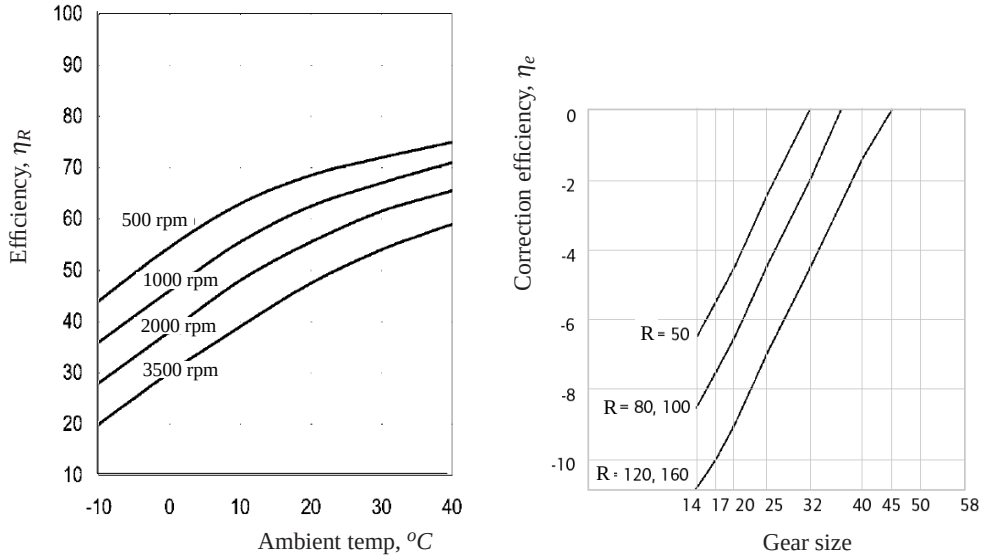

Figure 6.4: *(a) Efficient value based on working temperature and input speed for the CPU-H unit. (b) A correction of efficiency based on the friction from input sealing.*

Remaining efficiency data for the last two gear units can be reviewed in appendix D.

The last unknown in equation 6.2 is K that is a correction factor extracted from a plot that states the efficiency correction is based on input torque and rated torque. The efficiency correction η_e varies between 1 and 0.2 depending on V, which is calculated based on equation below.

$$V = \frac{T}{T_N} \quad 0.2 < V < 1 \tag{6.3}$$

T is the output torque for the gear at the current time step, T_N are the rated torque, see table 6.1. Generally the output torque calculated for each driving constraint will exceed T_N and therefore V would be larger then 1 and the correction factor K is therefore set to 1.

To calculate the total efficiency of the gear it is chosen that working temperature is set to 20^oC and the working input speed set to the 2000 rpm. This give an average efficiency factor $\eta_R =$ 64%. The average efficiency correction η_e is approximately -7.5. The correction factor K is set to 1. The calculated efficiency for the gears gives:

$$\eta_L = K(\eta_R + \eta_e) = 56.5\% \tag{6.4}$$

This is a low value compared to reachable and probably higher efficiency values if gear efficiency are calculated dynamic and based in correct selected gear. But as mentioned the calculated efficiency would secure that the selected motors (see next section) will be sufficient large to actuate the ARA.

6.1.2 Maxon Motors

Actuators used for the AAU-Bot1 is from the manufacture Maxon Motors [18], here DC motors of the series RE with graphite brushes. To keep the ARA design consistent with AAU-Bot1 these motors are used. The voltage used for AAU-Bot1 is the 48 voltage models. An illustration of the RE series is illustrated in figure 6.5.

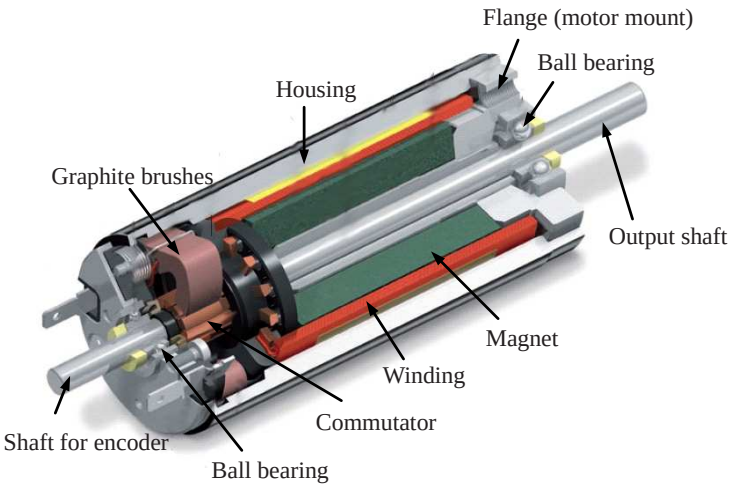

Figure 6.5: *The Maxon motors RE series. [18]*

Some of the advantage of these motors are according to [18].

- Excellent volume/performance ratio
- Highest efficiency
- Low inductance
- High acceleration thanks to a low mass inertia
- Linear characteristics
- High reliability
- Multiple combination possibilities with gears, feedback devices and control electronics

This type of motors have been used for space robots, aircraft seats, packaging systems, conveyors, chip mounting systems etc. [18]. At the same time motor documentation from Maxon are detailed that ease the selection procedure.

Motor	Mass [kg]	Stall torque, T_{st} [Nm]	Nominal torque, T_{nom} [Nm]	No load speed, n_0 [rpm]	Overload time [s]
RE-60	0.238	1.02	0.088	8490	16
RE-90	0.34	0.967	0.0965	7270	30
RE-150	0.48	2.5	0.184	7000	41

Table 6.3: *A short data list of two available RE motors from Maxon, [18]. The complete set of technical data for the motors can be found in appendix E.*

A short list of some of the Maxon DC RE series is shown in table 6.3.
The characteristics of the Maxon RE motors can be illustrated with a linear torque / speed relationship diagram, see figure 6.6 that is for the Maxon RE-60.

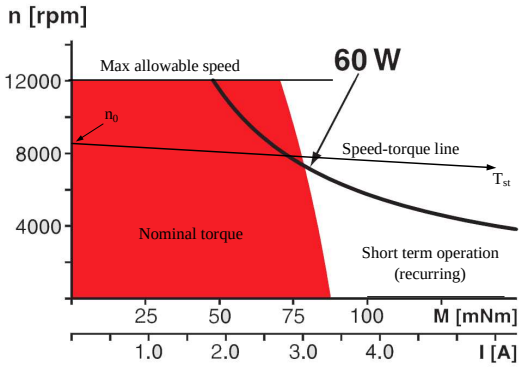

Figure 6.6: *A speed-torque diagram the RE-60 Maxon motor. [18]*

Here the no load speed n_0 and stall torque T_{st} is based on the nominal voltage. When the voltage is lowered the line is as well lowered parallel to the original line. If voltage is increased the line is moved higher. The motor operation area has to be below this line. At the same time, the motor working area should be within the nominal torque area (red) to ensure that the windings of the motor is not damage because of overheating.

Motor Selection Procedure

The selection of motors is heavy dependent on the gear ratio, but an idea to use direct drive with gears, the initial selection of motors will consider only motors sufficient large to actuate with direct drive. No additional gearing is introduced between motor and gear.

A motor selection procedure are available from Maxon Motors [19]. The selection procedure can be divided in to two steps, fist momentary peak load and second continuous load. The continuous load can be compared with motor characteristics, e.g. for RE-60 see figure 6.6.
The overall selection procedure is listed below.

1. Max torque, $T_{m|max}$ [Nm] <Stall torque, T_{st} [Nm]
2. Effective torque, $T_{m|RMS}$ [Nm] <Max nom torque, T_{nom} [Nm]
3. Motor speed n_m [rpm] <Speed-torque line, n [rpm]
4. Motor acceleration $\alpha_{m|max}$ [rad/s^2] <Max motor acceleration, α_{max} [rad/s^2]

Here the effective torque is defined as the root-mean-square (RMS) value of the working cycle, and can be calculated with equation 6.5, [19].

$$T_{m|RMS} = \sqrt{\frac{1}{T}\int T_m(t)^2 dt} \tag{6.5}$$

Here $T_m(t)$ is the required motor torque at the given time step and is calculated as equation 6.6. The motor torque is based on gear ratio, gear rotating parts' moments of inertia and motor rotating parts' moments of inertia.

$$T_m = \frac{T}{R\eta_L} + J_m\ddot{\psi}R + J_g\ddot{\psi}R \tag{6.6}$$

T is the calculated torque from DyP. R the gear ratio and η_L the gear efficiency calculated under gear selection. The moments of inertia for motor (J_m) shaft and gear (J_g) input shaft are available from Appendix D and E, the gear output shaft are not included in the calculation. The maximum motor torque $T_{m|max}$ are generally the static moment from table 5.2 and for that case the moments will be used along with the safety factor $f_s = 2$ from gear selection. If dynamic moments are larger than static they are used for maximum peak moment.

If the RMS torque exceeds the maximum continues nominal torque (T_{nom}) the motors can be overloaded in a given time period. As it is stated in the motor technical documentation, the motors may only be loaded with the maximum continuous torque because of thermal limits. But it is also stated that higher torque are permitted in short periods of time. The allowed recurring overloading period of the motor depends on the duration of cooling period of the motors, start temperature, torque and motor speed. An estimate of the allowed duration of maximum peak torque in percentage is based on an exponentially decreasing function from [19], see figure 6.7.

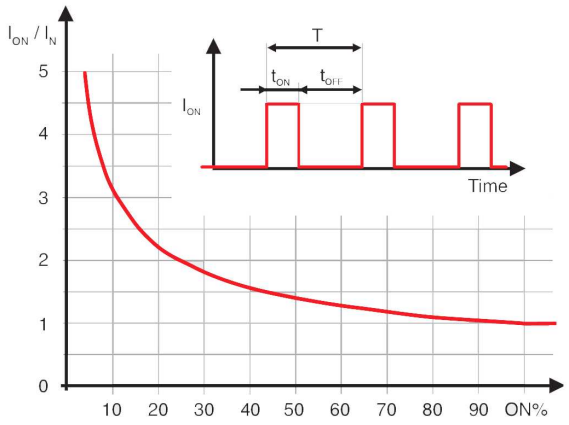

Figure 6.7: *Estimation of time overloading is allowed based on the maximum current I_{ON} and the permissible maximum current I_N. [19] As the current and torque have a linear relation the torque values can be used instead of current.*

Here T is the time period of one work cycle, t_{on} is the period of load and t_{off} is the time period when motor is in rest. I_{ON} is the maximum peak current or the max torque peak as the motor has a linear relation between current and torque. I_N is the permissible continuous nominal current or torque, see table 6.3.

Motor speed is compared in rpm and the results from DyP are in rad/s, therefore these are changed when motor speed is compared with the speed-torque line.

Motors can handle a limited maximum acceleration based on the mass moments of inertia and moment acting on motor shaft. The maximum acceleration can be calculated based on the allowed stall torque of the motor and the equivalent mass moment of inertia for motor, gear and body.

Shoulder Mount (A) motor selection

Shoulder mount joint (A) is the first revolute joint of the ARA and is as well the first driving constraint. The torque and velocity for handshake approach at this revolute joint have been plotted in figure 5.13. The complete handshake load case, handshake approach, the shake and return, will give the maximum load for this DOF. Besides load cases are the static outer position described in the end of chapter 5 compared with the motor maximum stall torque.

As the static analysis gives a moment of 88 Nm the motor stall torque has to be minimum as calculated below. The dynamic analyses for handshake load case gives smaller moments.

$$T_m = \frac{T_g}{R\eta_L} = \frac{88}{100 \cdot 0.56} \approx 1.6Nm$$

A stall torque of this magnitude require that the RE-150 model is chosen.

The root-mean-square for the complete handshake work cycle (handshake approach, the shake and return) gives the torque.

$$T_{m|RMS} \approx 0.32Nm$$

This value is exceeding the nominal maximum torque (T_{nom}) for each of the three motors shown in table 6.3. Motors larger than the three motors would increase the total weight of the ARA significantly and therefore not preferable. Another approach could be to select a gear with a higher gear ratio. To do this the gear have to be changed from size 14 to size 17 that has a max gearing of $R = 120$. But comparing the weights from gear and motors, it be seen that it would be preferable to go one step up in motor size. Another take is to create a secondary gearing between motor and gear with belt drive or similar. But as the motors are allowed to be overloaded in a given time period, this is checked for the RE-150 initial selected. A time-torque plot in figure 6.8 give an overview of the torque required for the motor in handshake approach. If these curves are compared with the three motor types it can be seen that the peak torque $T_{m|max} \approx 0.5$ and is around 3 times the nominal torque T_{nom} for the Maxon RE-150. For this overloading it is allowed that the peak torque occur approximately 11 % of the work cycle, see figure 6.7.

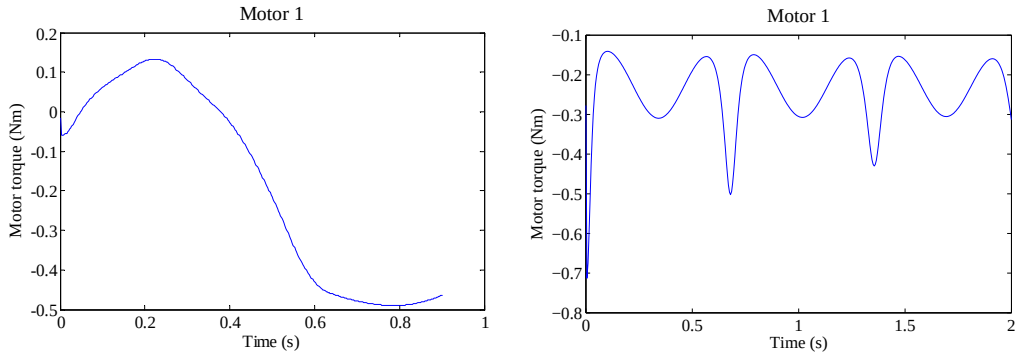

(a) (b)

Figure 6.8: *Plot of the handshake approach and the handshake. The peak at t=0 for (b) are not taken in to account because it occur from the linear calculation of motion.*

To give more effective overview of continues load in handshake load case, the result are plotted as a speed-torque diagram and compared with the motor characteristics. This is illustrated in figure 6.9. Here only the handshake approach is plotted

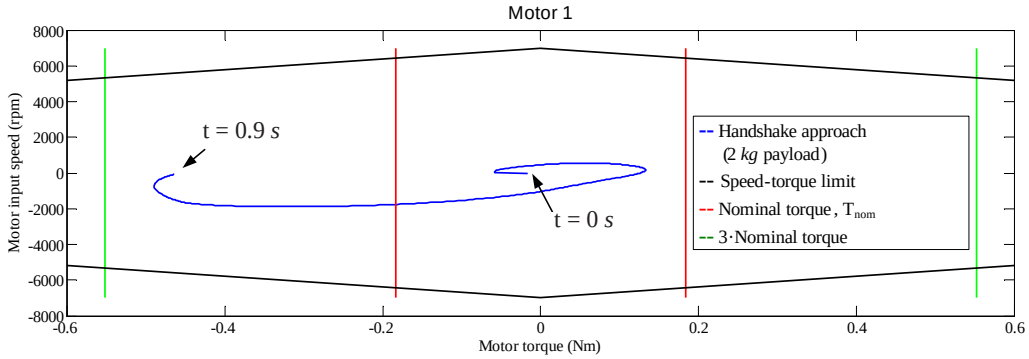

Figure 6.9: *Continuous load from the handshake approach motion plotted along with the motor characteristics for the selected motor.*

As the nominal torque $T_{nom} = 0.184$ for the RE-150 size, the handshake motion will generally exceed this value. But as the time of the complete handshake is only around 3 *s* and the technical data states that the overloading time can be up to 41 *s* the motor is assumed to be sufficient large.

All plots for each joint can be found from DyP placed at ”*CD-rom* → *dynamic_program*”.

Selected Motors

The selected motors to actuate the three remaining DOF are based on motion and forces with a payload of 2 *kg* and 5.8 *kg* as own mass. Table 6.4 gives an overview of the selected motors for each joint.

Joint	Size	Mass	Limit stall torque T_{st} [*Nm*]	Stall torque $T_{m\|max}$ [*Nm*]	Limit nominal torque·3 T_{nom}· 3 [*Nm*]	Peak torque $T_{m\|max}$ [*Nm*]
Shoulder Mount (A)	RE-150	0.48	2.5	1.6	0.552	0.35
Upper Arm 1 (B)	RE-150	0.48	2.5	1.6	0.552	0.08
Upper Arm 2 (C)	RE-90	0.34	0.967	0.55	0.2895	0.17
Lower Arm (D)	RE-90	0.34	0.967	0.55	0.2895	0.17

Table 6.4: *Selected gears for each of the revolute joints. The calculated maximum torqueses are shown along with the limits for the motor selected. A complete technical description of the motors can be found at [18] or in appendix E.*

It can bee seen that the sum of the masses gives 1.64 *kg* this is approximately 28 % of the allowed maximum mass of 5.8 *kg*. This mass can probably be lowered if smaller motors is selected and extra gearing is to be introduced. But for the initial ARA design approach these motors are used in the.

6.2 Mechanical Design

This section presents the ARA mechanical concept design. The presented design is based on selected gears and motors where structural parts are dimensioned based on calculated forces and moments from DyP. Because of the sizes of the selected gears and motors there is 1.8 *kg* available for structural design and other components. The mechanical design is in this section summarised in a design overview that are followed with a presentation of some of the design consideration. The structural design is in the end described in details. All the designed details have been dimensioned with simple calculation to ensure components will be sufficient strong. These calculations are not shown in this report. The overall mass of the designed ARA is found from Solid Works CAD model.

6.2.1 Design Overview

The initial suggested ARA design is illustrated in figure 6.10. A Solid Works CAD model is available at *"CD-tom → CAD → ARA-1.SLDASM"*.

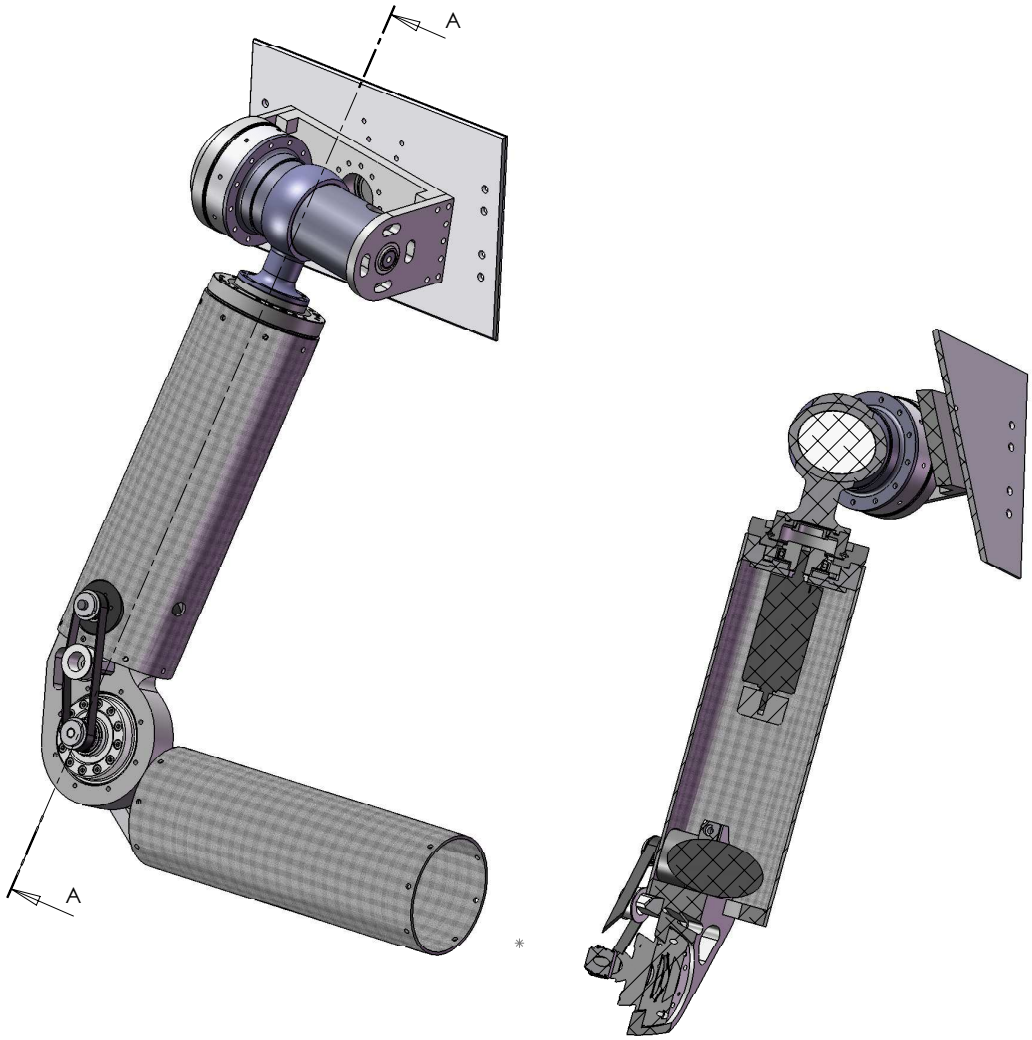

Figure 6.10: *ARA concept design that fulfil the listed requirements.*

The complete mass of the ARA with standard CPU gear units is 5.8 *kg*. The mass distribution of the ARA is listed in table 6.5 shown together with its AAU-Bot1 counterparts. The values are based on all components that connect the arm, here also gear and motor mounted inside AAU-Bot1 torso and is extracted from Solid Works. Screws, bolt, cables etc. are not included for the mass estimation.

Parts	ARA [*kg*]	AAU-Bot1 [*kg*]	Extra mass [*kg*]
Motors	1.64	0.25	1.39
Gears	2.42	0.64	1.78
Structural parts	1.70	0.90	0.8
Belt drive	0.04	0.01	0.03
Total	5.8	1.8	4

Table 6.5: *The mass distribution of the ARA design, all components that directly influence the arm movement are included. A comparison between AAU-Bot1 and ARA design are as well shown.*

6.2.2 Design Considerations

The ARA design is based on some considerations that first of all include an investigation of the AAU-Bot1 design. It is important that the mass of the arm is kept low to minimise gear and motors sizes and structural parts mass. Lowering the mass would minimise dynamic influence when the arm is moved around in space, which then would minimise power consumption, torque and forces. To minimise dynamic influence due to mass it was considered to move actuation and gearing inside AAU-Bot1 torso and the remote actuate each DOF through steel cables. But as the torso of AAU-Bot1 is filled with batteries and amplifiers, no space where available for the gears and actuators.

The structural parts are designed with the main criterion of minimising the mass and maximise the stiffness. Because the arm is moving around in a working space, it can hit either it self or people working around it. It was selected to design the ARA so outer surfaces would be relative smooth as well as keep fragile and moving parts inside design. As shown in above section the gear and motor mass was 3/4 of the total mass of ARA concept. Therefore to minimise the complete mass, gears and motors was considered to be a part of the carrying structure, without damaging the parts. The structural parts are designed based on simple calculation and intuitive design procedures.

It was noticed by Dept. of Electrical System that absolute sensors are required for defining standard initial position and the two outer positions of the revolute joints. The absolute position sensors minimise the need for moving parts to its two outer positions before motor encoder known the complete workspace. Both rotational sensors or on/off switches can be applied or this task.

The implementation of the last three DOF in the form of a special wrist joint has been taken in to account for the design of the lower arm. As the wrist joint will be a relative compact and advanced design there has to be space and flexibility in the ARA design so joint can be mounted on ARA with no or minimum amount of modification.

AAU-Bot1 Mounting
It was selected to use AAU-Bot1 arm mounting principle. This means the fist joint ”shoulder

mount (A)" are mounted at AAU-Bot1 shoulder plate, just as the case for original AAU-Bot1 arms, see figure 2.4.

Materials

As the mass of the ARA has to be minimised the selection of material is based on low density, high strength, and stiffness properties. It was chosen to use aluminium for the structural parts, as it gives a compromise between the three wanted properties of material. The aluminium are easy to machine and is therefore also easy to manufacture in-house structural parts. Besides was it chosen to use carbon fibres to create upper and lower arm, because mass could not be kept below 5.8 *kg* if aluminium where used for these parts. The aluminium used in the design has been the 6000 series aluminium available in Solid Works materials library. This grade of aluminium has a low density and relative high strength and stiffness properties.

6.2.3 Design Details

A detailed description of the ARA design is shown in this section.

Shoulder Joint

The shoulder joint is a combination of three revolute joints with intersecting rotating axes. The combined revolute joints have the same range of motion as a human shoulder joint. The design use two types of the CPU unit gears, one CPU-S and two CPU-M units. The design is relative compact where motors and gears have been combined as a structural carrying setup. All the structural parts in the shoulder joint are created of aluminium and can be designed with in-house machining processes. An overview of the joint design is illustrated in figure 6.11.

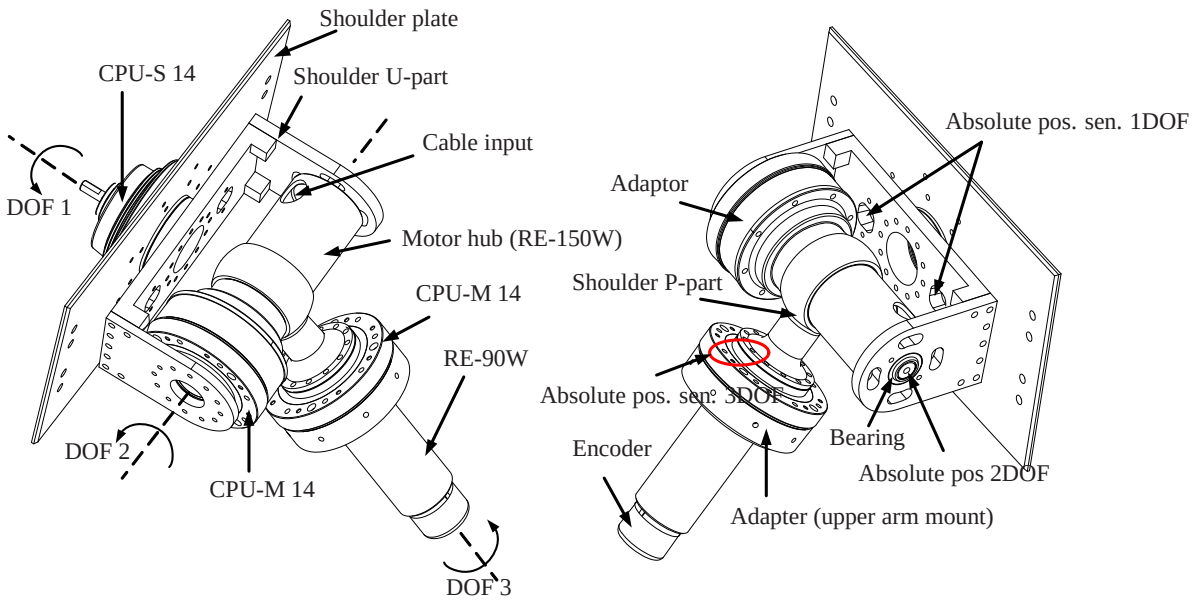

Figure 6.11: *Shoulder joint design.*

The shoulder plate, CPU-S and the motor connected to the gear are shared with the AAU-Bot1 design. It should be noted that the motor is connected to CPU-S in the AAU-Bot1 is the RE-60W model, but RE-150W are required. See figure 1.1 for AAU-Bot1 design overview.

The shoulder U-part is divided in to three components, the bottom plate, left and right plate. The U-part is designed in aluminium and is relative easy to manufacture. The left and right plate are connected to lower plate with screws that ease assembly of the part.

The motor hub is designed so the second DOF motor are placed inside the hub and then connected to the CPU-M gear via an in-house created adaptor. As the adaptor connects the motor and gear, the shaft from motor are placed inside the gear unit. The gear is filled with either grease or oil; a gasket is placed in the adaptor to seal opening between motor shaft and gear input shaft. Motor are fixed to hub with a secondary adaptor. The motor hub is supported with CPU-M bearings on left side and a standard ball bearing on right side. The extra bearing can slide along the 2 DOF rotating axis. An exploded overview can be seen in figure 6.12.

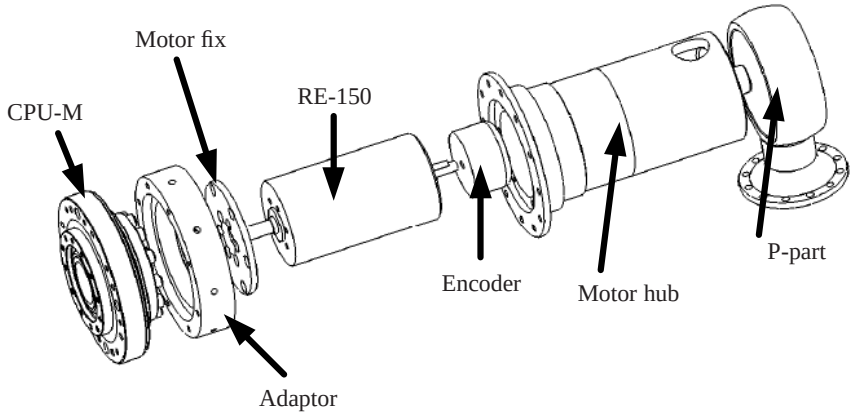

Figure 6.12: *Exploded view of the motor hub design.*

The assembly of P-part and motor hub are created as a shrink fit. The P-part can as well be fixed to motor hub with standard welding approach.

Third DOF is created with combination of a CPU-M gear unit and a RE-90W motor. The motor and gear are connected with an in-house designed adaptor. This adaptor does as well work as the mounting point of upper arm component. Output shaft of gear is connected to P-part.

The absolute position sensors are to be placed at marked areas highlighted from picture 6.11. The fist DOF sensor should be an rotational sensor as rotation of motor hub can be easy measured at this position. The second DOF absolute position is to be measured with two on/off pressure switches. The switches are activated when they passes mounted obstacles placed on the shoulder plate. The obstacles can be mounted with the screws that fix CPU-S gear unit. The third DOF absolute sensor is not shown in the figure but is to be created in same manner as second DOF sensor. The switches are to be mounted on the second DOF CPU-M spline and the obstacles are to be mounted on the P-part.

Elbow Joint

The elbow joint has moving parts exposed outside. To keep the mass down with used gears and motors it is necessary to take this design approach. The three first DOF of the four required DOF are placed at the shoulder joint and therefore the last DOF are created at the elbow joint. The joint are actuated with a RE-90W motor and uses a CPU-S gear unit. This joint range of motion is equivalent with the human elbow joint. The structural parts in the design are all create of aluminium and can be created with in-house machining. The elbow concept design is shown in figure 6.13.

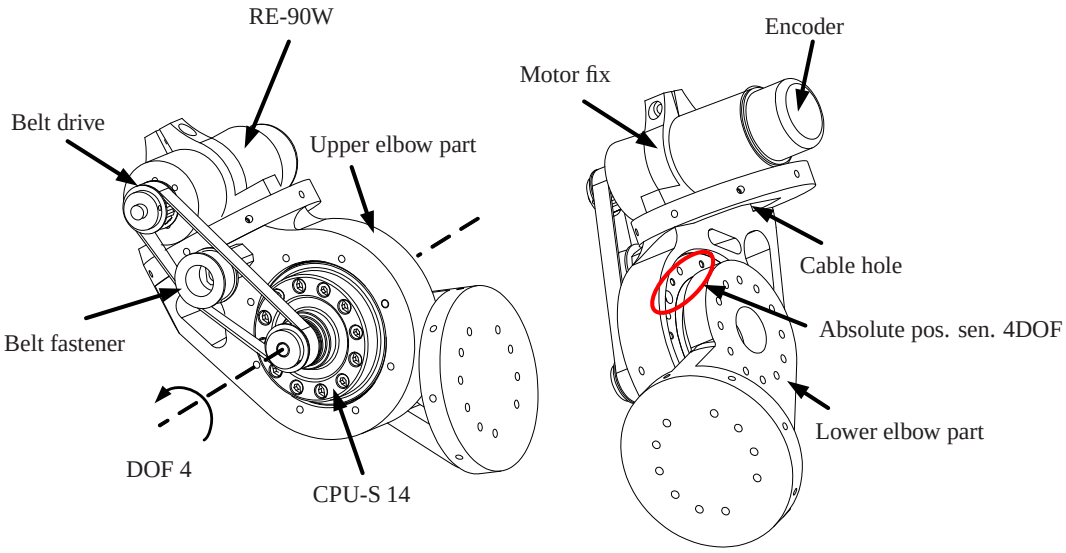

Figure 6.13: *Elbow joint design.*

The upper elbow joint is the main part of this design, where motor, gear belt drive etc. are mounted on. The motor is placed on the top of the upper elbow part; this position requires a hole in the upper arm. Motor are fixed with simple tightener. The motor actuate the gear through a belt drive system. The belt fastener is a simple offset mechanism. As a belt drive is used the motor will be affected by radial forces. They do not exceed the allowed for this motor model. The lower elbow part is only a part that connects lower arm and elbow joint.

Absolute position control for this joint is done with two on/off switches. The switches are mounted on the elbow CPU-S spline facing towards the lower elbow part. The switches are then activated when lower the elbow part is moved over the switches.

Upper/lower Arm

Upper and lower arm components are in overall the same components. The parts is created by aluminium. The components are carrying structure that gives a large stiffness feature because of relative large outer diameter. At the same time the design gives a good protection for wires, motors etc. which are placed inside these components. The upper/lower arm are illustrated in figure 6.14.

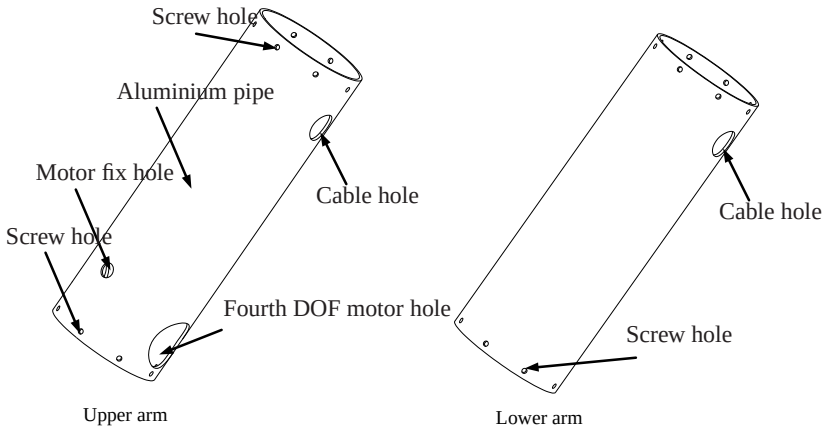

Figure 6.14: *Upper/lower arm.*

As the wrist joint is to be mounted on the lower arm no additional components have been placed at this part. The space available inside the lower arm aluminium pipe is relative large and can be filled with components used for wrist joint design. Holes for cables etc. are as well been introduced to ensure maximum compatibility.

6.3 Summary

The gears and motors selected in this chapter are based on modified selection criteria. The selected gears is found to be strong enough even for the smallest gear unit available. The selected motors are relative large even if some criterions was violated. It can be seen that the sum of motor and gear masses is 4.04 *kg* that is approximately 70 % of the allowed maximum mass of 5.8 *kg*. This leaves approximately 1.8 *kg* to be used for structural parts and extra components, e.g. cables. The mechanical design is created with gear and motors to be a part of the carrying structure. Even with this design approach the total mass of ARA would reach the 5.8 *kg*. For this mass estimation cables etc. was not taken into account. The structural components have been checked with simple calculation, not shown in this report, to ensure these are sufficient strong. The designed joints has the range of motion listed in table 2.1.

7
Conclusion and Future Work

The main focus of the project was to design an anthropomorphic robot arm (ARA). This arm is to be mounted on the AAU-Bot1 biped robot.

The designed ARA has four DOF, three at the shoulder and one at the elbow. Each of the joints has the equivalent range of motion as a human arm. Segment length follows the length of the upper and lower arm of a human. The selected gears and motors are calculated to fulfil the 1000 hour walking requirement as well as the handshake requirement of minimum 100 handshakes. Here these motion can be performed with 2 *kg* of payload. It is furthermore ensured that the ARA can work with other variants of motion. This is done by conducting simple static calculation of ARA position that gives maximum moments at each DOF. The estimated total ARA mass is 5.8 *kg*, (2.43 *kg* of gears, 1.64 *kg* of motors and 1.73 *kg* structural parts), which is equivalent to the maximum initially allowed ARA mass. The mass of designed ARA will give approximately 4 *kg* extra mass to the AAU-Bot1 per arm. The estimated mass does not include cables, switches etc. as well as the, not yet designed, 3DOF wrist joint.

The current ARA design is based on motion determined with two different optimisation procedures, a weighed damped pseudo inverse Jacobian (PIJ) method and a Complex optimising procedure used along with the PIJ. As the design parameters are the four input in the weighing matrix the values has to be chosen within a reasonable design space. Large values will introduce singular problems for the PIJ method and should therefore be avoided this is also the case for values that are negative. It can be seen that the optimising results, when minimising power consumption and removing intrusion, do only results in relative small improvements compared to optimising result where only intrusion is removed. This can be related to the fact that PIJ indirectly minimise energy usage.

The PIJ method is found to be an effective way of solving unknown driving motion for redundant systems. But the trajectory path of the endpoint will affect the results calculated with the method. If the endpoint is moved towards the workspace boundary or outside the boundary, singularity problems will occur. The calculated motion will then not be smooth, but give large velocity even for small time-steps. If endpoint is to be moved near boundary or outside, the use of the damping factor is found to be an effective approach to damp motion near singular position. The damping factor will introduce errors compared to endpoint reference velocity.

The use of complex optimisation procedure along with the weighing matrix of PIJ method is found to be an effective way to remove motion path that will give intrusion with AAU-Bot1. If intrusion control is to be used with for several obstacles placed differently in the work cycle, it will be necessary to divide the work cycle in to different steps. Optimisation objects that directly or indirectly is solved with the PIJ method is not improved significantly for this system

and intrusion control is found to be sufficient for initial calculation of the ARA motion.

The presented ARA concept in this report is the initial step of an ARA design. Here the initial steps have been taken to select gear, actuator sizes and design structural parts. To ensure that a finalised ARA with seven DOF will be below 5.8 *kg* the initial design shown in this report is to be reconsidered. It can bee seen that the mass contribution from the gears and motors is around 70% of the total mass. To minimise the gear mass, special designed gears with use of Harmonic Drive component set should be applied as the gear components has a high efficiency, stiffness and zero (or very little) backlash. Motors should be reselected based on additional gearing between motor and gear. This can at elbow joint be done with introducing a gearing with the toothed belt drive. The shoulder joint is to be redesigned if an extra gearing between motor and Harmonic Driver gear is to be applied.

Bibliography

[1] J.Ottnad C.Sauter K.Sedchaicham A.Albers, S.Brudniok. Upper body of a new humanoid robot - the design of armar iii. *IEEE*, 2002.

[2] J.Ottnad C.Sauter K.Sedchaicham A.Albers, S.Brudniok. Armar iii - design of the upper body. 2006.

[3] B.Rooks. The harmonious robot. *Industrial Robot: An International Journal*, 33:125–130, 2006.

[4] D.E.Whitney. Resolved motion rate control of manipulators and human prostheses. *IEEE Trans. on Man-Mach. Sys., 10*, 2:47–53, 1969.

[5] Harmonic Drive, 2008. www.harmonicdrive.de.

[6] Harmonic Drive, 2008. www.harmonicdrive.net/reference.

[7] Harmonic Drive, 2008. http://www.harmonicdrive.de/contenido/cms/upload/pdf/GK2007/english/2_Units/1_CPU-M/CPU_Technical20Data_en.pdf.

[8] Harmonic Drive, 2008. http://www.harmonicdrive.de/contenido/cms/upload/pdf/en/900030.pdf.

[9] Harmonic Drive, 2008. http://www.harmonicdrive.de/contenido/cms/upload/pdf/en/cpu_h7.pdf.

[10] A.Guignard & A.G.Billard F.Guenter, L.Roos. Design of a biomimetic upper body for the humanoid robot robota. *IEEE-RAS International Conference on Humanoid Robots*, 2005.

[11] L.Piccardi M.Calzascia A.Billard F.Guenter, A.Guignard. Development of a miniature articulated arm and pair of eyes for the humanoid robota. *IEEE/APS Conference on Mechatronics and Robotics*, 2005.

[12] Lei-Guang Huang. An extended form of damped pseudoinverse control of kinematically redundant manipulators. *Institute of Automation, Chinese Academy of Sciences*, pages 3791–3796, ?

[13] L.Finsen C.Jensen A.Jensen J.Merkel D.Ekner H.Christensen K.Hansen, H.Feveile. Kropsmål for danske arbejdstagere; antropometriske mål på 467 danske arbejdstagere. Technical report, 1999. Rapport nr. 7.

[14] N.Hamilton K.Luttgens. *Kinesiology: Scientific Basis of Human Motion*. Madison, 9. edition, 1997.

[15] Satoru Shibata Tomonori Yamamoto Mitsuru Jindai, Tomio Watanabe. Development of a handshake robot system. *The 15th IEEE International Symposium on Robot and Human Interactive Communication*, 15th:710–715, 2006.

[16] M.J.Box. A new method of constrained optimization and a comparison with other methods. *Computer Journal*, 8, 1965.

[17] L.F.Christiansen M.M.Pedersen, A.A.Nielsen. Design of biped robot aau-bot1. Master's thesis, IME Aalborg University, 2007.

[18] Maxon Motors, 2008. http://www.maxonmotorusa.com/.

[19] Maxon Motors, 2008. http://test.maxonmotor.com/docsx/Download/catalog_2008/Pdf/08_wichgtiges_dc_ec_motoren_e.pdf.

[20] T.O.Andersen M.R.Hansen. A method for derive the optimal operation of mobile hydraulic manipulators. *The Ninth Scandinavian International Conference on Fluid Power, SICFP'05*, 2005.

[21] M.Rygaard. System design optimization. Slides. IME Aalborg University.

[22] S.Bai M.Rygaard. Design and analysis of a human-like robotic arm. Project description, Depertment of Mechanical Engineering, 2008. ME Aalborg University.

[23] P.E.Nikravesh. *Computer-Aided Analysis of Mechanical Systems*. Prentice Hall, 1. edition, 1988. ISBN: 0 13 164220 0.

[24] Berret Technologies, 2008. www.berrett.com.

[25] T.J.Manetsch. Toward efficient global optimization in large dynamic systems - the adaptive complex method. *IEEE Transactions on system, Man, and cybernetics*, 20, 1990.

[26] Minoru Hashimoto Tomofumi Kasuga. Human-robot handshaking using neural oscillators. *Proceedings of the 2005 IEEE International Conference on Robotics and Automation*, 4:3813–3818, 2005.

[27] K.Shimomura H.Kondo & A.Morishima Y.Ogura, H.Aikawa. Development of a new humanoid robot wabian-2. *Proceedings of the 2006 IEEE International Conference on Robotics and Automation*, pages 76–81, 2006.

[28] C.Aoyama S.Matsunaga K.Higaki N.Fujimura Y.Sakagami, R.Watanabe. The intelligent asimo: System overview and integration. *IEEE International Conference on Intelligent Robots and Systems*, pages 2478–2483, 2002.

Nomenclature

a	=	scalar
$\underline{a}$	=	Vector
$\underline{\underline{a}}$	=	Matrix
$\sim$	=	Skew notation
$\dot{}$	=	First derivative with respect to time
$\ddot{}$	=	Second derivative with respect to time
$\underline{0}$	=	zero vector

Symbols

Section 5.2, Dynamic Analysis

$\underline{r}_i$	=	Translating position of body i	$\underline{s}_i$	=	Global joint coordinates of body i	$\underline{s}'_i$	=	Local joint coordinates of body i
$\underline{\underline{A}}_i$	=	Transformation matrix of body i	$\underline{\underline{\Phi}}_q$	=	Jacobian matrix of constraints	$\underline{\Phi}$	=	Vector of constraint equations
Φ	=	One constraint	$\underline{\underline{w}}$	=	Weighing matrix	ρ	=	damping factor
ρ_0	=	Constant damping factor	$\underline{\psi}$	=	Vector of driving angles	ψ_i	=	The angle of i^{th} input of the driving vector
$\underline{\underline{I}}$	=	Identity matrix	$\underline{q}_i$	=	Vector of coordinates of body i	x,y,z	=	Global Cartesian coordinate system
ξ_i, η_i, ζ_i	=	Local Cartesian coordinate system of body i	ϕ_1, ϕ_2, ϕ_3	=	Bryant angles	ε	=	Manipulability factor
t	=	Time	w_i	=	weighing value of i^i diagonal number in weighing matrix			

Section 5.3, Dynamic Analysis

$\underline{F}_i$	=	Vector of global reaction forces of body i	$\underline{M}_i$	=	Vector of global reaction moments of body i	m_i	=	Mass of body i
$\underline{F}'_i$	=	Vector of local reaction forces of body i	$\underline{M}'_i$	=	Vector of local reaction moments of body i	J	=	Mass moment of inertia
$\underline{g}$	=	Gravity vector	$\underline{w}_i$	=	Vector of gravity forces of body i	$\underline{\underline{J}}_i$	=	Global inertia tensor of body i
$\underline{\underline{J}}'_i$	=	Local inertia tensor of body i	$\underline{\omega}_i$	=	Global angular velocity vector of body i	$\dot{\underline{\omega}}_i$	=	Global angular acceleration vector of body i

Section 5.4, Dynamic Analysis

x_i	=	Design parameter	$\underline{x}_i$	=	Vector of design parameters of the i^{th} population	$\underline{x}_c$	=	Centroid of design vector parameters
α	=	Mirroring factor	λ	=	Tuning factor	n	=	Population size
β	=	Influence factor				f	=	Fitness function
K	=	Global fitness function	P_{av}	=	Root mean square power consumption	f_n	=	Normalising factor
S	=	Pseudo intrusion value	γ	=	shape tuning factor	a,b,c	=	Ellipsoid radius values
$\Delta a, \Delta b, \Delta c$	=	safety distance added to ellipsoid						

Section 6.1.1, Power Transmission

f_s	=	Safety factor	M_{TD}	=	Limit for dynamic tilting moment	M_{TS}	=	Limit for static tilting moment
T_A	=	Limit for average output torque	T_R	=	Limit for repeated peak torque	T_M	=	Limit for momentary peak torque
n_{max}	=	Limit for max input speed	n_{av}	=	Limit for average input speed	R	=	Gear ratio
η_L	=	Gear total efficiency	η_R	=	Speed-temp efficiency	η_e	=	Shaft sealing efficiency
K	=	correction factor	T_N	=	Rated torque			

Section 6.1.2, Power Transmission

T_{st}	=	Stall torque limit	T_{nom}	=	Limit for nominal torque	n_0	=	no load speed
J_m	=	Motor shaft mass moment of inertia	J_g	=	Gear input shaft mass moment of inertia	$T_{m\|RMS}$	=	Root mean square motor torque
I	=	Current	I_N	=	Nominal current	I_{ON}	=	Maximum peak current

Abbreviations

DOF	=	Degree of freedom	*ARA*	=	Anthropomorphic Robot Arm	*RMS*	=	Root Mean Square
CoM	=	Centre of Mass	*WJ*	=	Wrist Joint	*PIJ*	=	Pseudo Inverse Jacobian.
DyP	=	Dynamic Program	*EoM*	=	Equation of Motion	*TM*	=	Tilting Moment.
AM	=	Axial Moment	*IC*	=	Intrusion Control	*CO*	=	Complete Optimising
IDA	=	Inverse Dynamic Analysis						

APPENDIX

A
Constraint Equations

All the constraint equation and the respective transformation matrices are showed in this appendix.

Constraint Equations

The constraint equation for the ARA are based on figure A.1 and the complete set of 27 constraint equation are listed in equation A.4.

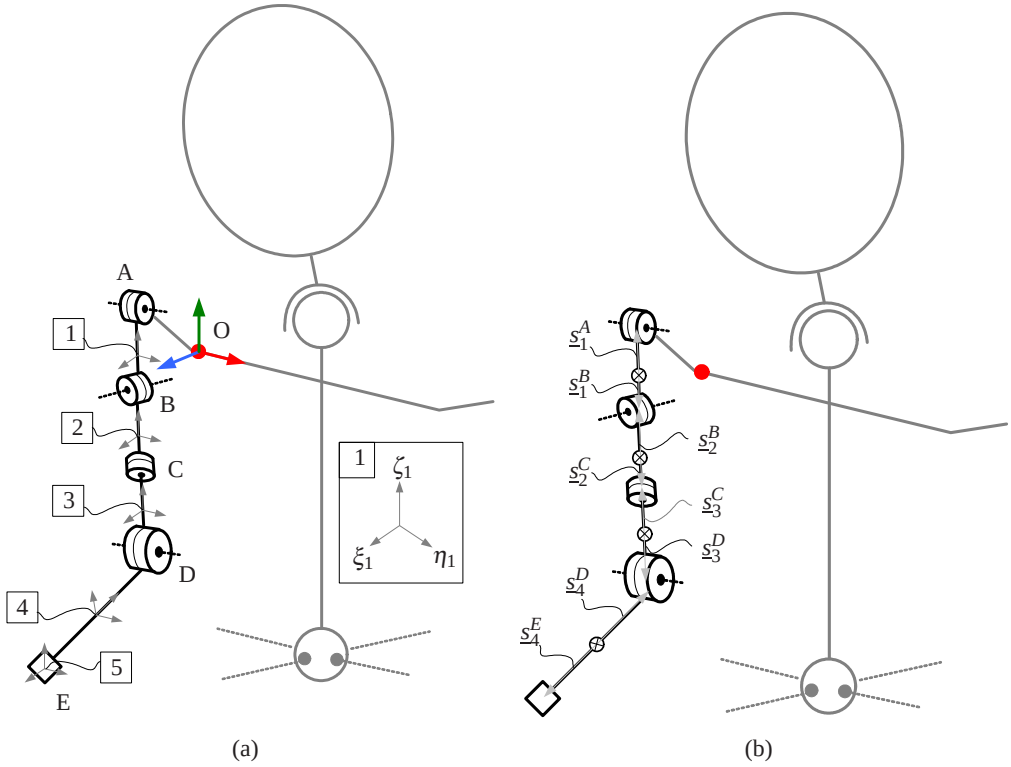

Figure A.1: *Kinematic definitions for the ARA used to establish constraint equation.*

Global - Body 1

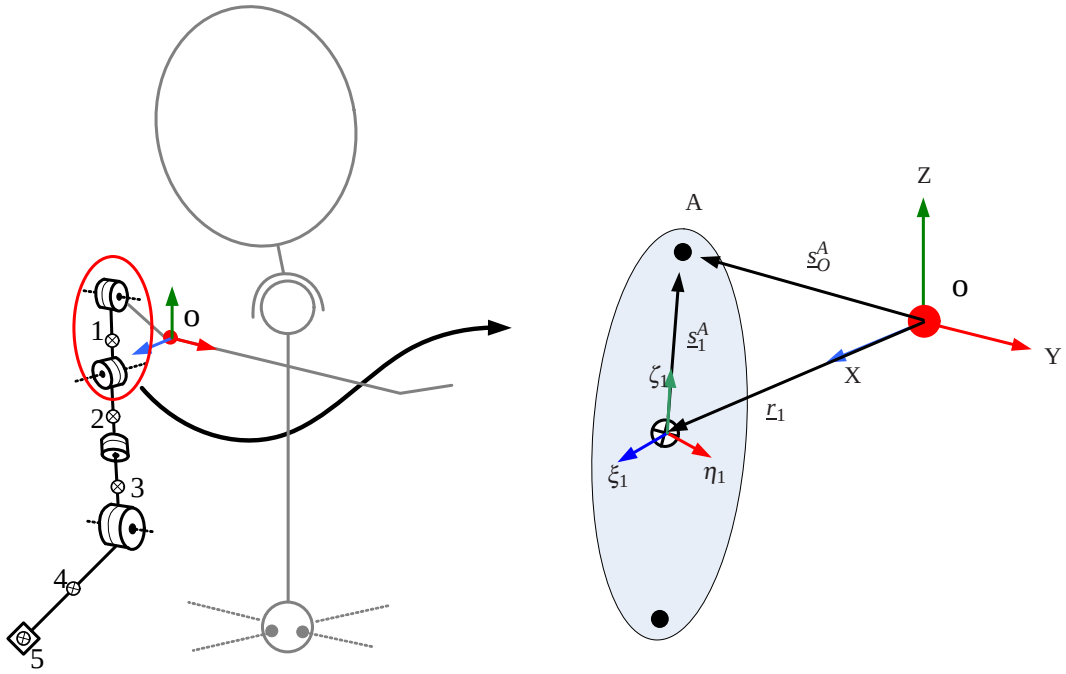

Figure A.2: *Kinematic constraint between Body 1 and reference.*

As $\underline{s}_O^A$ is set to zero the constraint equations of Body 1 are written as

$$\begin{aligned}
\underline{\Phi}_{1-3} &= \underline{r}_1 + \underline{\underline{A}}_1 \underline{s}_1'^A - \underline{s}_0^A = \underline{0} \\
\Phi_4 &= \phi_{11} = 0 \\
\Phi_5 &= \phi_{12} - \psi_1 = 0 \\
\Phi_6 &= \phi_{13} = 0
\end{aligned}$$

Where $\underline{\underline{A}}_1$ is

$$\underline{\underline{A}}_1 = \begin{bmatrix} c\phi_{12}c\phi_{13} & -c\phi_{12}s\phi_{13} & s\phi_{12} \\ c\phi_{11}s\phi_{13} + s\phi_{11}s\phi_{12}c\phi_{13} & c\phi_{11}c\phi_{13} - s\phi_{11}s\phi_{12}s\phi_{13} & -s\phi_{11}c\phi_{12} \\ s\phi_{11}s\phi_{13} - c\phi_{11}s\phi_{12}c\phi_{13} & s\phi_{11}c\phi_{13} + c\phi_{11}s\phi_{12}s\phi_{13} & c\phi_{11}c\phi_{12} \end{bmatrix}$$

Body 1 - Body 2

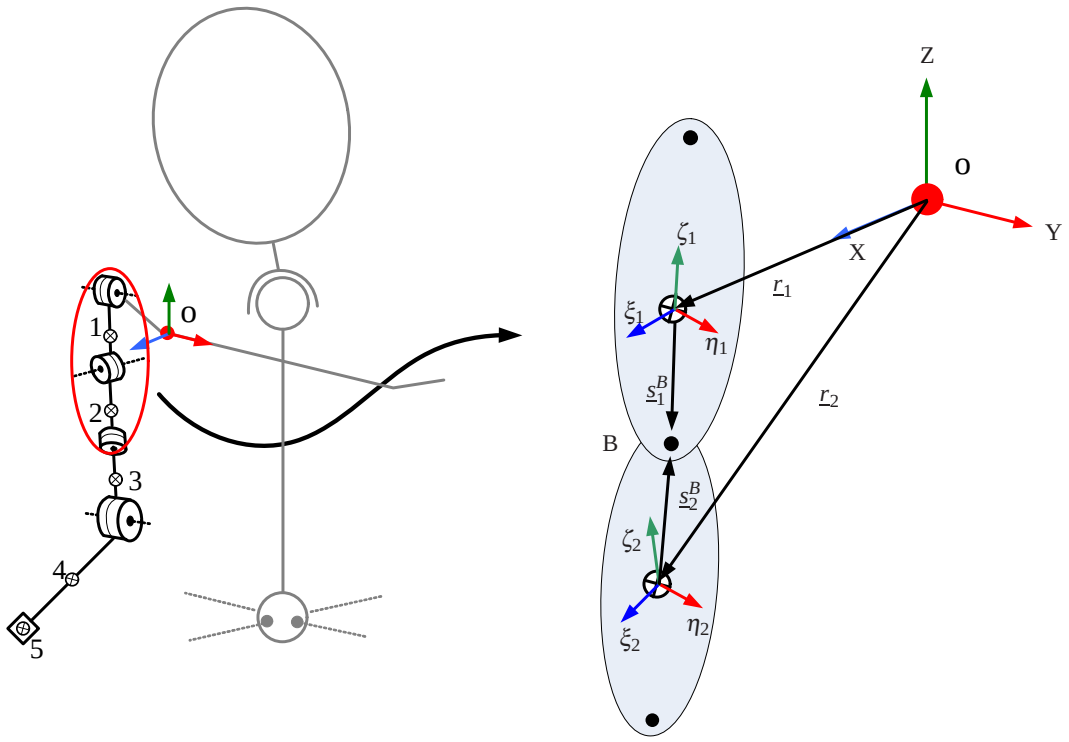

Figure A.3: *Kinematic constraint between Body 2 and 1.*

This give the constraint equations

$$\begin{aligned}
\underline{\Phi}_{7-9} &= \underline{r}_1 + \underline{\underline{A}}_1 \underline{s}'^B_1 - \underline{r}_2 - \underline{\underline{A}}_2 \underline{s}'^B_2 = \underline{0} \\
\Phi_{10} &= \phi_{21} - \psi_2 = 0 \\
\Phi_{11} &= \phi_{22} - \phi_{12} = 0 \\
\Phi_{12} &= \phi_{33} - \phi_{13} = 0
\end{aligned}$$

Where $\underline{\underline{A}}_2$ is

$$\underline{\underline{A}}_2 = \underline{\underline{A}}_1 \underline{\underline{A}}_{2/1} \tag{A.1}$$

$$\underline{\underline{A}}_2 = \underline{\underline{A}}_1 \begin{bmatrix} c\phi_{22}c\phi_{23} & -c\phi_{22}s\phi_{23} & s\phi_{22} \\ c\phi_{21}s\phi_{23} + s\phi_{21}s\phi_{22}c\phi_{23} & c\phi_{21}c\phi_{23} - s\phi_{21}s\phi_{22}s\phi_{23} & -s\phi_{21}c\phi_{22} \\ s\phi_{21}s\phi_{23} - c\phi_{21}s\phi_{22}c\phi_{23} & s\phi_{21}c\phi_{23} + c\phi_{21}s\phi_{22}s\phi_{23} & c\phi_{21}c\phi_{22} \end{bmatrix}$$

Body 2 - Body 3

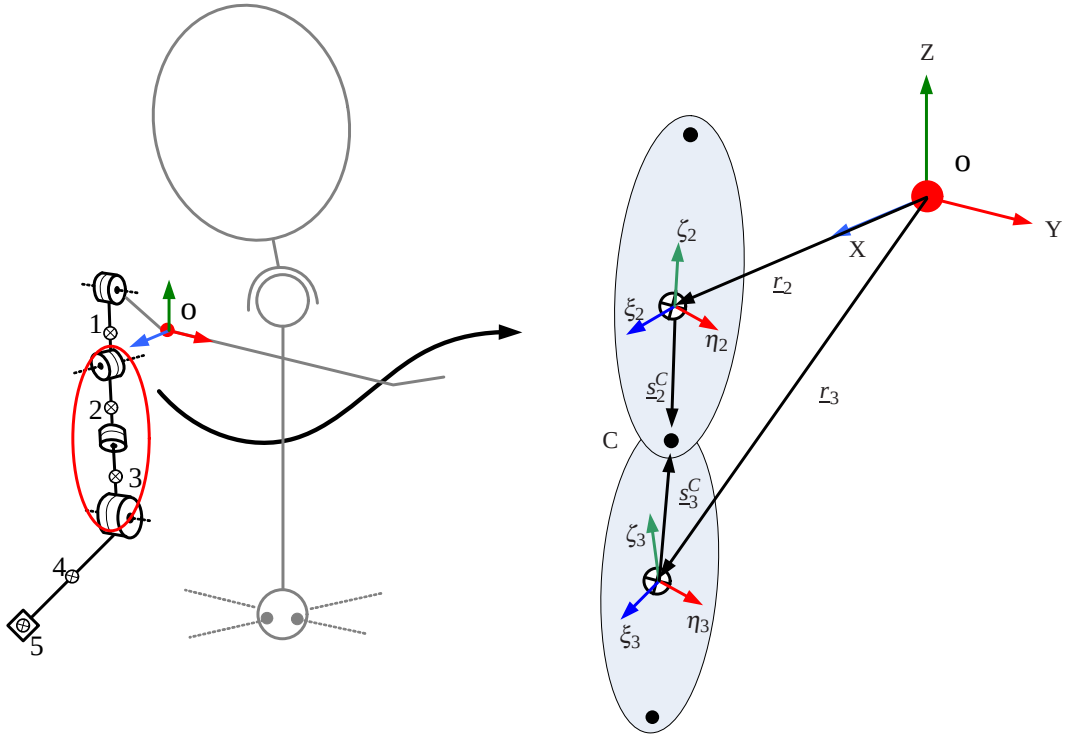

Figure A.4: *Kinematic constraint between Body 3 and 2.*

This give the constraint equations

$$\begin{aligned}
\underline{\Phi}_{13-15} &= \underline{r}_2 + \underline{\underline{A}}_2 \underline{s}'^C_2 - \underline{r}_3 - \underline{\underline{A}}_3 \underline{s}'^C_3 = \underline{0} \\
\Phi_{16} &= \phi_{31} - \phi_{21} = 0 \\
\Phi_{17} &= \phi_{32} - \phi_{22} = 0 \\
\Phi_{18} &= \phi_{33} - \psi_3 = 0
\end{aligned}$$

Where $\underline{\underline{A}}_3$ is

$$\underline{\underline{A}}_3 = \underline{\underline{A}}_2 \underline{\underline{A}}_{3/2} \tag{A.2}$$

$$\underline{\underline{A}}_3 = \underline{\underline{A}}_2 \begin{bmatrix} c\phi_{32}c\phi_{33} & -c\phi_{32}s\phi_{33} & s\phi_{32} \\ c\phi_{31}s\phi_{33} + s\phi_{31}s\phi_{32}c\phi_{33} & c\phi_{31}c\phi_{33} - s\phi_{31}s\phi_{32}s\phi_{33} & -s\phi_{31}c\phi_{32} \\ s\phi_{31}s\phi_{33} - c\phi_{31}s\phi_{32}c\phi_{33} & s\phi_{31}c\phi_{33} + c\phi_{31}s\phi_{32}s\phi_{33} & c\phi_{31}c\phi_{32} \end{bmatrix}$$

Body 3 - Body 4

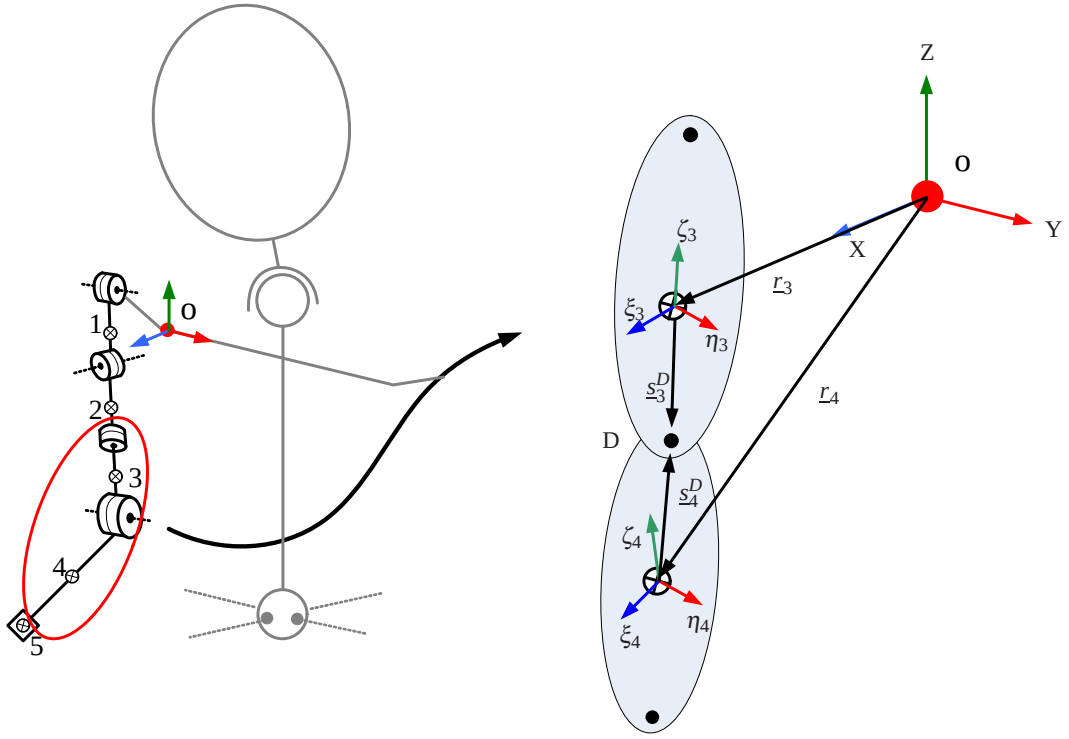

Figure A.5: *Kinematic constraint between Body 4 and 3.*

This give the constraint equations

$$\begin{aligned}
\underline{\Phi}_{19-21} &= \underline{r}_3 + \underline{\underline{A}}_3 \underline{s}'^D_3 - \underline{r}_4 - \underline{\underline{A}}_4 \underline{s}'^D_4 = \underline{0} \\
\Phi_{22} &= \phi_{41} - \phi_{31} = 0 \\
\Phi_{23} &= \phi_{42} - \psi_4 = 0 \\
\Phi_{24} &= \phi_{43} - \phi_{33} = 0
\end{aligned}$$

Where $\underline{\underline{A}}_4$ is

$$\underline{\underline{A}}_4 = \underline{\underline{A}}_3 \underline{\underline{A}}_{4/3} \tag{A.3}$$

$$\underline{\underline{A}}_4 = \underline{\underline{A}}_3 \begin{bmatrix} c\phi_{42}c\phi_{43} & -c\phi_{42}s\phi_{43} & s\phi_{42} \\ c\phi_{41}s\phi_{43} + s\phi_{41}s\phi_{42}c\phi_{43} & c\phi_{41}c\phi_{43} - s\phi_{41}s\phi_{42}s\phi_{43} & -s\phi_{41}c\phi_{42} \\ s\phi_{41}s\phi_{43} - c\phi_{41}s\phi_{42}c\phi_{43} & s\phi_{41}c\phi_{43} + c\phi_{41}s\phi_{42}s\phi_{43} & c\phi_{41}c\phi_{42} \end{bmatrix}$$

Body 4 - Body 5

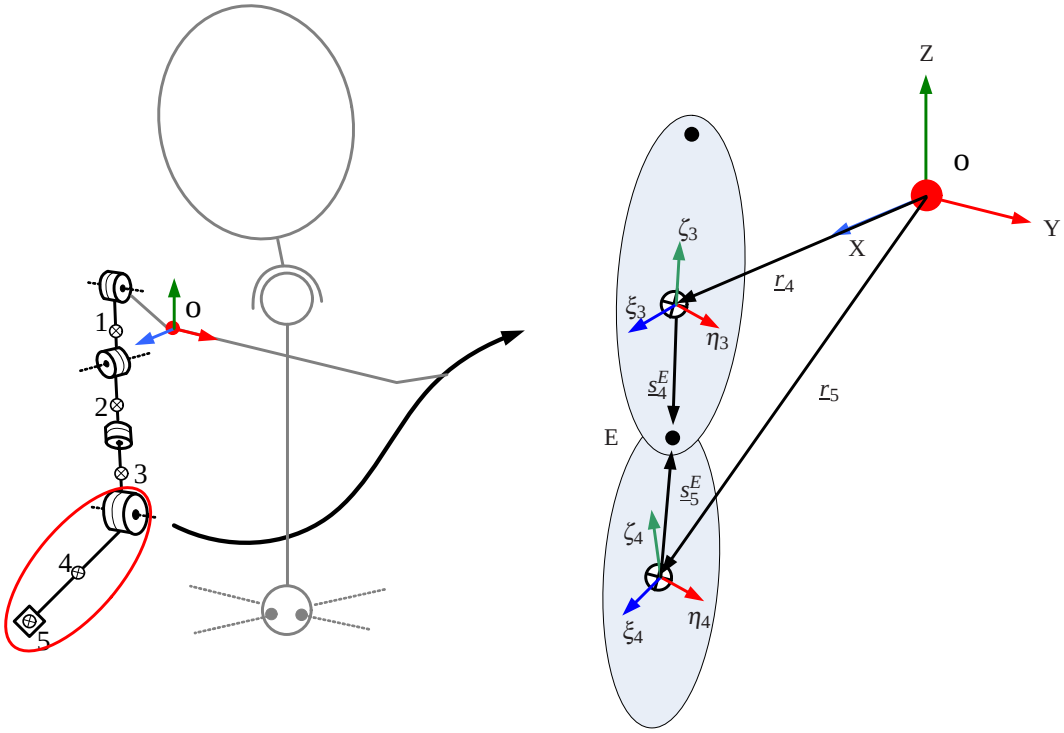

Figure A.6: *Kinematic constraint between Body 5 and 4.*

This give the constraint equations because $\underline{s}_4^E = 0$

$$\underline{\Phi}_{25-27} = \underline{r}_4 + \underline{\underline{A}}_4 \underline{s'}_4^E - \underline{r}_5 = \underline{0}$$

Collected

$$\Phi(\underline{q}) = \begin{bmatrix} \underline{r}_1 + \underline{\underline{A}}_1 \underline{s}'^A_1 \\ \phi_{11} \\ \phi_{12} - \psi_1 \\ \phi_{13} \\ \underline{r}_1 + \underline{\underline{A}}_1 \underline{s}'^B_1 - \underline{r}_2 - \underline{\underline{A}}_2 \underline{s}'^B_2 \\ \phi_{21} - \psi_2 \\ \phi_{22} - \phi_{12} \\ \phi_{33} - \phi_{13} \\ \underline{r}_2 + \underline{\underline{A}}_2 \underline{s}'^C_2 - \underline{r}_3 - \underline{\underline{A}}_3 \underline{s}'^C_3 \\ \phi_{31} - \phi_{21} \\ \phi_{32} - \phi_{22} \\ \phi_{33} - \psi_3 \\ \underline{r}_3 + \underline{\underline{A}}_3 \underline{s}'^D_3 - \underline{r}_4 - \underline{\underline{A}}_4 \underline{s}'^D_4 \\ \phi_{41} - \phi_{31} \\ \phi_{42} - \psi_4 \\ \phi_{43} - \phi_{33} \\ \underline{r}_4 + \underline{\underline{A}}_4 \underline{s}'^E_4 - \underline{r}_5 \end{bmatrix} = 0 \qquad \text{(A.4)}$$

B
Equation of Motion - ARA

The complete set EoM for the ARA are represented with figure B.1 and are represented with equations 5.20 and 5.21.

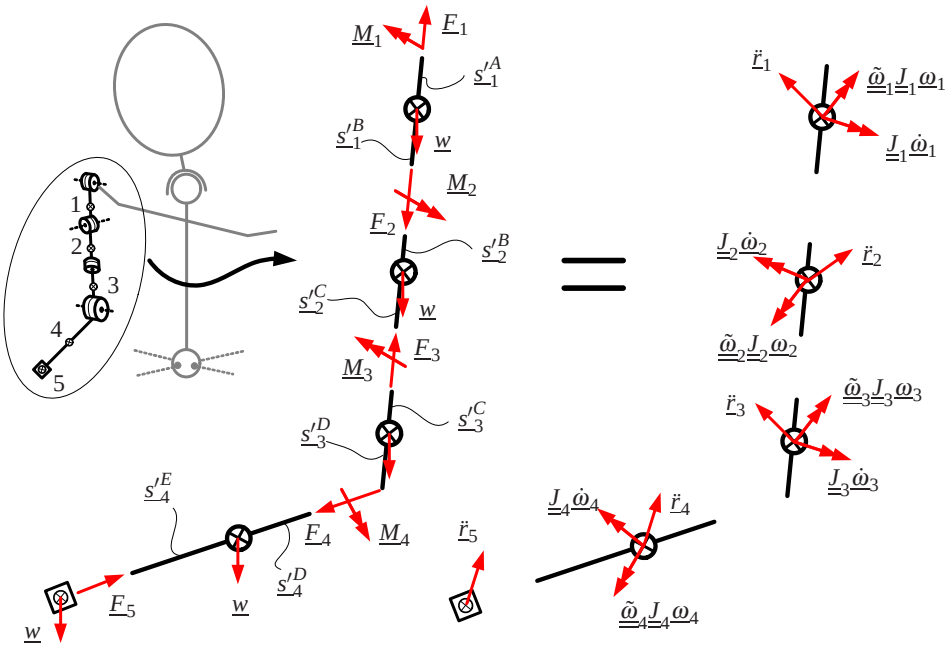

Figure B.1: *Complete set of equations of motion for ARA.*

From the notation of equation of motion and the FBD and KD showed in figure B.1. All EoM are written beneath for each body for the ARA.

Body 1

$$\sum \underline{F} \quad \Rightarrow \quad \underline{F}_1 - \underline{w}_1 - \underline{F}_2 = m_1 \ddot{\underline{r}}_1 \tag{B.1}$$

$$\sum \underline{M}_{CoG} \quad \Rightarrow \quad \underline{\tilde{s}}'^A_1 \underline{F}_1 + \underline{M}_1 - \underline{\tilde{s}}'^B_1 \underline{F}_2 - \underline{M}_2 = \underline{\underline{J}}_1 \dot{\underline{\omega}}_1 + \underline{\tilde{\omega}}_1 \underline{\underline{J}}_1 \underline{\omega}_1 \tag{B.2}$$

Body 2

$$\sum \underline{F} \quad \Rightarrow \quad \underline{F}_2 - \underline{w}_2 - \underline{F}_3 = m_2 \ddot{\underline{r}}_2 \tag{B.3}$$

$$\sum \underline{M}_{CoG} \quad \Rightarrow \quad \underline{\tilde{s}}'^B_2 \underline{F}_2 + \underline{M}_2 - \underline{\tilde{s}}'^C_2 \underline{F}_3 - \underline{M}_3 = \underline{\underline{J}}_2 \dot{\underline{\omega}}_2 + \underline{\tilde{\omega}}_2 \underline{\underline{J}}_2 \underline{\omega}_2 \tag{B.4}$$

Body 3

$$\sum \underline{F} \quad \Rightarrow \quad \underline{F}_3 - \underline{w}_3 - \underline{F}_4 = m_3 \underline{\ddot{r}}_3 \tag{B.5}$$

$$\sum \underline{M}_{CoG} \quad \Rightarrow \quad \underline{\tilde{s}}_3^{\prime C} \underline{F}_3 + \underline{M}_3 - \underline{\tilde{s}}_3^{\prime D} \underline{F}_4 - \underline{M}_4 = \underline{\underline{J}}_3 \underline{\dot{\omega}}_3 + \underline{\tilde{\omega}}_3 \underline{\underline{J}}_3 \underline{\omega}_3 \tag{B.6}$$

Body 4

$$\sum \underline{F} \quad \Rightarrow \quad \underline{F}_4 - \underline{w}_4 - \underline{F}_5 = m_4 \underline{\ddot{r}}_4 \tag{B.7}$$

$$\sum \underline{M}_{CoG} \quad \Rightarrow \quad \underline{\tilde{s}}_4^{\prime D} \underline{F}_4 + \underline{M}_4 - \underline{\tilde{s}}_4^{\prime E} \underline{F}_5 = \underline{\underline{J}}_4 \underline{\dot{\omega}}_4 + \underline{\tilde{\omega}}_4 \underline{\underline{J}}_4 \underline{\omega}_4 \tag{B.8}$$

Body 5

$$\sum \underline{F} \quad \Rightarrow \quad \underline{F}_5 - \underline{w}_5 = m_5 \underline{\ddot{r}}_5 \tag{B.9}$$

$$\sum \underline{M}_{CoG} \quad \Rightarrow \quad 0 \tag{B.10}$$

C
Dynamic Program

The MatLab code showed here are the Dynamic Program (DyP). The section are shown, to the extent as possible, in the order as the different function is used. The general overview of the program is illustrtated in figure C.1.

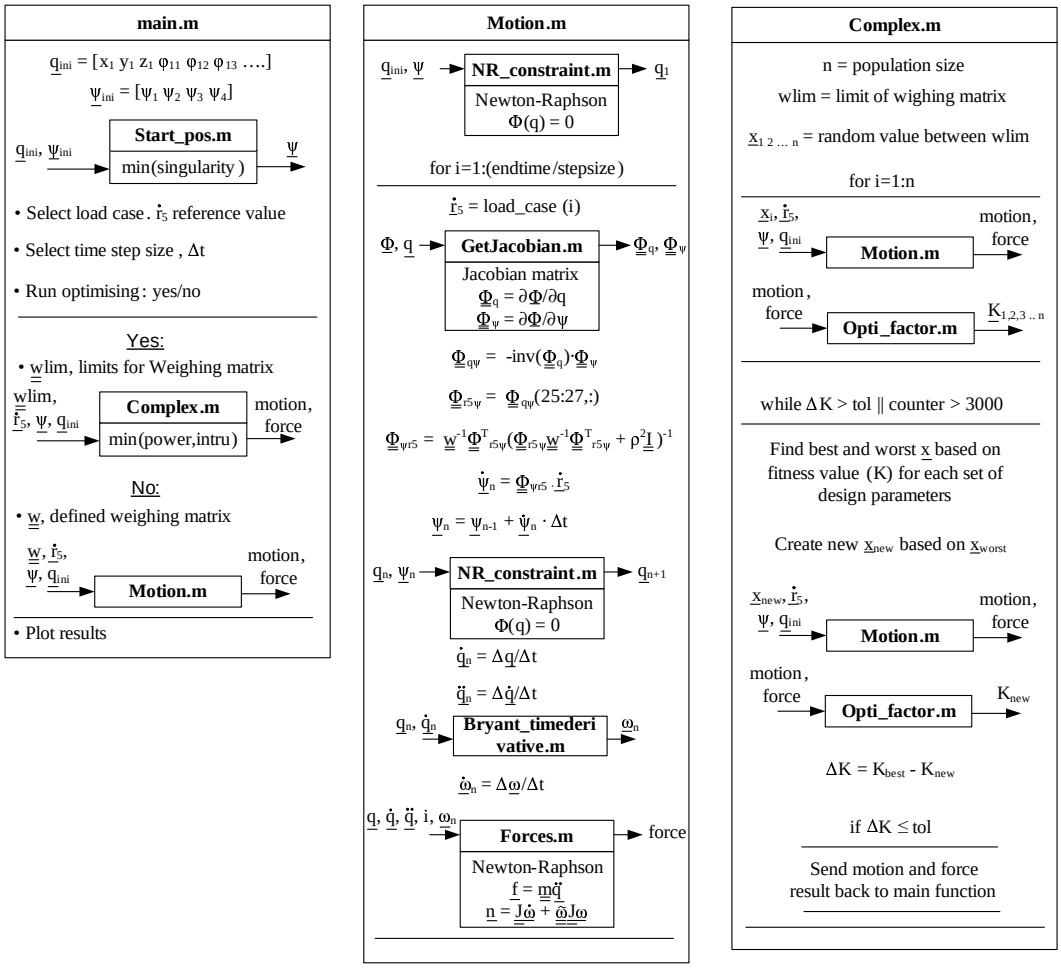

Figure C.1: *Overall working principle of DyP.*

The Matlab code for the program can be foound in the following pages.

D
Technical Data CPU units

E

Technical Data Maxon Motors

DESIGN OF MECHANICAL SYSTEMS

DMS 10 M.Sc.

Lee Richard Linnemann Nielsen